

8-2017

## MODIFICATION OF APLYSIA FEEDING NETWORK BY L-DOPA AND DOPAMINE-DEPENDENT LEARNING

Curtis Neveu

Curtis L. Neveu

Follow this and additional works at: [https://digitalcommons.library.tmc.edu/utgsbs\\_dissertations](https://digitalcommons.library.tmc.edu/utgsbs_dissertations)

 Part of the [Molecular and Cellular Neuroscience Commons](#)

---

### Recommended Citation

Neveu, Curtis and Neveu, Curtis L., "MODIFICATION OF APLYSIA FEEDING NETWORK BY L-DOPA AND DOPAMINE-DEPENDENT LEARNING" (2017). *The University of Texas MD Anderson Cancer Center UTHealth Graduate School of Biomedical Sciences Dissertations and Theses (Open Access)*. 802.  
[https://digitalcommons.library.tmc.edu/utgsbs\\_dissertations/802](https://digitalcommons.library.tmc.edu/utgsbs_dissertations/802)

This Dissertation (PhD) is brought to you for free and open access by the The University of Texas MD Anderson Cancer Center UTHealth Graduate School of Biomedical Sciences at DigitalCommons@TMC. It has been accepted for inclusion in The University of Texas MD Anderson Cancer Center UTHealth Graduate School of Biomedical Sciences Dissertations and Theses (Open Access) by an authorized administrator of DigitalCommons@TMC. For more information, please contact [digitalcommons@library.tmc.edu](mailto:digitalcommons@library.tmc.edu).

MODIFICATION OF APLYSIA FEEDING NETWORK BY L-DOPA AND DOPAMINE-  
DEPENDENT LEARNING

by

Curtis Lynn Neveu

APPROVED:

---

John H. Byrne, Ph.D.  
Advisory Professor

---

Andrew J. Bean, Ph.D.

---

Michael Beierlein, Ph.D.

---

Rebecca Berdeaux, Ph.D.

---

Ruth Heidelberg, M.D., Ph.D.

APPROVED:

---

Dean, The University of Texas  
MD Anderson Cancer Center UTHHealth Graduate School of Biomedical Sciences

MODIFICATION OF APLYSIA FEEDING NETWORK BY L-DOPA AND DOPAMINE-  
DEPENDENT LEARNING

A

DISSERTATION

Presented to the Faculty of

The University of Texas

MD Anderson Cancer

Graduate School of Biomedical Sciences

In Partial Fulfillment

Of the Requirements

for the Degree of

DOCTOR OF PHILOSOPHY

by

Curtis Neveu

Date of Graduation

August, 2017

This dissertation is dedicated to:

My wife, Ruthanne, and my daughter, Amelie.

## **Acknowledgements**

I would like to thank my wife for her love and support over the years. I would also like to thank my dad for getting me interested in science, my mom for teaching me to love solving puzzles, my step-dad for teaching me to be committed to working hard for things I want to achieve, and my brother for teaching me how to work hard, and my grandmother for teaching me the value of wisdom. I would also like to thank my Ph.D. advisor, Dr. Byrne, and Dr. Baxter for their guidance, Dr. Chen for her work on single-cell analogues of OC, and Dr. Smolen for his comments on early drafts of this dissertation.

# MODIFICATION OF APLYSIA FEEDING NETWORK BY L-DOPA AND DOPAMINE-DEPENDENT LEARNING

Curtis L. Neveu

Advisory Professor: John H. Byrne, Ph. D.

Dopamine (DA) is a ubiquitous neuromodulator of neuronal networks in the animal kingdom and has a well-established role in modulating motor behavior and encoding reward information. Although the effects of DA and DA-dependent learning at the behavioral and molecular levels are well-understood, many questions still remain concerning the effects of DA at the network level. DA-dependent learning effects on a neuronal circuit were examined by measuring the biophysical properties before and after *in vitro* operant conditioning (OC) of the feeding circuit of *Aplysia*. OC reduced the excitability of B4 and the B4-to-B51 synaptic connection, with a trend towards an enhancement of the B4-to-B8 synaptic connection. These data indicate that OC can decrease the excitability of neurons and modify synaptic connections. The effects of L-DOPA were examined by applying either low or high concentrations of L-DOPA (40 or 250  $\mu$ M) and then monitoring activity of up to 130 neurons simultaneously using a voltage-sensitive dye (RH-155). L-DOPA selected one of two distinct buccal motor patterns (BMPs): intermediate (low L-DOPA) or bite patterns (high L-DOPA). The selection of intermediate BMPs was associated with shortening of the second phase of the BMP (retraction), whereas the selection of bite BMPs was

associated with shortening of both phases of the BMP (protraction and retraction). Selection of intermediate BMPs was also associated with truncation of individual neuron spike activity (decreased burst duration but no change in spike frequency or burst latency) in neurons active during retraction and in neurons projecting an axon through nerves Rn or n3. In contrast, selection of bite BMPs was associated with compression of spike activity (decreased burst latency and duration, and increased spike frequency) in neurons projecting through nerves Rn, n2, and n3, as well as increased spike frequency of protraction neurons. The large-scale voltage-sensitive dye (VSD) recordings delineated the spatial distribution of neurons active during BMPs and the modification of that distribution by the two concentrations of L-DOPA. Finally, a system was established for identifying neurons in VSD recordings which will enable a detailed analysis of the effects of L-DOPA and OC.

## Chapter 1: Table of Contents

<b>Approval Sheet.....</b>	<b>i</b>
<b>Title Page.....</b>	<b>ii</b>
<b>Dedication.....</b>	<b>iii</b>
<b>Acknowledgements.....</b>	<b>iv</b>
<b>Abstract.....</b>	<b>v</b>
<b>Table of Contents.....</b>	<b>vii</b>
<b>List of Illustrations.....</b>	<b>xi</b>
<b>Abbreviations.....</b>	<b>xiv</b>
<b>Chapter 1: Introduction .....</b>	<b>1</b>
1.1 Feeding circuit of <i>Aplysia</i> .....	1
1.1.1 Neuron B4 .....	4
1.1.2 Neuron B8 .....	7
1.1.3 Neuron B51 .....	7
1.2 Neuron identification .....	11
1.3 Voltage-sensitive dye (VSD) imaging .....	11
1.4 Dopamine (DA).....	13
1.4.1 DA in animal behavior .....	13
1.4.2 L-DOPA and the synthesis of DA .....	14
1.4.3 Effects of DA on mammalian neurons .....	15
1.4.3.1 Effect of DA on intrinsic excitability .....	15
1.4.3.2 Effect of DA on synaptic connections.....	17



1.4.3 Effects of L-DOPA and DA on the feeding CPG.....	19
1.5 Operant conditioning (OC).....	20
1.5.1 Overview .....	20
1.5.2 Neuronal substrates of OC .....	21
1.5.3 Neuronal correlates of OC in mammals .....	22
1.5.4 Neuronal correlates of OC in <i>Aplysia</i> feeding.....	24
<b>Chapter 2: Operant conditioning (OC) modifies the synaptic and intrinsic properties of neurons within the feeding CPG.....</b>	<b>26</b>
2.1 Rationale and Hypothesis.....	26
2.2 Methods.....	29
2.2.1 Preparation.....	29
2.2.2 Classification of BMPs.....	30
2.2.3 <i>In vitro</i> analog of operant conditioning.....	30
2.2.4 Cell identification .....	32
2.2.5 Testing B4 properties in ganglia .....	32
2.2.6 Cell culture .....	33
2.2.7 Single-cell analog .....	33
2.2.8 Statistical analysis .....	34
2.3 Results.....	34
2.3.1 Contingent En2 stimulation reinforces iBMPs.....	34
2.3.1 B8 sag potential is modified by OC but not B8 excitability.....	37
2.3.2 B51-to-B8 synaptic connection is not modified by OC.....	41
2.3.3 B4-to-B51 synaptic connection is reduced by OC. ....	46

2.3.4 B4-to-B8 synaptic connection modulation by OC .....	49
2.3.5 B4 excitability is reduced by OC .....	52
2.3.6 Stimulation of En2 contingent with B4 stimulation suppresses B4 excitability <i>in vitro</i> . .....	54
2.3.7 DA contingent with B4 stimulation suppresses B4 excitability in culture. ....	57
2.3.8 Modeling operant conditioning in a conductance based model .....	60
2.3.8.1 Rationale .....	60
2.3.8.2 Modeling B8 motor neuron .....	60
2.3.8.3 Modeling retraction neurons B4, B51, and B71 .....	64
2.3.8.4 Contributions of correlates of OC .....	73
2.4 Discussion .....	78
<b>Chapter 3: Unique configurations of compression and truncation of neuronal activity underlie L-DOPA-induced selection of motor patterns in <i>Aplysia</i>. .....</b>	<b>80</b>
3.1 Rationale and hypothesis .....	80
3.2 Methods .....	81
3.2.1 Optical and electrophysiological recording .....	81
3.2.2 Classification of BMPs .....	83
3.2.3 Analysis of VSD imaging data .....	84
3.2.4 Analysis of extracellular nerve activity .....	85
3.2.5 Identification of axonal projections from neurons to nerves .....	86
3.2.6 Spike correlation .....	86
3.2.7 Burst analysis .....	86
3.2.8 Topographical analysis .....	88

3.2.9 Statistical analysis .....	88
3.3 Results.....	89
3.3.1 L-DOPA enhances specific fictive behaviors in a concentration dependent manner. ....	89
3.3.2 VSD imaging captures spike activity in a large number of neurons of the buccal ganglia. ....	93
3.3.3 L-DOPA modifies neuronal activity without increasing neuronal synchrony. ....	98
3.3.4 L-DOPA reconfigures activity of specific subgroups of neurons. ....	103
3.3.5 L-DOPA uniquely modifies the burst activity of specific subgroups of neurons .....	108
3.2.6 L-DOPA preferentially activates neurons located in different regions of the ganglia.....	112
3.3 Discussion .....	115
<b>Chapter 4: Identifying neurons using combined VSD imaging and extracellular nerve recording.....</b>	<b>120</b>
4.1 Hypothesis and rationale .....	120
4.2 Results.....	120
4.2.1 Catalogue of feeding CPG neurons.....	120
4.2.2 Neurons could be identified in VSD recordings .....	124
4.3 Discussion .....	128
<b>Chapter 5: Discussion and Future Directions .....</b>	<b>131</b>
<b>Bibliography .....</b>	<b>137</b>

<b>Vita .....</b>	<b>158</b>
-------------------	------------

## List of Illustrations

<b>Figure 1.1</b> Overview of the feeding CPG.....	3
<b>Figure 1.2</b> Synaptic connections and activity of B4.....	6
<b>Figure 1.3</b> Synaptic connections and activity of B51.....	9
<b>Figure 2.1</b> A subset of synaptic connections of the feeding CPG.....	28
<b>Figure 2.2</b> Buccal motor programs and their modulation by OC.....	36
<b>Figure 2.3</b> Excitability of B8 was not altered by OC .....	39
<b>Figure 2.4</b> OC increases sag potential of B8.....	40
<b>Figure 2.5</b> Synaptic depression is not modified by OC.....	43
<b>Figure 2.6</b> OC did not modify B51-to-B8 PPR.....	45
<b>Figure 2.7</b> Reversal potential of B4-to-B51. ....	47
<b>Figure 2.8</b> OC reduced the B4 to B51 synaptic connection.....	48
<b>Figure 2.9</b> Reversal potential of B4-to-B8 synaptic connection.....	50
<b>Figure 2.10</b> Effect of OC on the B4-to-B8 synapse. ....	51
<b>Figure 2.11</b> OC reduces the excitability of B4. ....	53
<b>Figure 2.12</b> Stimulation of En2 contingent with B4 stimulation suppresses B4 excitability. ....	56
<b>Figure 2.13</b> DA contingent with B4 stimulation reduced B4 excitability in culture. ..	59
<b>Figure 2.14</b> Modeling the $I_h$ current in B8.....	62
<b>Figure 2.15</b> $I_h$ does not affect excitability when neuron is clamped to -65 mV. ....	63
<b>Figure 2.16</b> Overview of the Model CPG network. ....	65
<b>Figure 2.17</b> Fitting of synaptic connections to empirical data.....	67
<b>Figure 2.18</b> Excitability was fit to empirical data.....	71

<b>Figure 2.19</b> Fits of input resistance and excitability to empirical data.....	72
<b>Figure 2.20</b> Correlates of OC were introduced into the feeding CPG.....	75
<b>Figure 2.21</b> Incorporating correlates of OC enhanced number of iBMPs and B51 activity.....	76
<b>Figure 3.1</b> Changes in fictive behavior by L-DOPA.....	91
<b>Figure 3.2</b> VSD imaging of neuronal activity in the buccal ganglia.....	95
<b>Figure 3.3</b> Changes in fictive behavior and neuronal activity by L-DOPA .....	100
<b>Figure 3.4</b> The temporal dynamics of specific groups of neurons are modified by L-DOPA.....	104
<b>Figure 3.5</b> L-DOPA differentially modified the burst properties of neurons. ....	110
<b>Figure 3.6</b> Spatial distribution of protraction, retraction, Rn, n2, and n3 projecting neurons.....	114
<b>Figure 3.7</b> L-DOPA recruits neurons with different spatial distributions. ....	114
<b>Figure 4.1</b> Catalog of all the identified neurons in the buccal ganglia.....	123
<b>Figure 4.2</b> Identification of neurons recorded by VSD.....	126
<b>Figure 4.3</b> Neuron identification reveals the functional role of each neuron.....	130

**Abbreviations**

BMP:	Buccal motor pattern
cAMP:	Cyclic adenosine monophosphate
CPG:	Central pattern generator
DA:	Dopamine
En2:	Esophageal nerve 2
EPSP:	Excitatory postsynaptic potential
FS:	Fast spiking
GABA:	$\gamma$ -amino butyric acid
iBMP:	Ingestion buccal motor pattern
IPSP:	Inhibitory postsynaptic potential
IPSC:	Inhibitory postsynaptic current
ISI:	Inter-stimulus interval
L-DOPA:	L-3,4-dihydroxyphenylalanine
n1:	Nerve 1
n2:	Nerve 2
n3:	Nerve 3
OC:	Operant conditioning
PKA:	Protein kinase A
PPF:	Paired-pulse facilitation
Rn:	Radular nerve
rBMP:	Rejection buccal motor pattern
SN:	Substantia nigra

TAN: Tonically active neuron

VSD: Voltage-sensitive dye

VTA: Ventral tegmental area



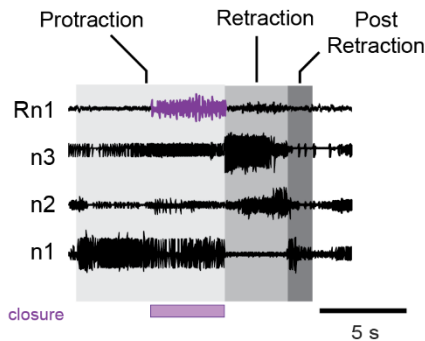
## Chapter 1: Introduction

### 1.1 Feeding circuit of *Aplysia*

*Aplysia* is well known as a model for understanding mechanisms underlying learning and memory. Studies using *Aplysia* have advanced the understanding of learning and memory mechanisms because of the simplicity of its behavior and the accessibility of its nervous system. The feeding behavior of *Aplysia* is ideal for studying learning and memory because the behavior is modified by both classical and operant learning paradigms and is simple enough to be mediated by central pattern generating (CPG) neurons within a single ganglia (i.e., buccal ganglia) (Fig. 1.1B) (Nargeot et al., 1997, 1999a,b, 2007, 2009; Brembs et al., 2002; Mozzachiodi et al., 2008; Seiling et al., 2009). In addition, isolated buccal ganglia continue to produce motor patterns (BMP) (Susswein and Byrne, 1988). A group of highly interconnected neurons within the buccal ganglia initiates patterns and mediates the first phase (i.e., protraction) of the BMP (Fig. 1.1C) (Hurwitz et al., 1994, 1996, 1997; Kabotyanski et al., 1998; Susswein and Byrne, 1988; Teyke et al., 1993). These neurons subsequently activate a second group of highly interconnected buccal ganglia neurons that mediate the retraction phase of the BMP and terminate the protraction phase through feedback inhibition (Church and Lloyd, 1994; Cropper et al., 2004; Evans and Cropper 1998; Hurwitz and Susswein 1996; Plummer and Kirk, 1990; Sasaki et al., 2013). The BMP is then terminated by neurons active during the post-retraction phase (Nargeot et al., 1999c). BMPs can be categorized into patterns that correspond to ingestion behaviors (iBMP) that bring food into the animal, patterns that correspond to rejection behaviors (rBMP) that move food out of the animal, and patterns that

correspond to intermediate behaviors that cause little to no movement of the food. Ingestion behaviors can be separated further into bites which cause a small inward movement and swallows which cause a large movement of food. In Chapter 2, patterns associated with bites and swallows will be combined into iBMPs, whereas in Chapter 4 bite patterns will be considered as a separate group. Some neurons such as B51 and B8 are more active during iBMPs, while other neurons such as B4 are more active during rBMPs, and some neurons within the pattern initiating group are active in both iBMPs and rBMPs such as B63, B65, B30 (Evans et al., 1998; Hurwitz et al., 1997; Morton and Chiel 1993b; Nargeot et al., 1999a,b, 2009; Seiling et al., 2014). The size, position, morphology, activity, and synaptic connections of each neuron is consistent between animals. Therefore, these properties can be used to locate and record from the same neuron across multiple preparations (Fig. 1.1B). Neurons within the buccal ganglia receive dopaminergic input either from the esophageal nerve or from a small group of neurons within the buccal ganglia. The buccal dopamine pathways will be described in more detail in Section 1.3.2. There are several limitations of the isolated buccal ganglia. For example, afferent sensory information and input from higher order structures are removed. Despite these differences, the buccal ganglia produce motor patterns that are remarkably similar to motor patterns *in vivo*. Although learning and memory are well established in *Aplysia* many questions still remain about the effects of DA-dependent learning.

### A1. Rejection (rBMP)



### A2. Ingestion (iBMP)

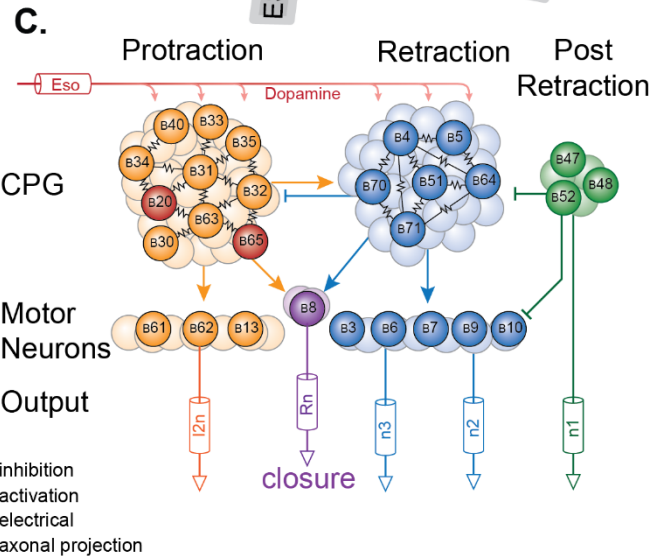
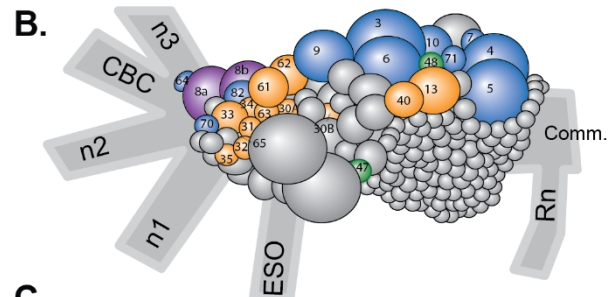
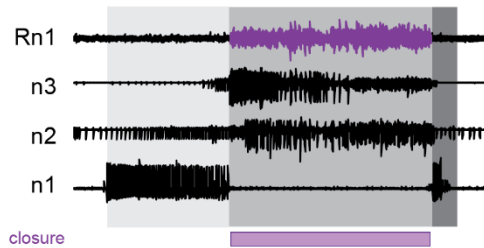


**Figure 1.1** Overview of the feeding CPG

**A1**, Example nerve recording of a rejection BMP. Each phase is indicated by grey shading. Closure activity is defined by large unit activity in the radula nerve. The majority of closure activity occurs during the protraction phase. **A2**, Example nerve recording of an ingestion BMP. The majority of closure activity occurs during retraction. **B**, The locations of some key neurons within the feeding CPG. **C**, A diagram showing the groups of neurons that mediate the phases of the BMP. DAergic neurons are red.

### 1.1.1 Neuron B4

In general, neurons in the buccal ganglia are numbered in the order at which they were first identified. So, B4 and its nearly identical counterpart B5 were discovered early in the investigation of buccal ganglia neurocircuitry. Daniel Gardner was the first to characterize this neuron and found that it synapses on many (if not all) neurons in the feeding CPG (Gardner and Kandel, 1971). Characterization of this neuron revealed that it released acetylcholine (ACh) and elicited both excitatory and inhibitory post-synaptic potentials (PSPs) (1977; Gardner and Kandel, 1971, 1977). Moreover, the PSPs of many of the B4 synaptic connections are biphasic in that they exhibit a fast excitatory component mediated by  $\text{Na}^+$  and then a slower inhibitory component mediated by  $\text{Cl}^-$  (Gardner and Kandel, 1973, 1977). These two components can be differentiated based on their sensitivities to different nicotinic ACh receptor inhibitors. The excitatory component is more sensitive to hexamethonium whereas the inhibitory component is more sensitive to curare (Gardner and Kandel, 1977). In addition, B4 is electrically coupled to many neurons in the buccal ganglia (Gardner 1977; Sasaki et al., 2013). A diagram of all the known synaptic targets of B4 is illustrated in Fig. 1.2A. B4 is active during every BMP but shows a greater level of activity during rBMPs as compared to iBMPs (Church and Lloyd, 1994; Susswein and Byrne, 1988; Sasaki et al., 2009). B4 biases the CPG towards rBMPs by its inhibitory synapses to neurons that promote iBMPs such as B51 and B8. Neuron B4 is a motor neuron that sends an axonal projection through the ipsilateral n3 and receives proprioceptive input from cerebral buccal interneurons (Church and Lloyd, 1991; Rosen et al., 1982). Taken together, these properties of B4 suggest that this neuron

may use proprioceptive input to reduce closure activity and strength of the retraction phase.

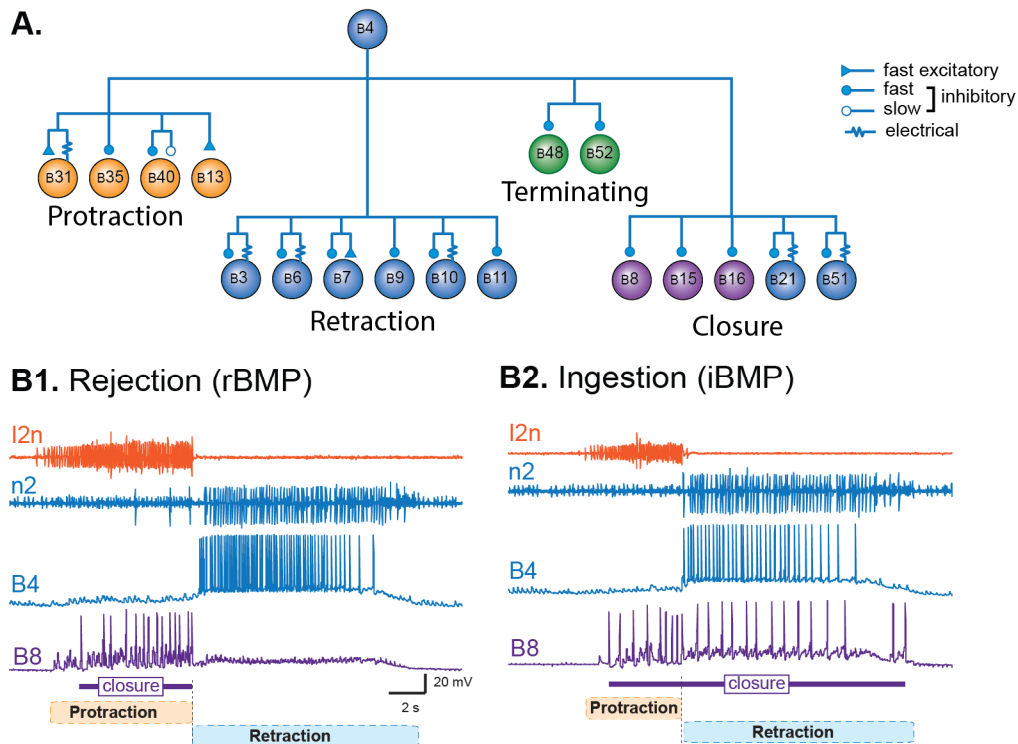


**Figure 1.2** Synaptic connections and activity of B4.

**A**, Diagram showing the targets of B4. The majority of the connections are inhibitory. **B**, Representative recordings of BMPs elicited by continuous, 4 Hz stimulation of n.2,3. The protraction phase was monitored via activity in I2 n. (orange trace, orange bar). The retraction phase was monitored via extracellular recording from n.2,1 (blue traces, blue bar). Closure motor activity was monitored by intracellular recordings from motor neuron B8 (purple traces, purple bar). **B1**, Rejection-like BMP (rBMP). B8 activity was restricted to the protraction phase. **B2**, Ingestion-like (iBMP). The majority of B8 activity (> 50%) occurred during the retraction phase.

### 1.1.2 Neuron B8

The designation B8 corresponds to a pair of neurons named B8a and B8b. Each B8 neuron sends bilateral axonal projections through the left and right radula nerves (Morton and Chiel, 1993b). B8a and B8b have identical properties, so these neurons will both be referred to hereafter as B8. The neuron B8 was first identified by Daniel Gardner (Gardner and Kandel, 1971). B8 became recognized as a key output neuron of the buccal ganglia when Morton and Chiel discovered that activity of this neuron mediates radula closure (Morton and Chiel, 1993b), indicating that B8 activity alone can be used to classify motor patterns into either iBMPs or rBMPs (e.g., Morgan et al., 2002; Church and Lloyd, 1994). Since then, a major focus of research on *Aplysia* feeding behavior has been on neurons which modulate B8 activity (Evans et al., 1998; Kabotyanski et al., 1998; Nargeot et al., 1999a,b; Teyke et al., 1993). Two important neurons in this regard are B51 and B4 which enhance or suppress B8 activity, respectively (Evans et al., 1998; Nargeot et al., 1999a,b; Plummer and Kirk, 1990). B8 also has a pronounced sag potential which shunts hyperpolarizing current injections and elicits rebound spike activity when the hyperpolarizing current injection is released (Kabotyanski et al., 2000). In principle, changes in the excitability of B4 or its synaptic connections to B51 or B8, or changes in the B8 sag potential could have strong effects on B8 activity during BMPs.

### 1.1.3 Neuron B51

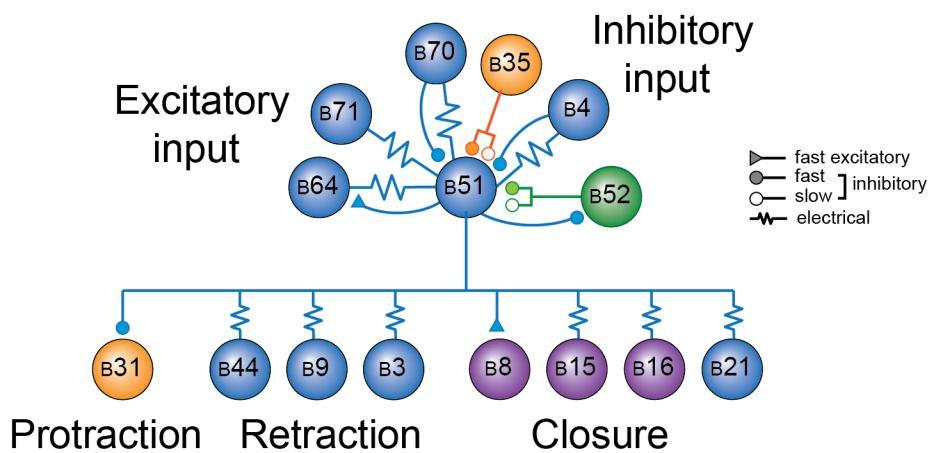
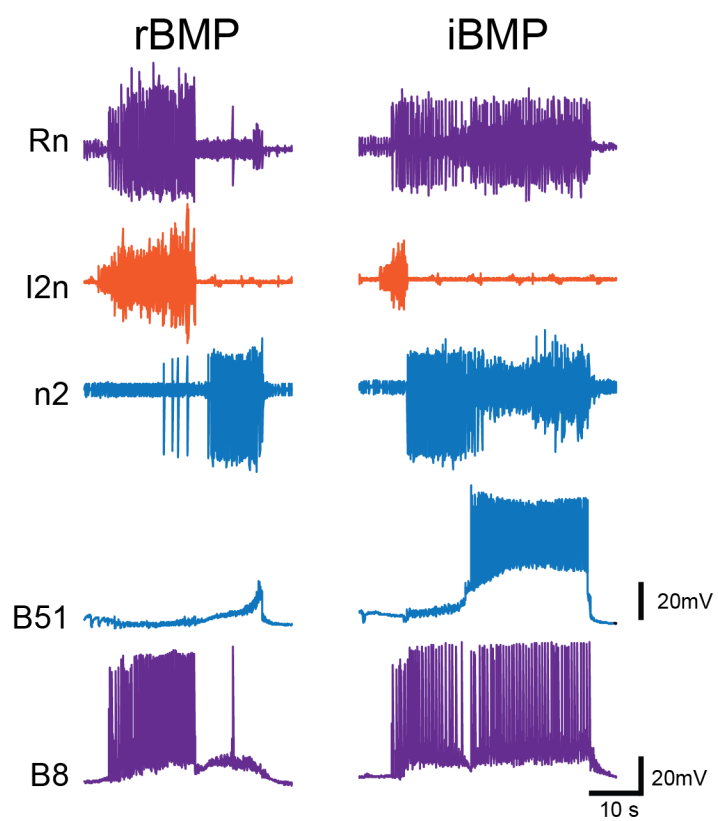
B51 is one of only two identified retraction neurons that activate neuron B8 during retraction. B51 was first characterized by Plummer and Kirk (1990) and its excitatory input to B8 was characterized by Evans and colleagues (Evans et al., 1998).

The most notable feature of B51 is its pronounced intrinsic  $\text{Ca}^{2+}$ -independent plateau potential (Fig. 1.4) which can be generated by a BMP or initiated by a depolarizing current injection in ganglia and when isolated in cell culture (Lorenzetti et al., 2008; Mozzachiodi et al., 2008; Nargeot et al., 1999a,b; Plummer and Kirk, 1990). To date, no chemical excitatory input has been found for B51. It appears that B51 is activated during a BMP by a combination of proprioceptive input from the radula surface and electrical coupling from retraction neurons. Indeed, distension of the radula tissue or activation of radula closure neurons B8 or B44 elicits spike activity of B51 (Evans et al., 1998). Increasing the resistance to backward rotation of the radula increases B51 activity during retraction (Evans et al., 1998). B51 provides chemical excitatory and electrical synaptic input to B64, another plateau generating neuron which maintains the retraction phase, as well as an inhibitory connection to B52, a BMP terminating neuron. The excitatory connection of B51-to-B64 and inhibitory connection of B51-to-B52 would extend the retraction phase. B51 also is electrically coupled to retraction motor neurons. Therefore, B51 activity would also increase the force of the retraction movement. For example, a large piece of food requiring a greater retraction force would increase proprioceptive input to B51 which would extend retraction, increase the retraction force, and increase the force of radula closure via its excitatory input to B8. OC increases the excitability of B51, which would increase the likelihood of eliciting a plateau potential during a BMP (more details provided in Section 1.4). These properties make B51 a crucial neuron for mediating ingestion behaviors (specifically swallowing) in order to bring food into the animal. What remains unclear is whether chemical synapses to and from B51 are altered by learning.



**Figure 1.3** Synaptic connections and activity of B51.

**A**, Diagram of the synaptic connections of B51. B64 and B71 drive B51 activity. B4 and other neurons suppress B51 activity. B51 extends retraction by activating B64 and inhibiting B52. B51 also activates B8 and retraction neurons. **B**, Representative recordings of B51 during an rBMP and iBMP. Note the pronounced plateau potential in B51 during iBMPs.

**A.****B.**

## 1.2 Neuron identification

In invertebrates, neurons are traditionally identified by size, position, axonal projections and activity during motor patterns or by synaptic connections (Gardner, 1977; Gardner and Kandel, 1971, 1973, 1977). In addition, active membrane properties (e.g., plateau potential in B51) or input/output excitability curves can be used (e.g., B52) (Plummer and Kirk, 1990). However, information pertaining to the synaptic connections, active membrane properties or excitability curves is often unavailable during voltage-sensitive dye (VSD) imaging.

Identifying neurons in optical recordings of invertebrates has been attempted by William Kristan and colleagues (Frady et al., 2016; Kapoor et al., 2015). This method involved building a medium-dimensional feature space of the properties of neurons, then using semi-supervised machine learning to build an atlas of neurons of the leech midbody ganglia. This atlas was built by first locating neurons which can be identified with certainty, then identifying the remaining neurons by their activity and relative position to the first set of neurons (Frady et al., 2016; Kapoor et al., 2015). Neuron identification methods would greatly benefit VSD recordings of *Aplysia*, however no attempts have been made to identify neurons in optical recordings of *Aplysia*.

## 1.3 Voltage-sensitive dye (VSD) imaging

Voltage-sensitive dye imaging has emerged as an important tool for recording neuronal activity because it can record from many neurons simultaneously. The first optical imaging of membrane potential changes of neurons was achieved in the 1950's where the light scattering of nerves were used to measure the waveform of an action

potential (for review see Cohen, 2010). The first study that used dyes to record membrane potentials was Tasaki et al. (1968). During the next several years, studies found that certain dyes change their absorbance during membrane depolarizations (Davila et al., 1974; Cohen et al., 1974; Ross et al., 1974, 1977). Afterwards, the voltage sensitivities of dyes were systematically investigated in search of improved dyes that signaled changes in membrane potential by either changes in light absorbance or changes in fluorescence (e.g., Bashford 1981; Fromherz and Müller 1993; Grinvald et al., 1989). Of these dyes, RH-155 has proven to be effective especially in recording neuronal activity in invertebrate nervous tissues (Bruno et al., 2015; London et al., 1987; Hill et al., 2010, 2012) and also in the mammalian brain (Zhang et al., 2010). The mechanism underlying the changes in optical properties varies between dyes. Although the mechanism has not been investigated specifically for RH-155, voltage sensing of this dye likely involves the a movement of the charge distribution of the dye from the extracellular surface of the cell membrane to the center of the cell membrane during membrane depolarization (Waggoner et al., 1977). RH-155 has been used to detect neuronal activity in the buccal ganglia of *Nanavax* and in recordings of the *Aplysia* abdominal ganglia (London et al., 1987; Zečević et al., 1989). Morton et al. used another absorbance dye JPW 1124 to record activity in the buccal ganglia of *Aplysia*. These results illustrate that VSD has enormous potential to provide novel insight into the *Aplysia* feeding network and its modification by DA and DA-dependent forms of learning and memory.

## 1.4 Dopamine (DA)

### 1.4.1 DA in animal behavior

DA is a ubiquitous neuromodulator in the animal kingdom and is well known to be an important signaling molecule in motor behavior (e.g., Schultz et al., 2013; Wise, 2004). In mammals, the majority of dopamine is released by a small population of neurons located in the ventral tegmental area (VTA) and the substantia nigra (SN) which send diffuse projections to the cortex and striatum. Single neuron recording of rodents and primates have indicated that dopamine signaling from the VTA and SN mediates reward and aversive prediction error (Schultz, 1997, 2016) and differentially modulates medium spiny neurons expressing either dopamine D1 or D2 receptors (Soares-Cunha et.al., 2016). In addition to reward prediction error, the neurons within the SN are important for initiating motor movements. The devastating deficits in voluntary motor behavior in Parkinson's disease serves as a potent example of the importance of these neurons in motor behavior (for review Goetz, 2011). Thus, in mammals DA mediates initiation of voluntary motor behavior and encodes information about rewards.

For *Aplysia* feeding behavior, BMPs are initiated by a small number of DA neurons located within the buccal ganglia while rewarding stimuli are encoded by the DAergic nerve En2. Blocking DA transmission by the DA receptor inhibitor methylergonovine suppresses the generation and reinforcement of BMPs by OC (Nargeot et al., 1999c). The DA neurons within the buccal ganglia include B20, B65 and an unidentified unilateral neuron. B20 and B65 are active during the protraction phase and are both able to initiate BMPs (Jing and Weiss, 2001; Kabotyanski et al.,

1998; Rosen et al., 1991; Teyke et al., 1993). B20 biases the feeding CPG towards rBMPs through its excitatory input to B8 and B4, while B65 biases the feeding CPG towards iBMPs through a slow EPSP to B8 (Jing and Weiss, 2001; Kabotyanski et al., 1998). En2 projects diffusely across the ganglia. For example, En2 stimulation elicits a fast EPSP in B4, a slow EPSP in B20 and B65, a slow IPSP in B40, and a combined fast IPSP and slow EPSP in B51, B52, and B64 (Nargeot et al., 1999c).

#### **1.4.2 L-DOPA and the synthesis of DA**

DA is a catecholamine neurotransmitter that is synthesized in the nerve terminal. The synthesis of DA begins with the conversion of L-tyrosine to the precursor L-3,4-dihydroxyphenylalanine (L-DOPA) by tyrosine hydroxylase using the coenzyme tetrahydrobiopterin and diatomic oxygen (Daubner et al., 2011). Tyrosine hydroxylase is the rate limiting enzyme for DA biosynthesis and is regulated by phosphorylation and feedback inhibition from DA (Daubner et al., 2011; Levitt et al., 1965). L-DOPA is then rapidly converted to DA by L-aromatic amino acid decarboxylase (AADC) using the coenzyme pyridoxal 5'-phosphate (Bertoldi, 2014). After synthesis, DA is packaged into synaptic vesicles via VMAT-2 (German et al., 2015), released via exocytosis, and taken back up into the presynaptic terminal by the dopamine transporter (Nirenberg et al., 1996). The rate at which AADC synthesizes dopamine is limited by the availability of L-DOPA. Thus, tyrosine hydroxylase tightly regulates the synthesis of DA. To bypass the regulation of tyrosine hydroxylase, L-DOPA can be exogenously added. The strong effect of L-DOPA supplementation was discovered by the pioneering efforts of Arvid Carlsson, Oleh Hornykeiwicz, and Walter Birkmayer. Carlsson found that reserpine induced Parkinsonian symptoms (e.g.,

decrease in behavior) by depletion of catecholamine neurotransmitters and these symptoms were rapidly ameliorated (within 15 minutes) by L-DOPA supplementation (for reviews see Abbott, 2010; Carlsson, 2001). Noradrenaline remained depleted when L-DOPA was administered to reserpine treated animals. However, DA levels were increased in reserpine treated animals and the increase in DA closely matched the time course of the increase behavior (Carlsson, 2001). His results were famously rejected by mainstream science but gained support after Oleh Hornykeiwicz and Walter Birkmayer demonstrated that L-DOPA reversed the effects of Parkinson's disease in 20 patients for a few hours (Abbot, 2010). The use of L-DOPA to treat Parkinson's disease was approved in 1970. The national center for bioinformatics (NCBI) protein database includes predicted proteins within the *Aplysia californica* genome that are homologous to tyrosine hydroxylase, AADC, and VMAT-2 indicating that the synthesis and transport of dopamine is conserved in *Aplysia*. Indeed, application of L-DOPA to isolated buccal ganglia of *Aplysia* enhances motor pattern activity possibly by increasing the release of DA (Kabotyanski et al., 1998, 2000).

### **1.4.3 Effects of DA on mammalian neurons**

#### ***1.4.3.1 Effect of DA on intrinsic excitability***

This section reviews the effects of DA application on mammalian inhibitory and cholinergic neurons in the striatum when these neurons were held near resting potential. The focus is restricted to striatal neurons because these neurons have been implicated in OC (e.g. Reynolds and Wickens, 2002). See Section 1.5.3-4 for a review on OC-induced changes in the biophysical properties of neurons. DA does not affect resting membrane potential or input resistance of medium spiny neurons (MSNs)

(Tritsch and Sabatini, 2012). DA increases the excitability of D1-expressing MSNs by prolonging and increasing the spike frequency of the “up” state. D1 receptor activation increases inward rectifying  $K^+$  current ( $K_{ir}$ ), decreases A-type  $K^+$  current ( $K_A$ ), increases L-type  $Ca^{2+}$  current, and decreases P/Q and N-type  $Ca^{2+}$  currents and voltage-gated  $Na^+$  current (Gerfen and Surmeier, 2011; Hernández-López et al., 1997; Pacheco-Cano et al., 1996; Schiffmann et al., 1995; Surmeier et al., 1995, 2007). Although some of these changes would theoretically decrease excitability of the neuron ( $\uparrow K_{ir}$  and  $\downarrow Na_v$ ), the combination of all of these changes has a net excitatory effect on D1 expressing MSNs (Gerfen and Surmeier, 2011; Tritsch and Sabatini, 2014; Surmeier et al., 2007). On the other hand, D2 receptor activation results in a net decrease in excitability of MSNs by decreasing  $K_{ir}$ , reducing L-type and R-type  $Ca^{2+}$  current, and enhancing depolarization-activated and ATP-sensitive  $K^+$  currents (Hernández-López et al., 2000; Higley and Sabatini, 2010; Sun et al., 2000).

In addition to MSNs, DA also modulates the excitability of striatal interneurons. DA activation of D1 receptors transiently depolarizes fast low threshold spiking (LTS) neurons which inhibit a wide range of MSNs (Centonze et al., 2002). DA activation of D5 receptors transiently depolarizes fast spiking (FS) neurons which inhibit D1 expressing MSNs (Bracci et al., 2002; Centonze et al., 2003). These transient depolarizations last only a few seconds after application of DA or DA receptor agonists. For Cholinergic neurons (a.k.a. tonically active neurons, TANs), reward predicting stimuli elicit a burst-pause-burst sequence of activity (Apicella 2007; Goldberg and Reynolds, 2011; Wieland et al., 2014). The pause in activity is D2-dependent and mediated by an increase in  $Na^+$  inactivation and decrease in rebound



excitation (Maurice et al., 2004; Wieland et al., 2014). The late burst of activity is D1 receptor dependent (Aosaki et al., 1998; Wieland et al., 2014).

#### *1.4.3.2 Effect of DA on synaptic connections*

This section reviews the effects of DA application on synaptic connections within the striatum when these neurons are held near resting potential. DA differentially affects the presynaptic release and postsynaptic PSP response (for review see Tritsch and Sabatini, 2012). DA primarily decreases neurotransmitter release in the striatum (Tritsch and Sabatini, 2012). This includes DA-induced decrease of release at the glutamatergic cortical synapses onto MSN (Bamford et al., 2004; Higley and Sabitini, 2010; Wang et al., 2012), the GABAergic synapse onto MSN (Delgado et al., 2000; Kohnomi et al., 2012), the GABAergic synapses between MSNs (Guzmán et al., 2003; Taverna et al., 2005; Tecuapetla et al., 2009), GABAergic but not glutamatergic synapses onto fast spiking (FS) interneurons (Bracci et al., 2002; Centonze et al., 2003) and GABAergic and cholinergic inputs to tonically active neurons (TANs) (Centronze et al., 2003; Momiyama et al., 2001; Pisani et al., 2000). Notable exceptions include mixed responses to D2 agonist on FS GABAergic synapses onto MSNs (Kohnomi et al., 2012) and enhancement of GABAergic synapses between MSNs by D1 receptor agonist (Guzmán et al., 2003). In one study, D1 agonist increased spontaneous release at the glutamatergic corticostriatal synapse whereas D2 agonist decreased spontaneous release (André et al., 2010). The DA-induced decrease in neurotransmitter release seems to be primarily mediated by activation of G-protein  $\beta\gamma$  signaling, which inhibits  $\text{Ca}^{2+}$  channels that mediate neurotransmitter release (P/Q-type and N-type) (Surmeier et al., 1995; Tritsch and

Sabatini, 2012; Yan et al., 1997; Simms and Zamponi, 2014). Other signaling cascades are likely involved. For example, endocannabinoid trans-synaptic signaling plays a role in modulating presynaptic release of the corticostriatal synapse (André et al., 2010).

The effect of DA on the postsynaptic neurotransmitter receptors is complex. D1 or D2 receptor activation leads primarily to an increase or decrease in postsynaptic receptor activation respectively (Tritsch and Sabatini, 2012). D1 receptor activation enhances response to NMDA and AMPA receptor agonists in dissociated striatal neurons whereas D2 receptor activation decreases response to NMDA and AMPA receptor agonist in dissociated MSNs (André et al., 2010; Flores-Hernández et al., 2002; Jocoy et al., 2011). D1 receptors facilitate AMPA receptors by activating PKA-mediated S845 phosphorylation of these receptors, and also by suppressing PP1 *via* activation of DARPP-32 (Snyder et al., 2000). On the other hand, D2 receptors inhibit PKA-mediated S845 phosphorylation of AMPA receptors, enhance PP1 activity, and decrease DARPP-32 activity (Håkansson et al., 2006). AMPA S845 phosphorylation increases channel open probability and is likely involved in DA-induced increases in surface expression (Shepherd and Huganir, 2007; Sun et al., 2008). However, it should be noted that changes in synaptically localized NMDA and AMPA receptors have yet to be observed (Higley and Sabatini, 2010; Tritsch and Sabatini, 2012). Despite the differential regulation of neurotransmitter release and postsynaptic response, the net effect of DA is generally to decrease synaptic efficacy (e.g., Bamford et al., 2004; Higley and Sabatini, 2010; Wang et al., 2012). For inhibitory synapses, D1 agonist decreases GABA<sub>A</sub> responses to GABA in dissociated MSNs and in TANs

in a PKA-dependent manner (Flores-Hernández et al., 2002; Yan and Surmeier, 1997). However, the amplitude of spontaneous IPSCs was not affected indicating that the decrease in inhibitory synaptic connections is primarily mediated by a decrease in presynaptic release (Centonze et al., 2003; Delgado et al., 2000).

#### **1.4.4 Effects of L-DOPA and DA on the feeding CPG**

As mentioned earlier, DA plays an important role in feeding behavior of *Aplysia*. Application of L-DOPA (250  $\mu$ M), DA (50  $\mu$ M) and 5-HT (5  $\mu$ M) to buccal ganglia in a semi-intact preparation increased the number of ingestion behaviors as well as the total number of feeding behaviors. L-DOPA and DA increased mainly bite behaviors whereas 5-HT increased mainly swallow behaviors (Kabotyanski et al., 2000). DA also increased the number of iBMPs (presumably bites) in isolated buccal ganglia whereas 5-HT tended to decrease BMPs. DA decreased the excitability of neurons B4, B34, and B51 and their activity during BMPs (Kabotyanski et al., 2000). Neurons B4 and B34 bias the CPG towards rejections whereas B51 bias the CPG towards swallows (Jing and Wiess, 2001). DA also appeared to decrease B63 excitability and the strength of the B4-to-B8 inhibitory and the B64-to-B4 excitatory synapse, which would decrease B4 activation disinhibiting B8 and biasing the CPG towards iBMPs (Kabotyanski et al., 2000). In addition, DA enhanced the B64-to-B31/32 and the strength of the B64-to-B34 inhibitory synapse which may increase the number of BMPs by reducing the duration of the protraction phase (Kabotyanski et al., 2000). DA also increased the rebound excitation of B8 which may help to excite this neuron during retraction (see Section 2.3.8.2). Similar results were obtained with L-DOPA, which decreased the excitability of B4, B34, and B65 and enhanced the strength of

synaptic connections from B64 and B31/32 while decreasing the strength of the B64-to-B4 synaptic connection (Kabotyanski et al., 2000). These data highlight the strong effect L-DOPA and DA has on the feeding CPG. Several questions still remain unanswered. For example, how are these cellular changes manifested in circuit-wide activity? Are there consistent changes to the activity of protraction or retraction neurons? Are the changes induced by L-DOPA similar to those induced by DA-dependent forms of learning like OC? What are the physiological consequences of some of these changes?

## **1.5 Operant conditioning (OC)**

### **1.5.1 Overview**

Operant conditioning (OC) is when an animal learns the consequences of its behavior (Thorndike, 1911; Skinner, 1938). Traditionally, OC refers to the increased or decreased expression of a learned behavior when a contingency is formed between the behavior and a salient stimuli (e.g. lever press is paired with food or the emetic lithium chloride). In this thesis, OC is operationally defined as an increase in a specific behavior (i.e., ingestion) in an animal that receives rewards contingent with that specific behavior.

The study of OC began with Edward Lee Thorndike who used “puzzle boxes” to investigate the ways in which animals acquire behavior (Thorndike, 1911; for review see Leahey, 2000). Thorndike avoided the prevailing method of inferring thought processes or intentions underlying behavior, but rather considered an animal’s behavior as acts of trial and error. Behaviors which resulted in reward were repeated. This was Thorndike’s law of effect which he stated, “Of several responses made to

the same situation, those which are accompanied or closely followed by satisfaction to the animal will, other things being equal, be more firmly connected with the situation, so that, when it [the situation] occurs they [the responses] will be more likely to recur (Thorndike, 1911)."

B.F. Skinner created a more simplified learning paradigm now called the Skinner box to reinforce (increase the expression of) lever pressing (Skinner, 1938). This widely used technique has been adapted to a variety of training protocols (for review see Staddon and Cerutti, 2003). The main advantage of the Skinner box was that it allowed for the "free operant" procedure. In the free operant procedure, the animal is free to respond as many times as the animal desires. This allowed the experimenter to estimate the level of learning by a simple metric: the number of lever presses (i.e., the operant) (Skinner, 1938). The Skinner box also allowed for independent variables to be manipulated such as the schedule of reinforcement. The simplest schedule of reinforcement which has the closest resemblance to the training used in Chapter 2 is the continuous reinforcement schedule where an animal receives a reward after each behavior or operant. This schedule was chosen to study OC in *Aplysia* because of its simplicity. The use of Skinner boxes and advancements of electrophysiological techniques have allowed for the neuronal substrates of OC to be investigated.

### **1.5.2 Neuronal substrates of OC**

In this dissertation, neuronal substrates refer to neuronal activity that encode learning and neuronal correlates refer to the OC-changes in the properties of neurons. A major advancement in elucidating the neuronal substrates of OC was from the

experiments of Wolfram Schultz (Schultz et al., 1986, 1993). In these experiments, a monkey was given a reward if it pressed a key in response to light. Schultz found that before training the reward activated DA neurons but the light did not. However, after training the light activated DA neurons but the reward did not (Schultz et al., 1993). These results were clarified by the theoretical work of Sutton and Barto who developed a modified version of the Rescorla-Wagner learning algorithm to infer the learning mechanisms of Pavlovian and OC (for review Niv, 2009). Sutton and Barto's model used reward prediction error estimates to approach the behavior that yielded the greatest reward. In brief, the model compares the reward obtained with the reward that was expected. Behaviors associated with a reward were reinforced whereas behaviors not associated with a reward were suppressed (Barto, 1994). It was suggested that DA neurons could be encoding reward prediction error because they are activated when the reward is greater than expected. So, in the beginning of training, DA neurons are activated by the reward because it is unexpected but by the end of training DA neurons are not activated by the reward because it is predicted by the light (Schultz, 1997). The downstream effects of DA neurons are discussed in Section 1.4.3. The major difference between the OC model used in this dissertation and *in vivo* OC models is that the DA neurons will be activated directly rather than indirectly through a reward.

### **1.5.3 Neuronal correlates of OC in mammals**

Investigations of the mechanisms underlying OC in mammals have focused on the effects of DA on the excitability and synaptic efficacy of striatal neurons (see Section 1.4.3). However, only a few studies have examined OC-induced changes in

excitability or synaptic efficacy of neurons. These studies have examined the effect of lever pressing for reward on the corticostriatal synapse (see review Reynolds and Wickens, 2002) and excitatory input to the VTA (Chen et al., 2008), effect of olfactory learning on the pyramidal neurons of the piriform cortex (Lebel et al., 2001; Quinlan et al., 2004; Saar et al., 1999, 2002), the effect of spatial discrimination task on the dentate gyrus (Uzakov et al., 2005), and the effect of motor skill learning on intracortical connections in the M1 motor cortex (Rioult-Pedotti et al., 1998).

Intracranial self-stimulation of the DAergic SN potentiates the corticostriatal synapse *in vivo* in a D1-receptor dependent manner (Reynolds et al., 2001; Reynolds and Wickens, 2002). The corticostriatal synapse was also potentiated in a cellular model of OC where high-frequency stimulation (HFS) of cortical neurons and MSN depolarization was paired with DA application (Wickens et al., 1996; Reynolds and Wickens, 2000). HFS of cortical neurons when the MSN is held at resting potential requires  $Mg^{2+}$ -free solution (Calabresi et al., 1992; Kerr and Wickens, 2001). NMDA receptors are blocked by  $Mg^{2+}$  at resting potentials, but this blockade is removed in depolarized conditions (Nowak et al., 1984). The  $Mg^{2+}$ -free solution is presumably required to remove the  $Mg^{2+}$  block of NMDA receptors highlighting the need for both presynaptic activity and postsynaptic depolarization to potentiate the corticostriatal synapse (Reynolds and Wickens, 2002). Sucrose and food reinforcement of lever presses increased the AMPA/NMDA receptor ratio and increased the spontaneous EPSP frequency onto VTA DA neurons (Chen et al., 2008). Therefore, lever pressing for reward seems to increase synaptic efficacy to the striatum and VTA.

Olfactory discrimination task increases the NR2a/NR2b ratio and suppresses LTP and paired-pulse facilitation (PPF) while enhancing LTD in the piriform cortex (Lebel et al., 2001; Quinlan et al., 2004; Saar et al., 1999). Olfactory learning also decreased the stimulation intensity of intrinsic fibers necessary to elicit a PSP in layer Ib pyramidal neurons of the piriform cortex (Saar, 2002). Therefore, olfactory learning decreases synaptic plasticity and possibly neuronal excitability in the piriform cortex. Motor skill learning increased the strength of horizontal connections in layer II/III of the motor cortex (Riout-Pedotti et al., 1998). Motor skill learning increased the activity of the majority of striatal and cortical neurons (Costa et al., 2004). However, it is unclear whether the striatal neurons are D1 or D2 MSNs or whether these changes are upstream or intrinsic to the recorded neurons. Lastly, holeboard training where the animal learns the pattern of baited holes enhances LTP in the dentate gyrus (Uzakov et al., 2005). Therefore, much more work remains to elucidate the neuronal correlates of OC in mammals. For example, does OC modulate the excitability or synaptic connections of inhibitory or cholinergic neurons in the striatum? These gaps in knowledge can be answered by investigating the connections of a cholinergic neuron in a more simple system such as B4 in *Aplysia*.

#### **1.5.4 Neuronal correlates of OC in *Aplysia* feeding.**

When *Aplysia* ingestion behavior is paired with seaweed extract the animal increases the frequency of ingestion behaviors (Nargeot et al., 2007). After ingestion, food traveling through the esophagus causes distention of the esophageal tissue which activates sensory neurons located within the esophageal tissue (Martínez-Rubio et al., 2009). These sensory neurons send dopaminergic afferents which



project (*via* the esophageal nerve) diffusely across the buccal ganglia. In an *in vitro* OC protocol, stimulation of the esophageal nerve (En2) contingent with the occurrence of an iBMP reinforces this pattern in a DA-dependent manner (Nargeot et al., 1997, 1999a,b,c, 2001, 2009; Bédécarrats et al., 2013). This increase in iBMPs was correlated with an increase in the input resistance and decrease in the burst threshold of neuron B51 which persisted for at least 24 h (Mozzachiodi et al., 2008; Nargeot et al., 1999a) and increased the input resistance, firing threshold, and electrical coupling of the pattern initiating neurons B30, B63, and B65 (Seiling et al., 2014). In a single-cell analogue of B51 OC, pairing B51 stimulation with En2 stimulation in ganglia or with iontophoretic application of DA in culture also increased the input resistance and decreased the burst threshold of B51, indicating that these changes were intrinsic to B51 (Brembs et al., 2002; Nargeot et al., 1999b; Lorenzetti et al., 2008). The single-cell OC analogue in culture allowed the biochemical signaling cascade to be investigated in detail. Stimulation of B51 induced the influx of  $\text{Ca}^{2+}$ , which activated a  $\text{Ca}^{2+}$ -dependent protein kinase C, while DA application activated a G-protein second messenger. These two cascades converged onto adenylyl cyclase to produce cyclic adenosine monophosphate (cAMP) which then activated protein kinase A (Lorenzetti et al., 2008). Many questions remain unanswered. For example, what effect does OC have on the excitability of inhibitory neurons which suppress the expression of iBMPs? Also, what effect does OC have on chemical synaptic connections? Chapter 2 investigates these two questions.

## **Chapter 2: Operant conditioning (OC) modifies the synaptic and intrinsic properties of neurons within the feeding CPG.**

### **2.1 Rationale and Hypothesis**

As mentioned earlier, OC is widely expressed in the animal kingdom (Byrne, 1987; Kelley, 2004). Rhythmic movements during feeding in *Aplysia* are mediated by a CPG, which is an advantageous model system for investigating the mechanisms underlying OC (Nargeot et al., 1997, 1999a,b,c; Brembs et al., 2002; Mozzachiodi et al. 2008). The CPG is multifunctional and mediates at least two mutually exclusive behaviors; ingestion and rejection. *In vivo* ingestion is reinforced by the presentation of food or stimuli that mimic food contingent with ingestion behavior (Brembs et al., 2002; Nargeot et al., 2007). *In vitro* the neural activity that mediates ingestion (ingestion-like buccal motor patterns, iBMPs) can be modified by an analog of OC (Nargeot et al., 1997). Because the cells and synaptic connections within the CPG are well characterized and amenable to detailed cellular analyses (for reviews see Elliott and Susswein, 2002; Cropper et al., 2004; Baxter and Byrne, 2006), the neural circuitry that mediates feeding is a useful model to identify loci and mechanisms of learning-induced plasticity underlying operant conditioning.

Previously identified neuronal correlates of the conditioning include increases in the excitability of B30, B63 and B65, which are involved in initiating BMPs (Nargeot et al., 2009), and B51, which is involved in the specific selection of iBMPs (Nargeot et al., 1999a,b; Lorenzetti et al., 2006, 2008; Mozzachiodi et al., 2008). Given the learning-induced increased excitability of a neuron (B51) that promotes the reinforced

behavior, we hypothesized that a complementary decrease in excitability and strength of inhibitory synaptic connections might be present in neurons that suppress iBMPs. Therefore, we examined the excitability and synaptic connection of B4, a neuron that suppresses iBMPs, in part, by its inhibitory synaptic connections to B8 and B51(Fig. 2.1) (Plummer and Kirk, 1990; Kabotyanski et al., 1998; Sasaki et al., 2009; Dacks et al., 2012). In addition, we examined whether the B51-to-B8 excitatory synaptic connection or B8 intrinsic excitability was modified by OC.

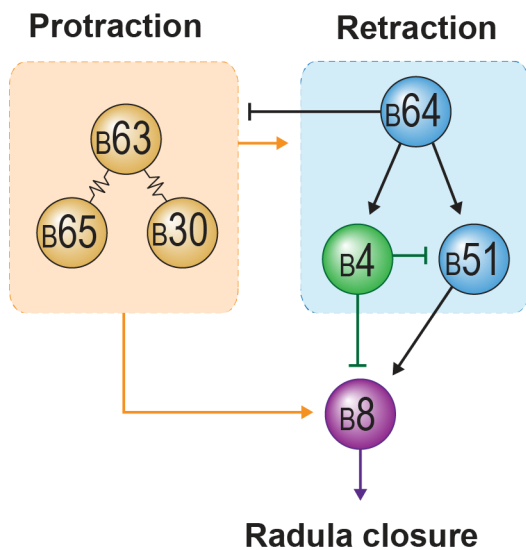


**Figure 2.1** A subset of synaptic connections of the feeding CPG

Simplified schematic of the feeding CPG. Activity in some neurons (e.g., B30, B63, B65) underlies protraction (orange), whereas activity in other neurons (e.g., B64) underlies retraction (blue). B51 plays a role in the expression of iBMPs through its excitatory connection to B8. Conversely, B4 inhibits B51 and B8. Thus, the level of activity in B4 plays a role in the expression of iBMPs. Arrows indicate excitation whereas bars indicate inhibition.

We found that the *in vitro* analog of operant conditioning decreased B4 but did not modify B8 excitability. The decrease in B4 excitability was recapitulated in a single-cell analog of operant conditioning in which B4 activity was paired with DA iontophoresis or esophageal nerve stimulation. We also found that operant conditioning reduced the strength of the inhibitory synaptic connection from B4-to-B51, tended to increase the B4-to-B8 connection relative to yoke control, but did not modify the B51-to-B8 synaptic connection. Inserting these changes into a computational model of the feeding CPG indicated that either the increase in B4 excitability alone or decrease in B4-to-B51 alone are sufficient to induce a strong bias towards iBMPs. These results indicate that contingent reinforcement of iBMPs reduced the intrinsic excitability of a neuron and modified its synaptic connections to relieve suppression of the reinforced behavior.

## 2.2 Methods

### 2.2.1 Preparation

*Aplysia californica* (120-210g) were obtained from Alacrity Marine Biological Specimens (Redondo Beach, CA) and Marinus (Westchester, CA). Animals were housed individually in perforated plastic cages in aerated seawater tanks at a temperature of 15 °C. Animals were fed ~1 g of dried seaweed three times per week. Two distinct but complementary approaches were used in this study: 1) an *in vitro* analog of operant conditioning in isolated preparations of buccal ganglia dissected from naïve animals, 2) a single-cell analog of operant conditioning in cell culture with neurons isolated from buccal ganglia of naïve animals.

### 2.2.2 Classification of BMPs

Both ingestion and rejection consist of two phases that involve an outward (protraction) and inward movement (retraction) of the radula, a grooved tongue-like structure. Radula closure during the retraction phase is a distinguishing feature of ingestion behavior. Feeding behavior is controlled by a CPG within the buccal ganglia, which continues to produce patterned motor activity in isolated ganglia. These buccal motor patterns (BMPs) were monitored *in vitro* by extracellular nerve recordings of I2 n. and n.2,1 and intracellular recording from radula closer motor neuron B8 (Fig. 1A). As in our previous studies (Nargeot et al., 1997), fictive protraction was monitored as activity in I2 n., and fictive retraction was monitored as large-unit activity in n.2,1. Large unit activity in n2,1 is spike activity with an amplitude greater than spike activity during protraction. Activity in B8 served as a measure of radula closure. Patterns with >50% of the total duration of closer motor neuron activity occurring during retraction were classified as iBMPs (Nargeot et al., 1997, 1999a,b,c; Brembs et al., 2002; Mozzachiodi et al., 2008). For simplicity, patterns that did not fit the criteria for iBMPs were grouped into a general category of 'other' BMPs.

### 2.2.3 *In vitro* analog of operant conditioning

To ensure all animals were at the same motivational state, animals were food-deprived for 3-5 d before the experiment and fed a piece of seaweed 45 min and immediately before dissection, at which time animals were anesthetized by isotonic MgCl<sub>2</sub> with a volume in ml equal to half the animal's body mass in mg (Brembs et al., 2004). The protocol for the *in vitro* analog of operant conditioning has been described previously (Nargeot et al., 1999a). Briefly, the buccal ganglia were isolated and

pinned out in a Sylgard-coated Petri dish containing artificial seawater (ASW). The left hemi-ganglion was desheathed on the rostral side in presence of high divalent cation ASW. The composition of the ASW and high divalent cation ASW solution have been described previously (Nargeot et al., 1997). The ASW was then exchanged for normal ASW which was maintained at 13-15°C by means of a Peltier cooling device for the remainder of the experiment. Neural activity was monitored via extra- and intra-cellular recordings (see above).

First, pre-test measurements of input resistance ( $R_{in}$ ), spike threshold and excitability were made following a 10 min rest period after the beginning of intracellular recordings. Then, sustained rhythmic BMP activity was elicited by continuous low-frequency stimulation of nerve n.2,3 (7 V, 0.5 ms, 4 Hz). A 10 min training period was initiated with the first occurrence of an iBMP. Immediately following training, n.2,3 stimulation was paused briefly while the post-test  $R_{in}$ , threshold, and excitability were measured. Then, n.2,3 stimulation resumed for 20 min during which time the effect of training on BMP expression was assessed (post-test). The En.2 nerve contains dopaminergic afferents to the buccal ganglia (Kabotyanski et al., 1998; Martinez-Rubio et al., 2006). Stimulation of En.2 (7 V, 0.5 ms, 10 Hz for 6 s) served as reinforcement (Nargeot et al., 1997, 1999a,c). This study included two groups: a contingent group that received En.2 stimulation immediately following the expression of iBMPs and a yoke control group that received En.2 stimulation that was uncorrelated to pattern expression. The experiments were done sequentially with a yoke experiment following each contingent experiment. The sequence of En.2

stimulation of each contingent preparation served as the template for the sequence of En.2 stimulation for its corresponding yoke preparation.

#### **2.2.4 Cell identification**

Neurons were identified by their relative size, location, and physiological characteristics. For example, B51 was identified based on its characteristic plateau potential (Plummer and Kirk, 1990) and excitatory synaptic connection to B8 (Evans et al., 1998); B8 was identified by its axonal projections in the radular nerve (Nargeot et al., 1997); and B4 by its inhibitory inputs to B8 (Rosen et al. 2000) and B51 (Plummer and Kirk, 1990).

#### **2.2.5 Testing B4 properties in ganglia**

Conventional two-electrode intracellular recording and current-clamp techniques were performed with an Axoclamp-2A (Molecular Devices, Sunnyvale, CA) and fine-tipped glass microelectrodes (resistance 10-15 M $\Omega$ ) filled with 2 M potassium acetate.  $R_{in}$  was measured by injecting a -3 nA, 5 s current. The threshold of B4 was measured by injecting depolarizing current pulses (5-s duration) that increased by 0.5 nA increments until a single action potential was elicited. The lowest current intensity necessary to elicit an action potential was considered as the threshold. The excitability of B4 was measured as the number of spikes elicited during 4 and 6 nA (5-s duration) depolarizing current injections. The intrinsic properties of B4 were measured in the absence of n2,3 stimulation. While measuring the intrinsic properties of B4 in either *in vitro* or in cell culture preparations, the membrane potential was held at -70 mV, which was slightly more negative than the average resting potential ( $-63 \pm 0.7$  mV) of B4 in ganglia. For IPSP measurements, B4 and B51 were current clamped



to -70 mV. A rest period of at least 4 min preceded the measurements of IPSPs before and after training.

### 2.2.6 Cell culture

Culturing procedures for B4 followed those described in Brembs et al. (2002) and Lorenzetti et al. (2008). Briefly, ganglia from adult *Aplysia* were treated with Dispase® II (10 units/ml) (neutral protease, grade II) (Roche, Indianapolis, IL) at 35°C for ~3 h and then desheathed. Fine-tipped glass microelectrodes were used to remove individual B4s from the ganglia. Each cell was plated on poly-L-lysine coated petri dishes with culture medium containing 50% hemolymph, 50% isotonic L15 (Invitrogen, Carlsbad, CA). L15 was adjusted with 350 mM NaCl, 25 mM MgSO<sub>4</sub>, 11.4 mM CaCl<sub>2</sub>, 29 mM MgCl<sub>2</sub>, 10 mM KCl, streptomycin sulfate (0.10 mg/mL), penicillin-G (0.06 mg/mL), dextrose (mg/mL) and 15mM Hepes. The pH of the culture medium was adjusted to 7.5. Cells were allowed to grow for 4-5 days. Prior to recording, the culture medium was exchanged for a solution containing 50% ASW and 50% isotonic L15.

### 2.2.7 Single-cell analog

The procedures for the single-cell analog were similar to those established previously (Brembs et al., 2002; Lorenzetti et al., 2008). The intensity of the depolarizing current injection into B4 during training was adjusted for each cell to match the level of activity (2.5 - 5 Hz) during a typical iBMP (Sasaki et al. 2012). Cells in culture had a higher  $R_{in}$  and lower firing threshold ( $R_{in} = 8.1 \pm 0.6 \text{ M}\Omega$ ; threshold =  $0.6 \pm 0.1 \text{ nA}$ ) than cells in ganglia ( $R_{in} = 3.2 \pm 0.2 \text{ M}\Omega$ ; threshold =  $3.3 \pm 0.4 \text{ nA}$ ), which is presumably due, at least in part, to the absence of the electrical coupling in the

isolated neurons.  $R_{in}$  was measured by injecting a -1 nA, 5 s current. The threshold of B4 was measured by injecting depolarizing current pulses (5-s duration) that increased by 0.1 nA increments until a single action potential was elicited. Therefore, excitability of cultured B4 was measured as the number of spikes elicited by 1.5 and 2 nA (5-s duration) depolarizing current pulses. Dopamine was iontophoresed through a fine-tipped glass microelectrode (resistance 10-15 M $\Omega$ ) (Fig. 3A). The concentration of DA in the electrode was 200 mM with an equal concentration of ascorbic acid to reduce oxidation of DA. A retaining current of -3 nA was used during the course of the experiment. The current was transiently stepped to +1 nA (6-s duration) to eject the DA. The single-cell analog in ganglia was similar to the single-cell analog in culture however in ganglia the En2 stimulation similar to OC was used in place of DA and the En2 stimulation was delayed by 5 s. High divalent cation ASW was used for the single-cell in ganglia experiment to prevent B4 activity during En2 stimulation.

### **2.2.8 Statistical analysis**

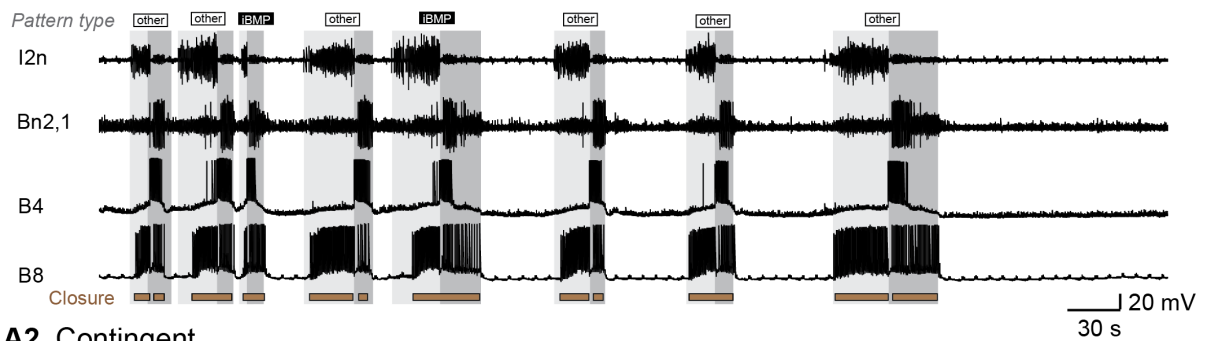
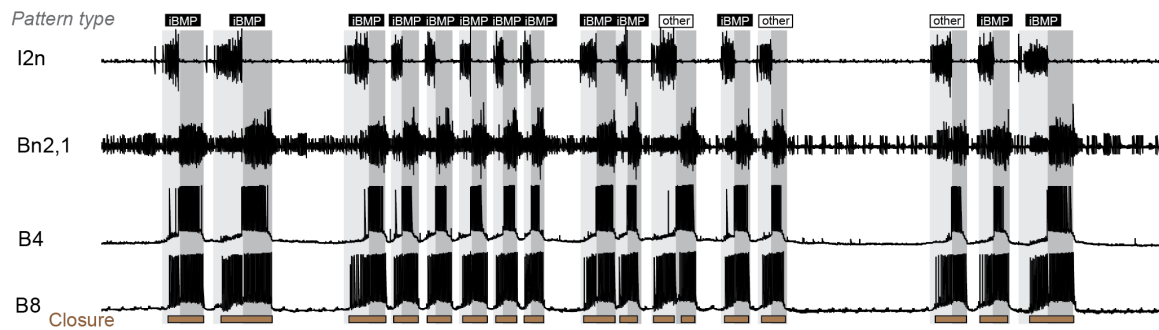
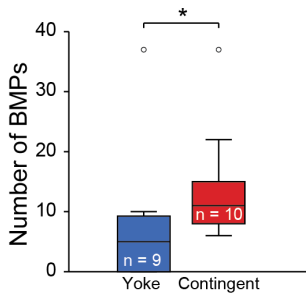
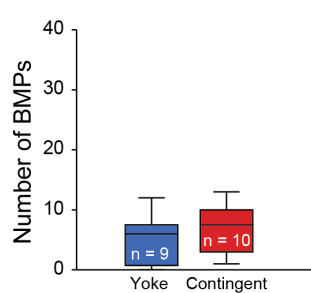
Statistical significance was set at  $P < 0.05$ . Comparisons between two groups were made using paired t-tests or student's t-tests. Comparisons between multiple groups were made using a two-factor ANOVA. Statistics were performed using SigmaStat 12.0 (Systat Software, San Jose, CA) or MATLAB.

## **2.3 Results**

### **2.3.1 Contingent En2 stimulation reinforces iBMPs**

This study used a previously developed protocol in which En.2 stimulation was contingent upon the expression of iBMPs. As in previous studies (Nargeot et al., 1997, 1999a), preparations that received contingent training expressed a greater number of

iBMPs compared to the yoke control group (Wilcoxon rank sum,  $Z = -2.22$ ,  $P = 0.026$ ) during the post-test observation period (Fig. 2.3B1). No difference was observed in the expression of other types of BMPs (Wilcoxon rank sum,  $Z = -1.025$ ,  $p = 0.306$ ) (Fig. 2.2B2).

**A1. Yoke****A2. Contingent****B1. iBMP****B2. other****Figure 2.2** Buccal motor programs and their modulation by OC.

The feeding CPG is multifunctional and generates at least two types of patterned activity: one that mediates rejection (rBMP) and another that mediates ingestion (iBMP). **A**, Representative recordings of BMPs produced by continuous, 4 Hz stimulation of n.2,3. The protraction phase was monitored via activity in I2 n. (orange trace, orange bar). The retraction phase was monitored via intracellular recordings from B4 and extracellular recording from n.2,1 (blue traces, blue bar). Closure motor activity was monitored by intracellular recordings from motor neuron B8 (purple traces, purple bar). **B**, Summary data for the number of iBMPs (**B1**) and other BMPs (**B2**).

### 2.3.1 B8 sag potential is modified by OC but not B8 excitability.

The increase in B8 activity during retraction following OC could be mediated in part by an increase in B8 excitability. To examine this possibility, B8 was held near resting potential (-70 mV) while the excitability was measured with suprathreshold depolarizing current injections (1 – 4 nA). The excitability was examined before and after OC. There was no significant difference in the number of elicited spikes between the yoke and contingent groups (rm ANOVA,  $F_{(1,16)} = 0.104$ ,  $p = 0.75$ ) nor was there a difference between these groups prior to training (rm ANOVA,  $F_{(1,16)} = 0.054$ ,  $p = 0.82$ ).

As mentioned earlier, B8 also expresses rebound excitation which is produced by the activation of an h-current (see section 2.3.5.1). The h-current shunts the effect of inhibitory input creating a sag potential (Fig. 2.3A). In addition, the h-current depolarizes the resting membrane potential, bringing the neuron closer to the firing threshold (see section 2.3.5.1). The effect of the h-current was measured by injecting a hyperpolarizing intracellular current injection (-6nA, 10 s) and measuring the percent sag potential and rebound excitation before and after training. Percent sag was calculated as the difference between the membrane potential measured at the beginning and end of the current injection divided by the membrane potential at the beginning of the current injection. This value was multiplied by 100 to get the percent sag. The change in percent sag (posttest – pretest) was compared between yoke and contingent groups (Fig. 2.4A-C). A Wilcoxon rank sum indicated a significant difference in change in percent sag between the yoke and contingent group ( $Z = -2.261$ ,  $p = 0.024$ ) (Fig. 2.4A-B). However, there was no significant difference in the percent change of rebound excitation between yoke and contingent groups (Wilcoxon

rank sum,  $Z = -0.304$ ,  $p = 0.76$ ). The difference in change of percent sag could be due to differences in the amount of hyperpolarization induced by the current injection. To examine this possibility, the change in initial hyperpolarization was compared between yoke and contingent groups. There was not a significant difference between yoke and contingent groups (Wilcoxon rank sum,  $Z = -1.395$ ,  $p = 0.16$ ). These data indicate that OC conditioning induces a  $\sim 5\%$  increase in the sag potential of B8 relative to yoke. However, this effect was not reflected by changes in rebound excitation. Therefore, these results need to be confirmed by measuring the h-current directly using voltage clamp techniques.

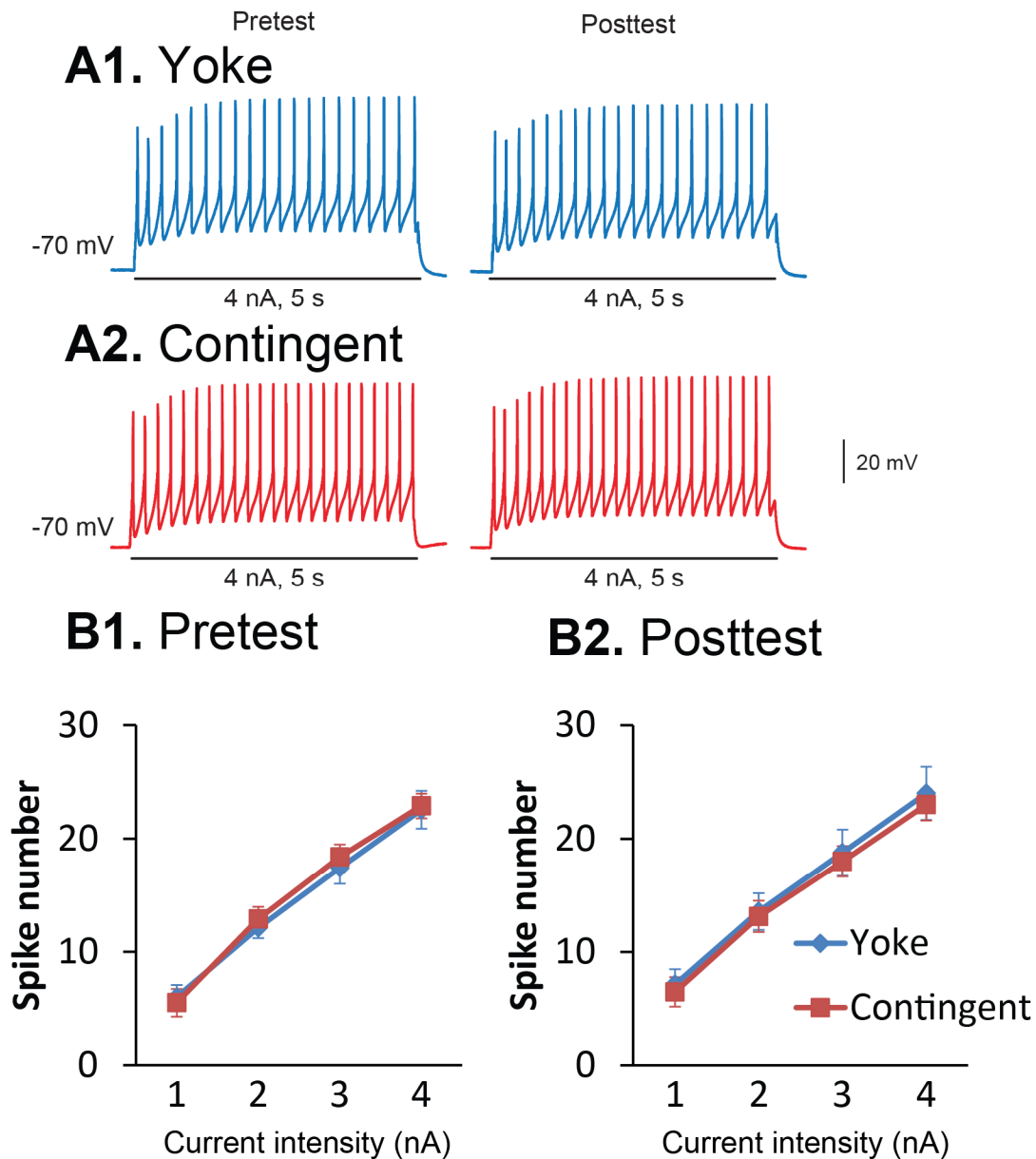


**Figure 2.3** Excitability of B8 was not altered by OC

**A**, Representative measurements of excitability before (pretest) and after (post-test) training. **B**, Summary data for the number of spikes elicited by intracellular current injections for the pretest (**B1**) and posttest (**B2**) measurements. Sample size is 9 for both groups.

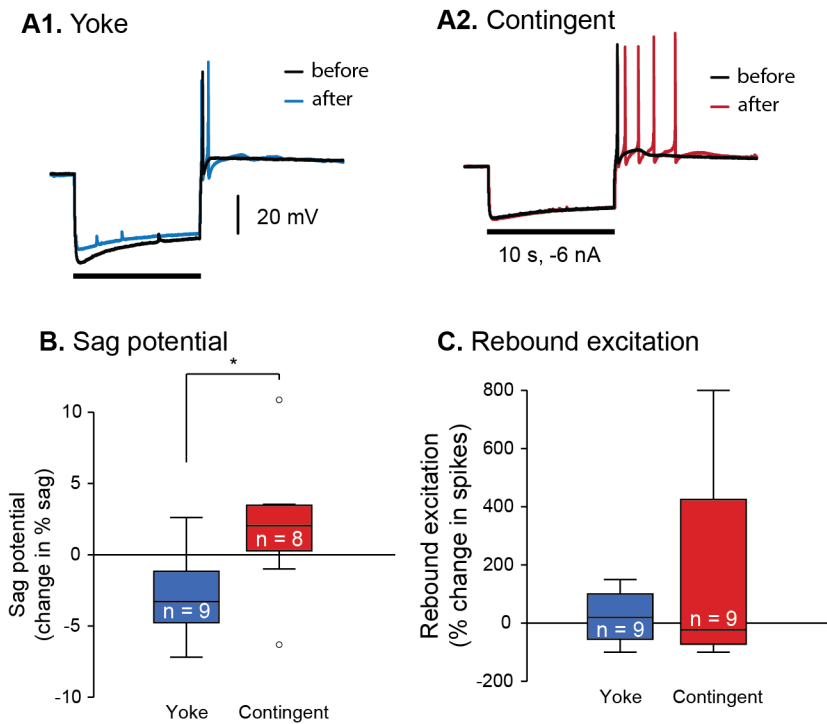


**Figure 2.4** OC increases sag potential of B8.

**A**, Example recordings of sag potential and rebound excitation in yoke (**A1**) and contingent (**A2**) groups before (black trace) and after (red or blue trace) training. **B**, Summary data for the change (posttest – pretest) in percent sag. **C**, Summary data for percent change in rebound excitation. Rebound excitation is measured as the number of spikes immediately following hyperpolarization. \*  $p < 0.05$ .

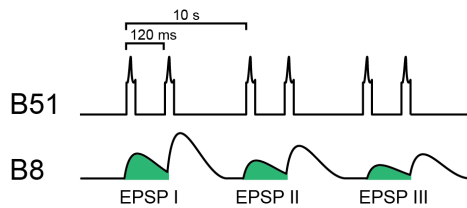
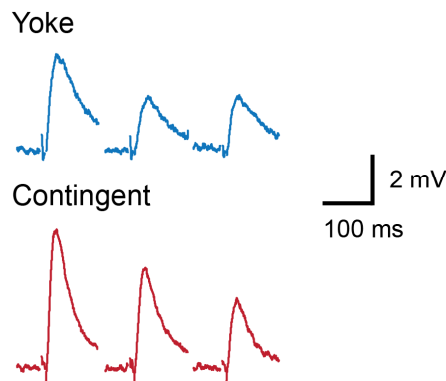
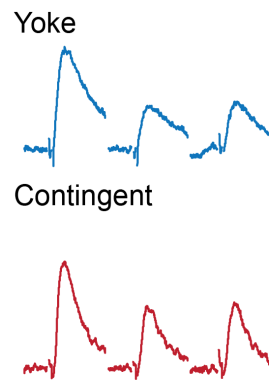
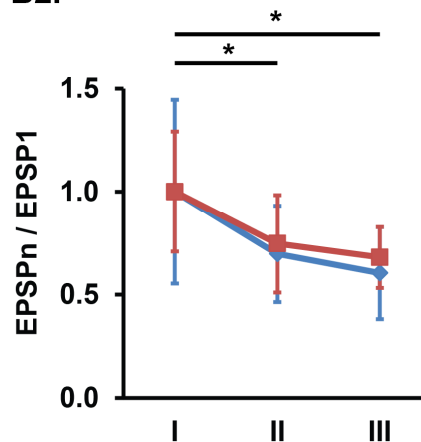
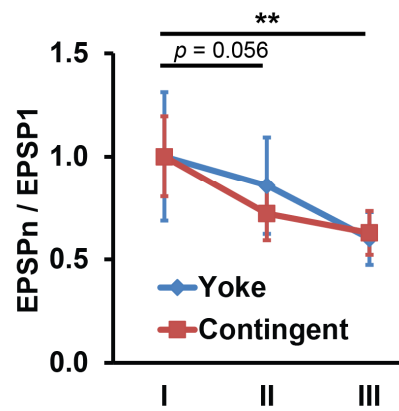


### 2.3.2 B51-to-B8 synaptic connection is not modified by OC.

B51 drives activity in B8 through an excitatory synaptic connection biasing the motor pattern towards a more ingestion-like BMP (Fig. 2.3). Preliminary experiments indicated that the B51-to-B8 synapse exhibits synaptic depression and paired-pulse facilitation within the time frame of a single BMP. Therefore, OC could facilitate the production of iBMPs by either enhancement of the initial amplitude of the EPSP, enhancing paired pulse facilitation, or by reducing synaptic depression of this connection.

Synaptic depression and paired-pulse facilitation was measured using a single stimulation protocol. This protocol consisted of three sets of paired stimuli injected into B51 (100 nA, 10 ms) where each pair was separated by 10 s and each stimuli within the pair was separated by 120 ms (see Fig 2.3A). 10 s interval was chosen because this is approximately the interval between *in vivo* motor patterns. B51 was held at -70 mV and B8 held at -100 mV. The first EPSP in each pair of stimuli was used to measure synaptic depression. This protocol elicited synaptic depression of the B51-to-B8 synapse of the second (repeated measures ANOVA,  $F_{(2,36)} = 5.155$ ,  $p = 0.016$ ; 1<sup>st</sup> vs 2<sup>nd</sup>,  $q = 3.516$ ,  $p = 0.022$ ) and third pair of EPSPs (1<sup>st</sup> vs 3<sup>rd</sup>,  $q = 4.185$ ,  $p = 0.020$ ). There was no significant differences between yoke and contingent groups in pretest (rmANOVA,  $F_{(1,11)} = 0.048$ ,  $p = 0.830$ ). Next, synaptic depression was compared between after yoke and contingent training. After training, the protocol elicited synaptic depression in both yoke and contingent groups (rmANOVA,  $F_{(2,36)} =$

7.129,  $p = 0.004$ ; 1<sup>st</sup> vs 2<sup>nd</sup>,  $q = 2.857$ ,  $p = 0.056$ ; 1<sup>st</sup> vs 3<sup>rd</sup>,  $q = 5.336$ ,  $p = 0.003$ ), however there was no significant difference in depression between yoke and contingent groups (rmANOVA,  $F_{(1,11)} = 0.211$ ,  $p = 0.655$ ). This result does not support the hypothesis that OC reduces the synaptic depression of the B51-to-B8 synapse.

**A. Stimulation protocol****B1. Pretest depression****C1. Posttest depression****B2.****C2.****Figure 2.5** Synaptic depression is not modified by OC

**A**, Diagram of the stimulus protocol. Three pairs of stimuli with 10 s separating each pair and 120 ms separating the stimuli within each pair were given to B51. EPSPs were measured in B8. Synaptic depression was measured as the change in amplitude of the first EPSP elicited in each pair (green). **B1**, Example recordings illustrating the depression of EPSPs during pretest. **B2**, Summary data of EPSP amplitude of 1<sup>st</sup>, 2<sup>nd</sup>, and 3<sup>rd</sup> (I – III) stimulus pair during pretest. **C1**, Example recordings illustrating the depression of EPSPs during posttest. **B2**, Summary data of EPSP amplitude of 1<sup>st</sup>, 2<sup>nd</sup>, and 3<sup>rd</sup> (I – III) stimulus pair during posttest. Sample size is 7 for both groups.

The first pair of stimuli (see Fig. 2.6A) measured paired-pulse facilitation and consisted of two depolarizing intracellular current injections into B51 separated by a 120 ms inter-stimulus interval (ISI). The amplitude of the first EPSP was measured from the peak of the EPSP relative to the baseline. The amplitude of the second EPSP was measured from the peak relative to an exponential curve fitted to the downward slope of the prior EPSP (Fig. 2.6A). Paired pulse ratio was calculated as the amplitude of the second EPSP divided by the amplitude of the first EPSP. One experiment with a small EPSP in pretest (0.2 mV) was excluded from the analysis. Paired pulses separated by 120 ms reliably facilitated the EPSP (black trace in yoke Fig. 2.6B, C) (Wilcoxon sign rank,  $Z = -2.201$ ,  $p = 0.028$ ). Next, the PPR was measured before and after OC. There was a significant difference in PPR between yoke and contingent prior to training (Wilcoxon rank sum,  $Z = 2.044$ ,  $p = 0.041$ ). The percent change in PPR from pretest to posttest was compared between yoke and contingent groups. There was no significant difference in the percent change in PPR between yoke and contingent groups (Wilcoxon rank sum,  $Z = 0.929$ ,  $p = 0.35$ ).

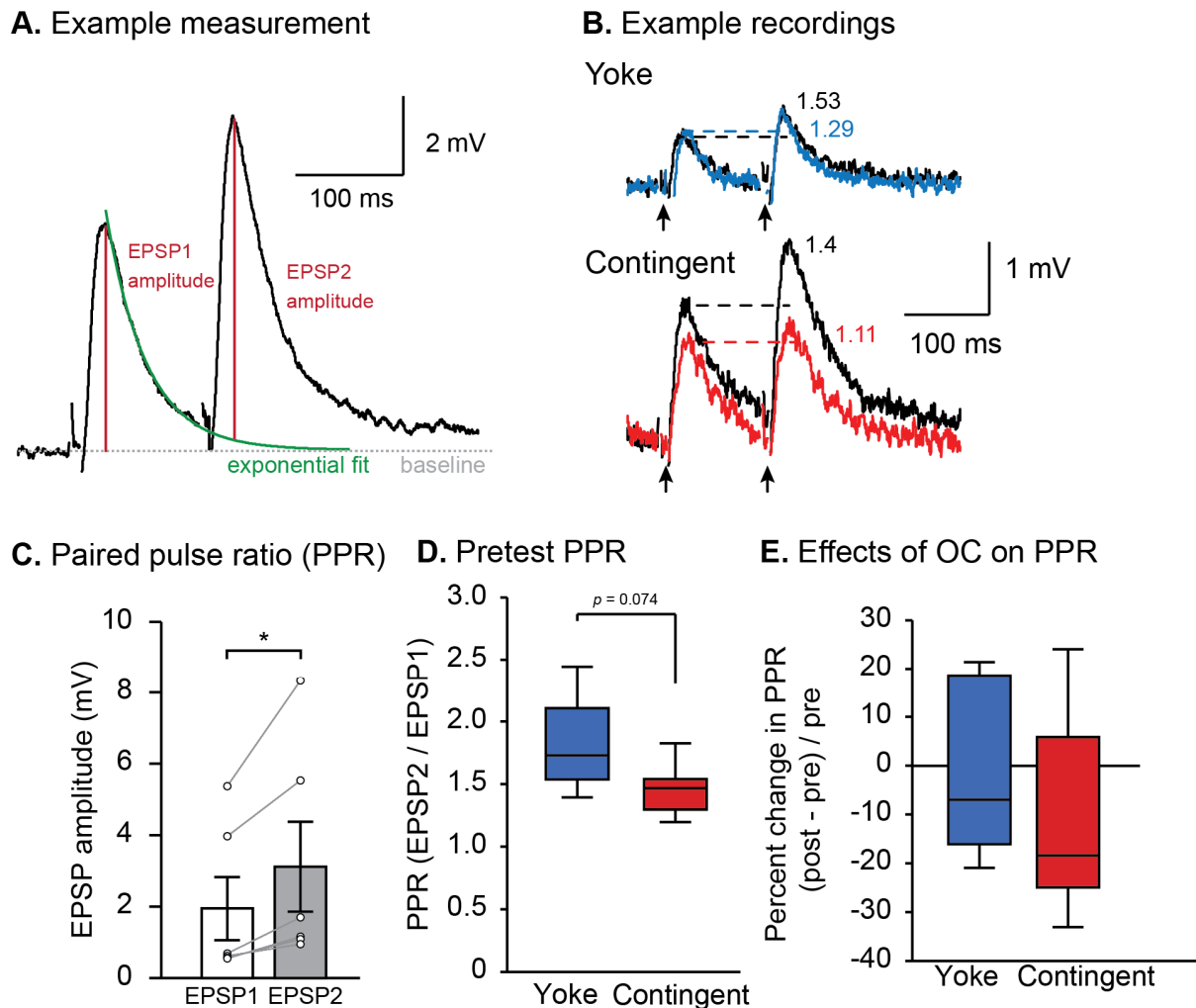


**Figure 2.6** OC did not modify B51-to-B8 PPR

**A**, Measurements of the EPSP amplitude. The exponential fit is indicated by a green line. The baseline is indicated by grey dotted line. **B**, Representative recordings of the PPR before and after contingent (bottom) and yoke (top) training. **C**, Paired-pulse facilitation for yoke prior to training. **D**, Pretest PPR. **E**, Percent change in PPR. Sample size is 7 for both groups.

The amplitude of the first EPSP of the first pair of stimuli was compared before and after OC to examine whether OC induced an overall enhancement of the B51-to-B8 synapse. There was no significant difference in EPSP amplitude prior to training (yoke =  $1.71 \pm 0.78$ , contingent =  $2.48 \pm 0.72$ ; Wilcoxon rank sum,  $Z = -1.15$ ,  $p = 0.25$ ) nor was there a difference in percent change in EPSP between yoke ( $72.3 \pm 35$ ) and contingent groups ( $52.4 \pm 27$ ) (Wilcoxon rank sum,  $Z = 0.128$ ,  $p = 0.90$ ). Taken together, these results suggest that OC does not modify the B51-to-B8 synaptic connection.

### **2.3.3 B4-to-B51 synaptic connection is reduced by OC.**

In principle, reducing the B4-to-B51 inhibitory synaptic connection could increase the likelihood of B51 firing and therefore increase the likelihood of an iBMP (Fig. 1B). Although this connection is well known, this synapse has not been extensively characterized. Therefore, as a first step, the reversal potential of this synaptic connection was measured by stimulating B4 with an intracellular current injection (30 ms, 20 nA) while varying the holding potential of B8 (Fig. 2.7). This analysis revealed that the reversal potential is about 100 mV. To determine whether the B4-to-B51 IPSP was modulated by operant conditioning, its amplitude was measured before (pre-test) and after (post-test) the *in vitro* analog of operant conditioning. B4 and B51 were current clamped to -70 mV. A rest period of at least 4 min preceded the measurements of IPSPs before and after training. IPSPs from the contingent group were reduced to a greater extent than the yoke group (Fig. 2.8B) (Contingent,  $0.74 \pm 0.1$  mV; Yoke,  $0.16 \pm 0.2$  mV; paired t-test,  $t_{(3)} = 4.158$ ,  $P = 0.025$ ,  $n = 4$  in each group).

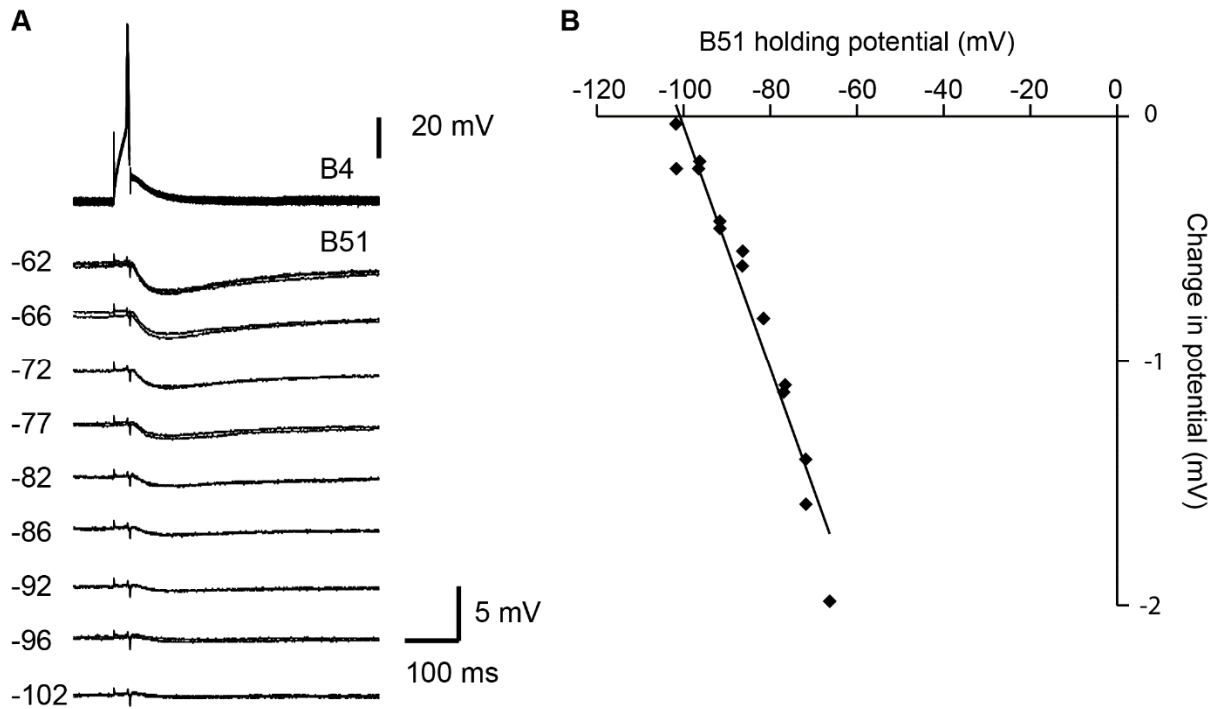


**Figure 2.7** Reversal potential of B4-to-B51.

**A**, Representative intracellular recordings of B4 (top) and B51 (bottom) illustrating the measurement of the IPSP at different holding potentials of B51. Horizontal bar indicates current injection. **B**, Summary data. Diamonds are individual data points. The linear regression is the black line. The reversal potential is indicated next to the regression line. Sample size is one.

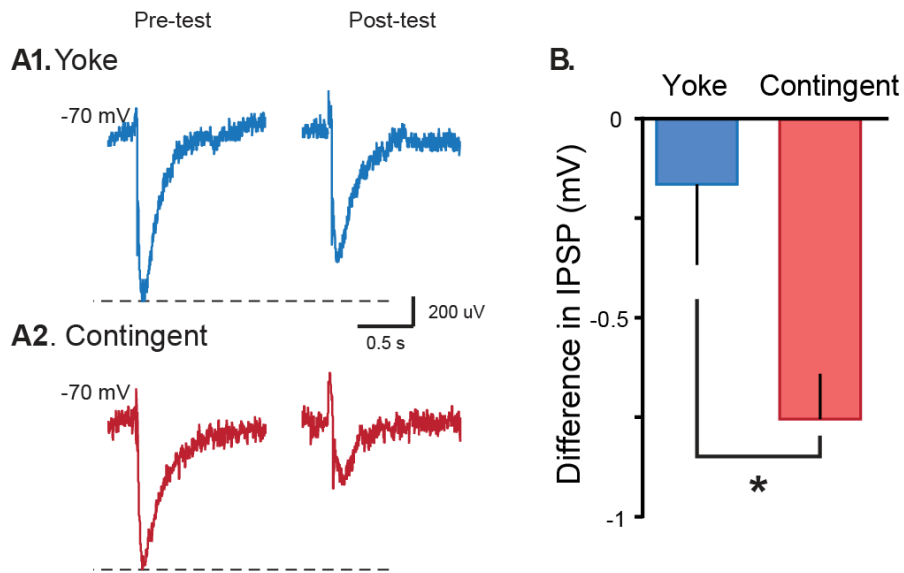


**Figure 2.8** OC reduced the B4 to B51 synaptic connection.

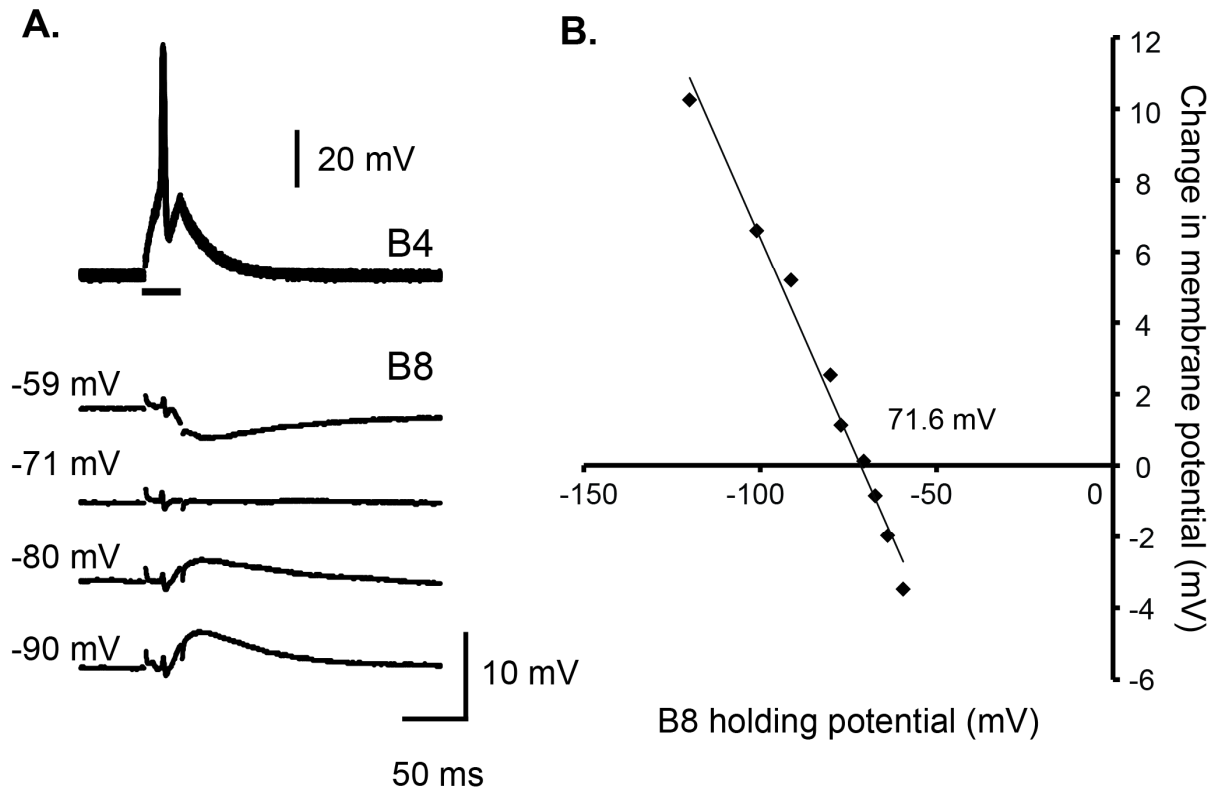
**A**, Representative intracellular recordings illustrating the measurement of the IPSP amplitude before (pre-test) and after (post-test) yoke control (**A1**) and contingent training (**A2**). **B**, Summary data. Sample size if 4 in both groups.



### 2.3.4 B4-to-B8 synaptic connection modulation by OC

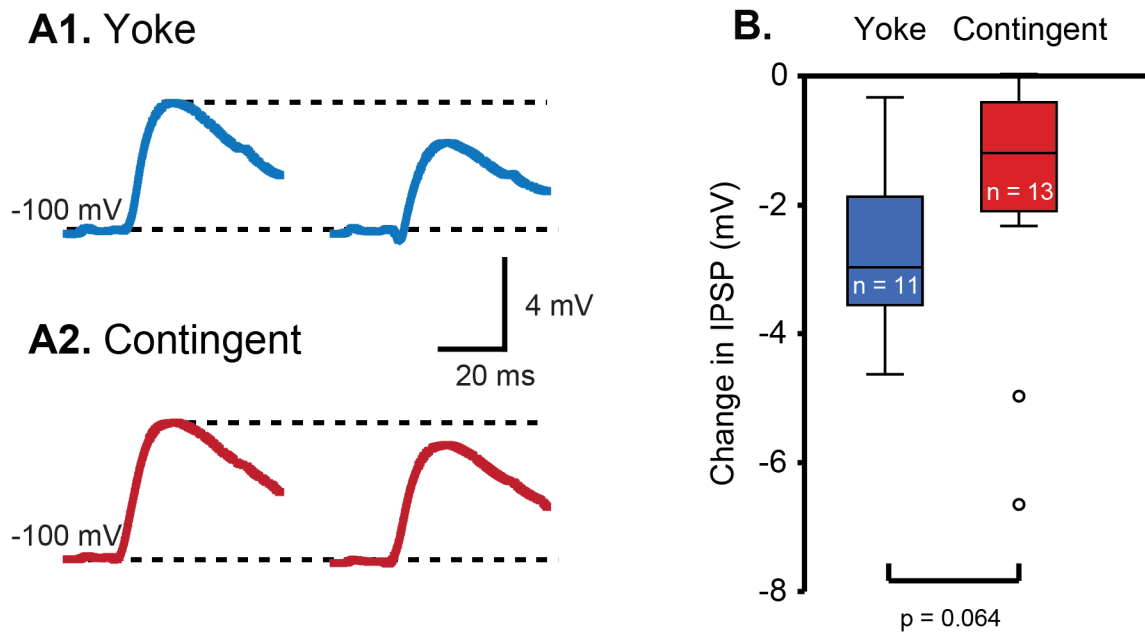
The B4-to-B8 inhibitory synaptic connection was first identified by Gardner (Gardner, 1977). This connection can reduce the activity of B8 during the retraction phase (Fig. 2.1), which could bias the motor pattern toward more rejection-like BMPs. Therefore, a reasonable hypothesis is a suppression of this connection by OC in order to increase the bias towards more ingestion-like BMPs. Although this connection is well known, this synapse has not been extensively characterized. Therefore, as a first step, the reversal potential of this synaptic connection was measured by stimulating B4 with an intracellular current injection (30 ms, 20 nA) while varying the holding potential of B8 (Fig. 2.9). This analysis revealed that the reversal potential is about 72 mV which is slightly more negative than the resting potential of B8 (approximately - 65 mV).

Next, the effect of OC on the strength of this synapse was examined. To measure the B4-to-B8 synaptic strength, an action potential was elicited in B4 by a 5 s depolarizing current injection into B4 which was adjusted to be near the action potential threshold. The membrane potential of B8 was held at -100 mV, a potential substantially more negative than the reversal potential of the B4-to-B8 synaptic connection. One experiment with a small IPSP in pretest (1.6 mV) was excluded from the analysis. The strength of the B4-to-B8 synaptic connection was measured before and after OC (Fig. 2.10). The strength of the B4-to-B8 synapse tended to be reduced to a greater extent in the yoke group as compared to the contingent group however this result was not significant (Wilcoxon rank sum test,  $U = -1.854$ ,  $p = 0.064$ ). There was no significant difference in pretest IPSP (t-test,  $t_{(22)} = -0.357$ ,  $p = 0.73$ ).



**Figure 2.9** Reversal potential of B4-to-B8 synaptic connection

**A**, Representative intracellular recordings of B4 (top) and B8 (bottom) illustrating the measurement of the IPSP at different holding potentials of B8. Horizontal bar indicates current injection. **B**, Summary data. Diamonds are individual data points. The linear regression is the black line. The reversal potential is indicated next to the regression line. Sample size is one.

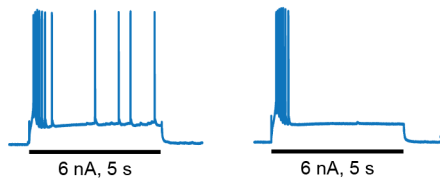
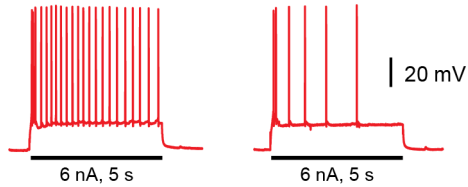
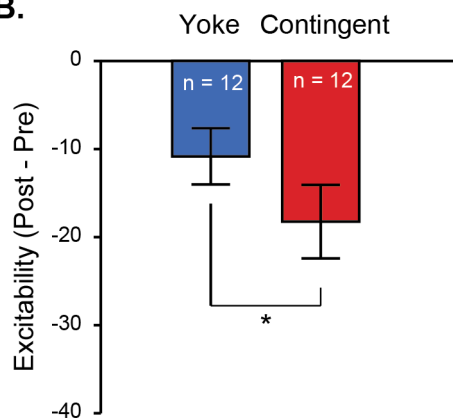


**Figure 2.10** Effect of OC on the B4-to-B8 synapse.

**A**, Representative intracellular recordings illustrating the measurement of the IPSP amplitude before (left) and after (right) yoke (**A1**) and contingent (**A2**) training. **B**, Summary data.

### 2.3.5 B4 excitability is reduced by OC

As mentioned earlier, OC increases the excitability of neurons that initiate motor patterns (B30, B63, and B65) as well as neurons that bias the motor patterns towards iBMPs (B51). Possible OC-induced changes in excitability of neurons (e.g., B4) which bias the motor patterns toward rBMPs have not been examined. A plausible hypothesis is that OC decreases excitability of B4, which would relieve the inhibition of B51 and B8 and bias the motor patterns towards iBMPs. Excitability was measured by counting the number of spikes elicited by a 5-s duration depolarizing (6 nA) current injection. The change in number of spikes (posttest – pretest) was compared between yoke and contingent groups. The contingent group had a greater reduction in excitability compared to yoke (Wilcoxon sign rank,  $Z = 2.046$ ,  $p = 0.041$ ) (Fig. 2.11). There was no significant difference in percent change of input resistance for yoke ( $-7.14 \pm 1.7\%$ ) and contingent groups ( $-7.72 \pm 2.0\%$ ) (Wilcoxon sign rank,  $Z = 0.267$ ,  $p = 0.79$ ). These data indicate that OC reduces the excitability of B4.

**A1. Yoke****A2. Contingent****B.**

**Figure 2.11** OC reduces the excitability of B4.

**A**, Representative measurements of excitability before (pretest) and after (post-test) training. **B**, Summary data for the change in number of spikes elicited by 5 s intracellular current injections (6 nA) for yoke and contingent groups.

### **2.3.6 Stimulation of En2 contingent with B4 stimulation suppresses B4 excitability *in vitro*.**

We next examined whether activating B4 directly *in vitro*, in a ganglia preparation and in cell culture, modified B4 excitability, by measuring its properties before and after a single-cell analog of operant conditioning in which application of DA or En2 was contingent on activity in B4. DA was used because it appears to mediate reinforcement of iBMPs during operant conditioning of feeding in *Aplysia* (Nargeot et al., 1999c; Brembs et al., 2002; Lorenzetti et al., 2008). In addition, B4 receives monosynaptic excitatory input from En.2 and this EPSP is reduced by the DA receptor inhibitor methylergonovine (Kabotyanski et al., 1998; Nargeot et al., 1999c). Methylergonovine blocks reinforcement of iBMPs (Nargeot et al., 1999c). In addition, iontophoretic application of DA to B4 elicited depolarizing responses in cell culture indicating that dopamine receptors are expressed on B4 (data not shown). As mentioned in Chapter 2, B4 suppresses the expression of iBMPs. We hypothesize that pairing B4 with DA or stimulation of dopaminergic afferents would decrease the excitability of B4.

The input resistance, threshold, and excitability were measured before and after the single-cell analog of operant conditioning. Two training protocols were used, which differed in the delay between B4 and En2 stimulation. The contingent group received seven 5 s intracellular current injections to B4 (inter-stimulus interval of 2 min) followed, after 5 s, by a 6 s stimulus (9 V, 10 Hz) to the En2 nerve, whereas for the non-contingent yoke control, the En2 stimulus was instead delayed by 35 s. The intensity of the depolarizing current injection into B4 during training was adjusted for

each cell to match the level of activity (2.5 - 5 Hz) during a typical iBMP (Sasaki et al. 2012). The spike frequency was measured during each stimulus throughout training. Preparations were excluded from the analysis if the average spike frequency during training stimuli exceeded 4.0 Hz. Contingent En2 stimulation significantly reduced the excitability of B4 (t-test,  $t_{(14)} = 2.405$ ,  $p = 0.031$ ) (Fig. 2.12). However, there was no significant difference in percent change in threshold in the contingent ( $10.9 \pm 4.4$ ) compared to yoke ( $3.7 \pm 2.7$ ) (t-test,  $t_{(14)} = 1.177$ ,  $p = 0.259$ ). No significant differences were observed in  $R_{in}$  between the contingent ( $-8.4 \pm 1.4\%$ ) and the non-contingent control group ( $-9.8 \pm 1.1\%$ ) (t-test,  $t_{(14)} = 0.752$ ,  $p = 0.464$ ). These data indicated that the single-cell *in vitro* analog of operant conditioning reduced B4 excitability, and this decrease appeared independent of a change in input resistance.

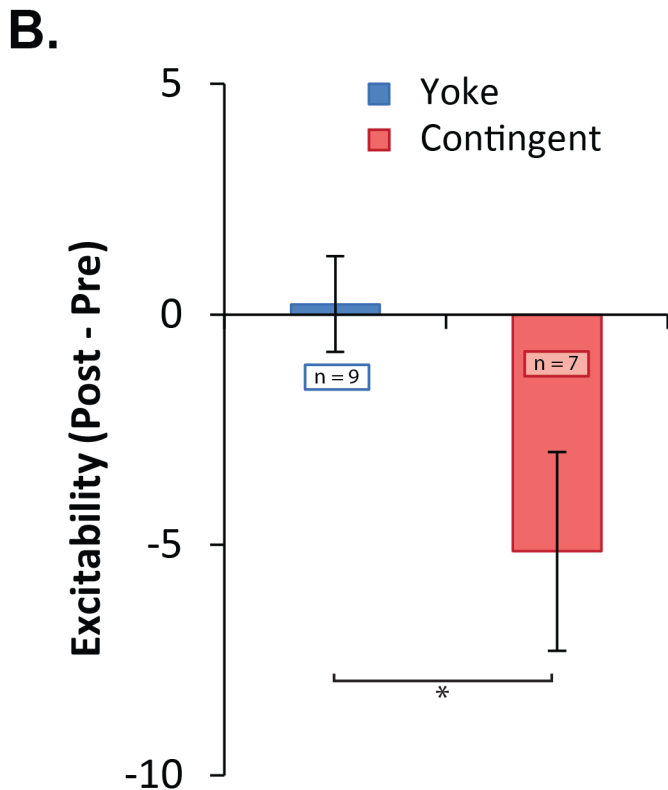
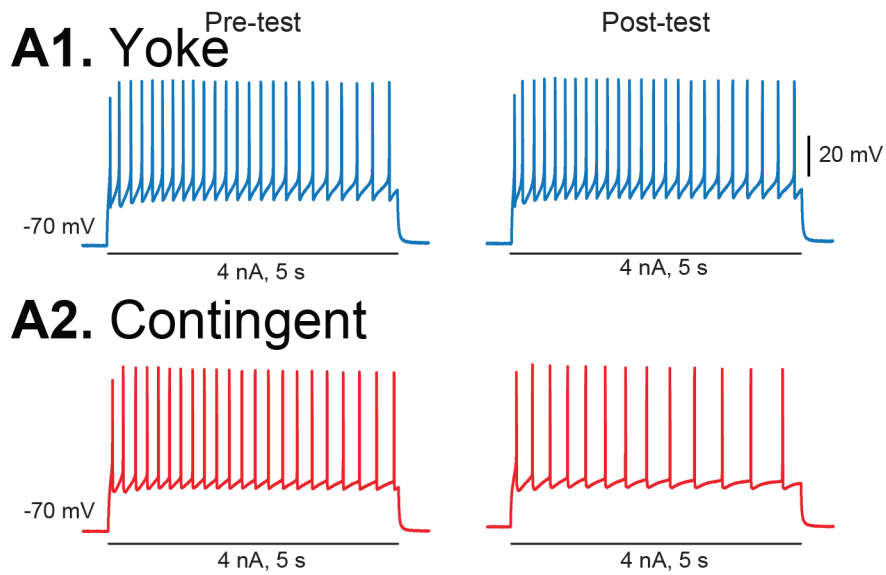


**Figure 2.12** Stimulation of En2 contingent with B4 stimulation suppresses B4 excitability.

Representative intracellular recordings illustrating measurement of excitability before (pre-test) and after (post-test) contingent DA application (**A1**) and non-contingent control (**A2**). **B**, Summary data.



### 2.3.7 DA contingent with B4 stimulation suppresses B4 excitability in culture.

The  $R_{in}$ , threshold, and excitability were measured before and after the single-cell analog of operant conditioning. Two groups of cells were used, which differed in the delay between B4 stimulation and DA iontophoresis (Fig. 2.13A). The contingent group received DA iontophoresis (6-s duration) immediately following suprathreshold depolarizing current injections (5 s) into B4, whereas for the non-contingent control group, this DA iontophoresis occurred 35 s after B4 stimulation. While measuring the intrinsic properties of B4 in either *in vitro* or in cell culture preparations, the membrane potential was held at -70 mV, which was slightly more negative than the average resting potential ( $-63 \pm 0.7$  mV) of B4 in ganglia. A two-way ANOVA indicated a greater decrease in excitability of the contingent group as compared to the non-contingent control group ( $F_{(1,14)} = 4.739$ ,  $P = 0.047$ ,  $n = 4$  to 5 in each group) (Fig. 3.2.2). Neurons that received contingent DA tended to have a greater increase in threshold ( $98.3 \pm 31.0\%$ ) as compared to the non-contingent control group ( $18.2 \pm 7.2\%$ ), but the effect was not statistically significant (t-test,  $t_{(7)} = 2.245$ ,  $P = 0.060$ ,  $n = 4 - 5$  in each group). No significant differences were observed in  $R_{in}$  between the contingent ( $-12.7 \pm 4.8\%$ ) and the non-contingent control group ( $-21.7 \pm 5.4\%$ ) (t-test,  $t_{(7)} = -1.227$ ,  $P = 0.259$ ,  $n = 5 - 6$  in each group).

These data indicated that the single-cell analog of operant conditioning reduced B4 excitability, and similar to *in vitro* conditioning, this decrease appeared independent of a change in input resistance. Moreover, these results indicated that the contingent-dependent decrease in B4 excitability was intrinsic to B4.



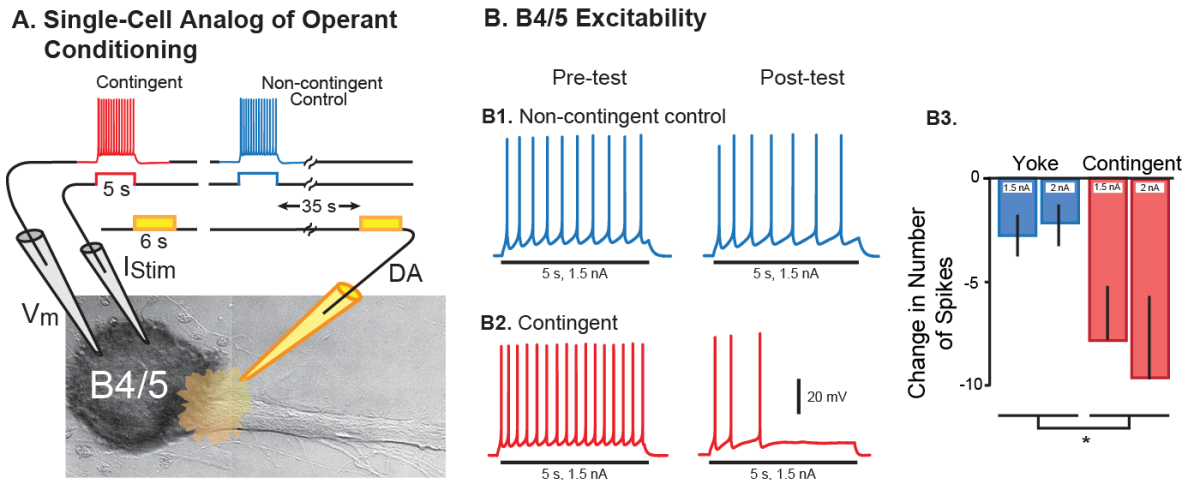


**Figure 2.13** DA contingent with B4 stimulation reduced B4 excitability in culture.

Single-cell analog of operant conditioning reduced B4 excitability. **A**, Diagram illustrating the protocol for the single-cell analog of operant conditioning. In the contingent group, DA was applied extracellularly to the axon hillock region by iontophoresis immediately following a train of spikes in B4, which were elicited by a 5-s suprathreshold depolarizing current injection, whereas in the non-contingent group DA was applied 35 s after stimulation of B4. **B**, Contingent DA application decreased the excitability of B4 in cell culture. Representative intracellular recordings illustrating measurement of excitability before (pre-test) and after (post-test) contingent DA application (**B2**) and non-contingent control (**B1**). **B3**, Summary data. Courtesy of Hsin-Mei Chen.

### 2.3.8 Modeling operant conditioning in a conductance based model

#### 2.3.8.1 Rationale

The empirical study discussed above identified two sites of plasticity (decreases in B4 intrinsic excitability and in the B4-to-B51 IPSP) and two putative sites of plasticity (increase in B4-to-B8 IPSP and increase in B8 sag potential). The decrease in B4 excitability and strength of B4-to-B51 connection and increase in B8 sag potential would bias the CPG towards iBMPs, whereas the increase in B4-to-B8 may bias the CPG towards rBMPs (See Fig. 2.1). Intuitively, the increase in B4-to-B8 could nullify the changes in the B4-to-B51 synapse. However, B51 has highly non-linear membrane properties such as a plateau potential, whereas B4 is a more linear regular spiking neuron, which may increase the effectiveness of the B4-to-B51 relative to B4-to-B8 synapse. In addition, B51 is bi-stable in that it is either inactive or active in a high frequency burst (see Fig. 1.3). Therefore, a small change in the B4-to-B51 synapse may yield very large changes in the activity of B51. The changes in excitability of B4 may also reduce the potency the B4-to-B8 synaptic changes. In order to test the relative contributions of each of these sites of plasticity, these changes were inserted into a preliminary computational model of the feeding CPG (Fig. 2.15). The changes in B8 sag were not examined in these preliminary analysis, but may be included in future versions of the CPG model.

#### 2.3.8.2 Modeling B8 motor neuron

As a first step, a model for B8 was constructed which included an h-current ( $I_h$ ), leakage conductance,  $Na_{fast}$ , and  $K_{fast}$  ionic conductances, with parameters adjusted to match empirical data. The properties of  $I_h$  were measured by placing B8 in culture

and using voltage-clamp techniques to measure  $I_h$  activation at different membrane potentials (Fig. 2.14A). B8 was clamped to -40 mV to deactivate  $I_h$ , then stepped to different membrane potentials to activate  $I_h$ . Then, the membrane potential was stepped to -140 mV to measure the tail-current at this potential as an indicator of  $I_h$  activation (Fig. 2.14A2, C). The time constant of activation was measured by fitting an exponential equation to the currents associated with each step potential (Fig. 2.14D). The model for  $I_h$  was fitted to these data (Fig. 2.14B) and reproduced the sag potential of B8 (Fig. 2.14E). Additional parameters were modified to fit the model to the excitability of B8 measured in ganglia. The membrane capacitance was measured for B8 in ganglia by injecting a hyperpolarizing current pulse (-3 nA) into B8 and fitting an exponential curve to the voltage response. The capacitance was calculated as the input resistance divided by the time constant of this exponential equation. The parameters of the leakage conductance,  $N_{fast}$ , and  $K_{fast}$  were adjusted to fit the model of B8 to the I/O curve of B8 in ganglia (Fig. 2.15A).

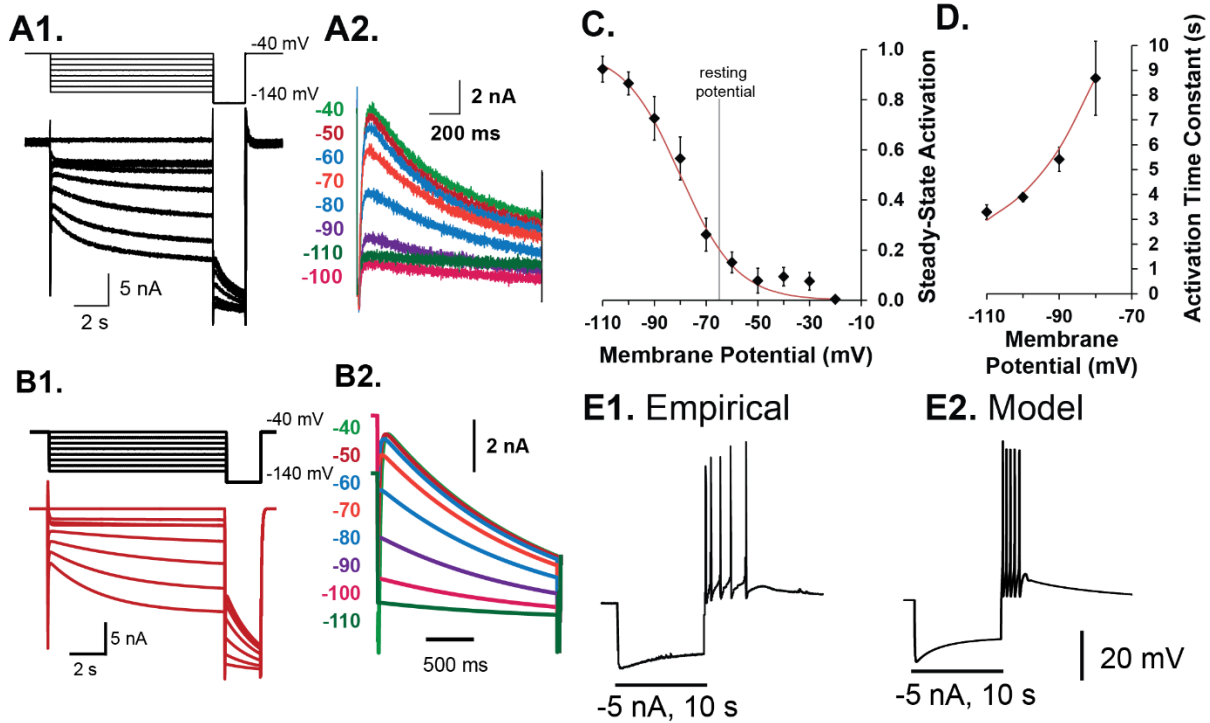


**Figure 2.14** Modeling the  $I_h$  current in B8

**A1**, B8 was voltage-clamped to a holding potential where  $I_h$  is deactivated (-40 mV).  $I_h$  was activated by stepping to potentials that ranged from -40 to -110 mV (10 mV increments) for 10 s. This step was followed by a step to -140 mV. **A2**, High-gain plot of tail-currents. **B**, Voltage clamp simulation using the same protocol as (**A**). **C**, Plot of the amplitude of the tail-currents measured at the beginning of the step to -140 mV. X axis is the potential of the step immediately prior. **D**, Plot of the activation time constant as a function of membrane potential. The activation time constant was measured as the time constant of an exponential curve fitted to the current trace associated with each step potential. **E1**, Empirical example of a current-clamp recording illustrating the sag potential and rebound excitation of B8. **E2**, The model of B8 which included  $I_h$  reproduced the sag potential and rebound excitation in (**E1**).

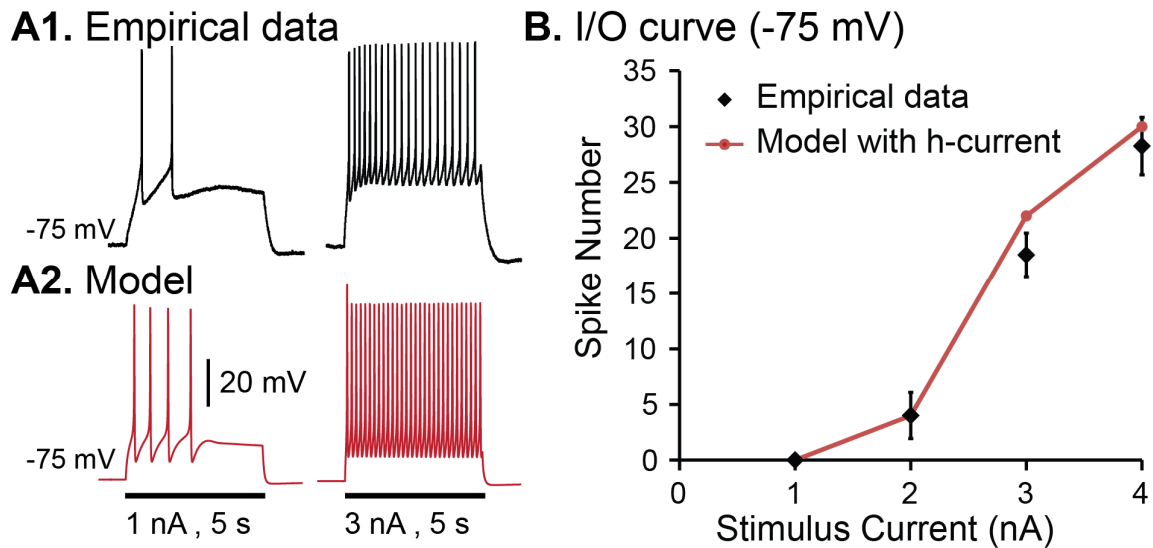


**Figure 2.15**  $I_h$  does not affect excitability when neuron is clamped to -65 mV.

**A**, Excitability of B8 (**A1**) and B8 model (**A2**) measured from a holding potential of -75 mV, which is 10 mV more negative than the resting potential. Spike activity was elicited by 5 s depolarizing current injections (1 – 4 nA). **B**, I/O properties of B8 (black diamonds) and B8 model with  $I_h$  (red line).

### 2.3.8.3 Modeling retraction neurons B4, B51, and B71

A second step to inferring the contributions of the correlates of OC was to modify an expanded model of the feeding CPG. Douglas A. Baxter and colleagues expanded the 10-cell model of the feeding CPG (Cataldo et al., 2006) by removing the fictitious Z-cell and adding the cerebral-buccal interneuron 2 (CBI-2), B20, B30, B40, and B65, and adding a second compartment to B64. Extensions of this model, for the current study, included adding a two-compartment cell (B71), including the modified model of B8 (see section 2.3.5.2), adding a second compartment to B51 and B4, and adding synaptic depression and PPF to the B51-to-B8 synapse. An overview of this model is provided in Fig. 2.15. This model now includes 14 neurons, 35 fast and 8 slow inhibitory synapses, 34 fast and 26 slow excitatory synapses, and 21 electrical synapses. Example simulations of the extended CPG model are provided in Fig. 2.21.



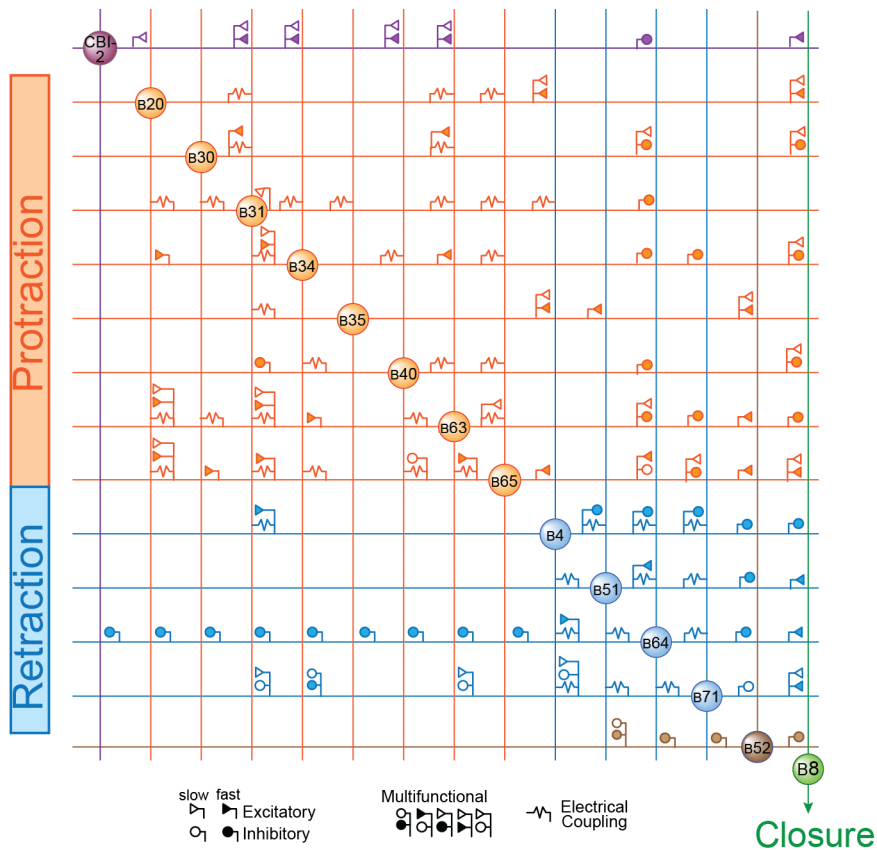


**Figure 2.16** Overview of the Model CPG network.

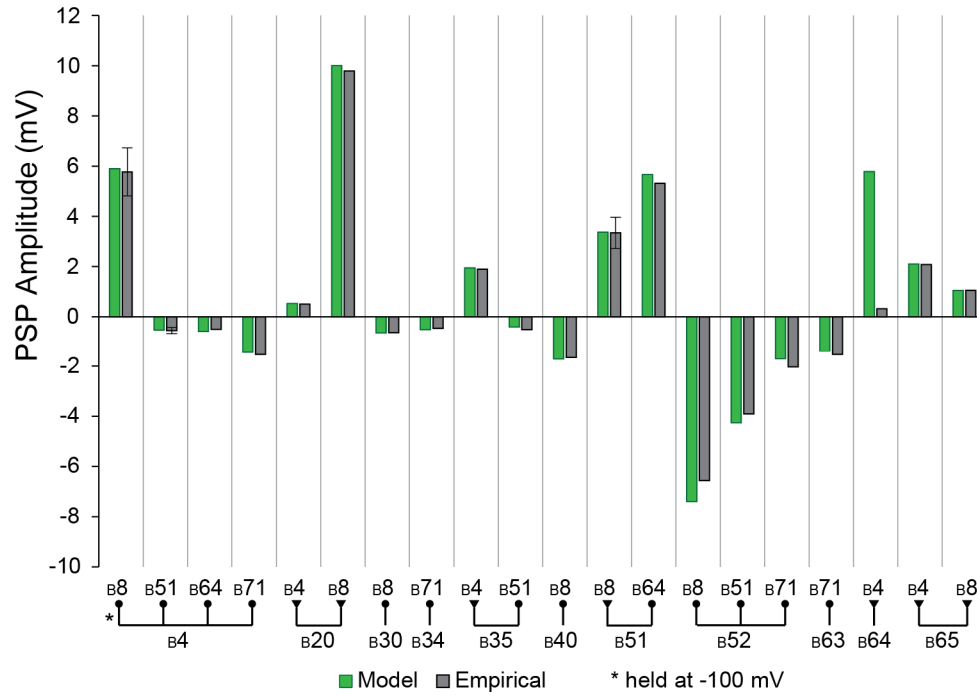
Connectivity matrix of all the synaptic connections included in the model CPG network. Protraction neurons are represented in orange. Retraction neurons are represented in blue. Cerebral ganglia neuron is purple. Closure neuron is green and BMP terminator neuron B52 is brown.

The maximum conductance parameter was adjusted so that the PSPs of the chemical and electrical synapses matched published data (Fig. 2.17). The strength of a few chemical and electrical synaptic connections needed to be larger than published values so that the postsynaptic neuron's activity reached the level of activity observed during a BMP. For example, the chemical B64-to-B4 synapse and the electrical B51→B71, B64→B51, and B64→B71 synapses all had a larger PSP or coupling ratio than in published recordings (Sasaki et al., 2013; Seiling et al, 2014). The need for greater excitatory input to B4, B51, and B71 suggests that there may be additional neurons or synaptic connections within the retraction CPG feeding circuitry that are not included in the model. Indeed, there is a second B51-like neuron (i.e., B53) which exhibits a plateau potential and is coupled to B51. Additional experiments are needed to characterize B53's intrinsic properties and synaptic connections before this neuron can be added to the CPG model. The need for increased strength of the B64-to-B4 electrical connection suggests the presence of a yet to be identified slow excitatory synapse to B4 from a protraction neuron or synaptic connection from a neuron active in the beginning portion of retraction.

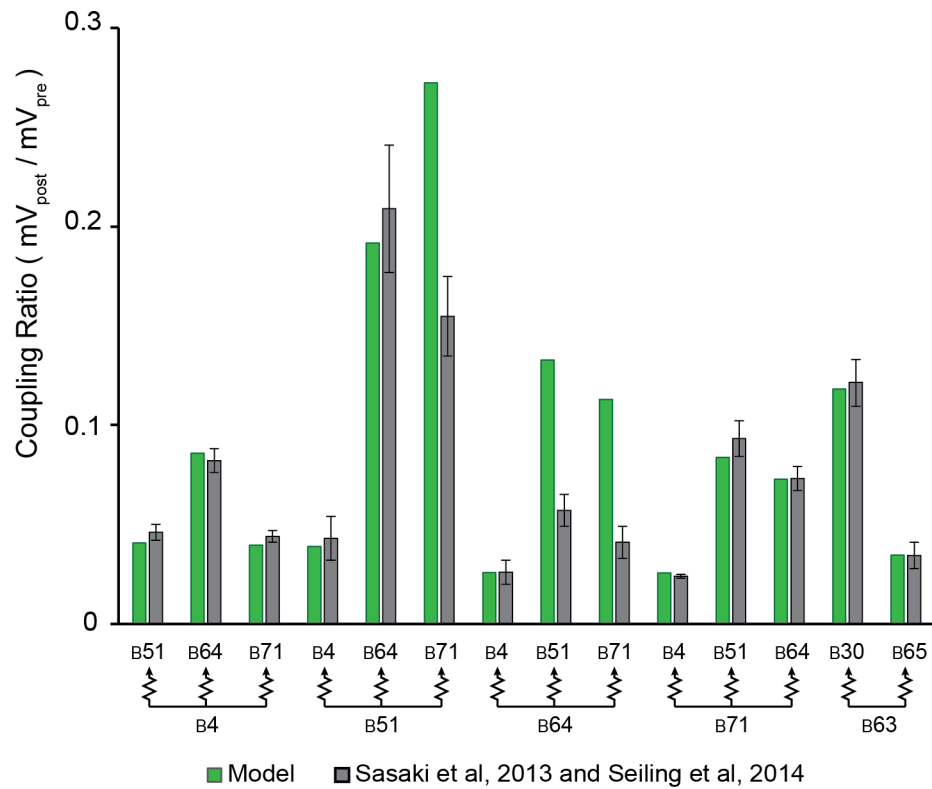
**Figure 2.17** Fitting of synaptic connections to empirical data.

**A**, Comparison of empirical data (Sasaki et al., 2013; Seiling et al., 2014) to the synaptic connection strengths to and from retraction neurons in the CPG model.  
**B**, Comparison of empirical data (Sasaki et al., 2013; Seiling et al., 2014) to the coupling ratios between retraction neurons and three key protraction neurons in the CPG model.

## A. Chemical synaptic connections



## B. Electrical synaptic connections



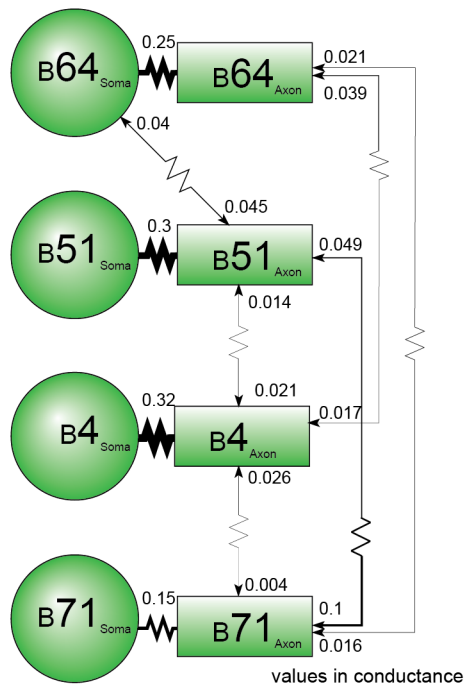
In order for the CPG model to better replicate the physiological properties of B4, B51, and B71, these neurons were each subdivided into a soma and axon compartment. The compartments and electrical synaptic connections between them are depicted in Fig. 2.17. The electrical synapses between these neurons are rectified in that the junctional conductance differs depending on the direction of the current flow (Sasaki et al., 2013). For example, the junctional conductance from B4→B64 is 0.039 whereas the junctional conductance from B64→B4 is 0.017. The majority of electrical synapses were modeled connecting axon compartments, however the B64→B51 synapse was modeled connecting the soma of B64 to the axon of B51. This was necessary to drive B51 activity during BMPs. Addition of B53 in the future may remove the need for this axosomatic electrical synapse. In the model, the plateau potential in B51 was modeled to be mediated in large part by a tetrodotoxin (TTX) insensitive sodium current ( $Na_{pp}$ ) and facilitated by the activation of the TTX sensitive sodium current ( $Na_{fast}$ ) (Fig 2.17B). These currents rectified the steady-state IV relationship to the extent that the IV plot crossed the X-axis with a positive slope at two points, creating two stable membrane potentials: the resting potential and plateau potential. The plateau was terminated by a slowly activating potassium current ( $K_{slow}$ ) and by slow inactivation of  $Na_{pp}$  (Fig 2.17B).

Finally, the ionic conductances were modified so that the input resistance and excitability of the model matched empirical data (Sasaki et al., 2013; Seiling et al., 2014) (Fig. 2.19). The input resistance was calculated as the change in membrane potential of the soma during a simulated hyperpolarizing current injection (-3 nA, 5 s)

to the soma (Fig. 2.19A). The excitability was calculated as the threshold for eliciting an action potential during a simulated depolarizing current injection (Fig. 2.19B) or as the number of spikes elicited by a 5 s simulated intracellular depolarizing current injection into the soma (Fig. 2.19C). All the values except the B51 threshold closely matched empirical data. The threshold for B51 was reduced so that its level of activity during a BMP matched empirical data. As mentioned above, adding neuron B53 may remove the need to reduce the B51 threshold.

Although there are some differences between empirical data and the modified model of the feeding CPG (e.g., coupling between B51, B64, and B71), the similarity of the model with a large portion of the empirical data indicates that this model serves as a good approximation of the biophysical properties of the feeding neural network. Thus, this CPG model serves as a good test bed to investigate the relative contributions of OC-induced changes in the B4-to-B8 and B4-to-B51 synapses, and in B4 intrinsic excitability.

### A. Compartments

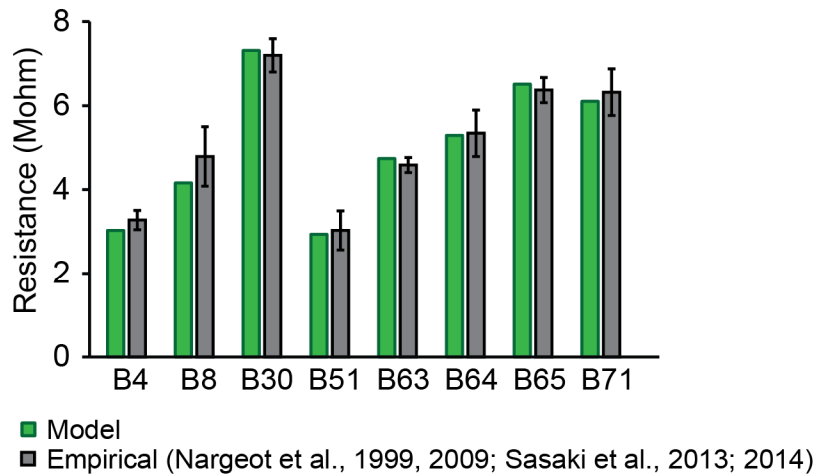
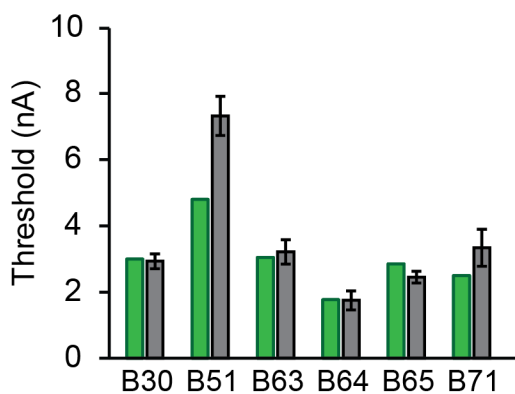
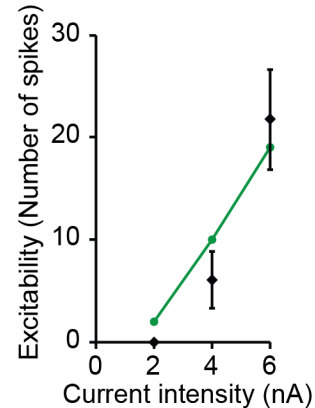
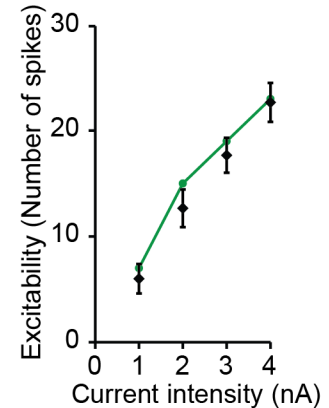


### B. Table of conductances

<b>B4</b>	<b>B51</b>	<b>B64</b>	<b>B71</b>
<b>Soma</b>	<b>Soma</b>	<b>Soma</b>	<b>Soma</b>
Leak	Leak	Leak	Leak
$K_{slow}$	$Na_{pp}$	$Na_{pp}$	$Na_{pp}$
$K_{fast}$	$K_{fast}$	$K_{fast}$	$K_{fast}$
$Na_{fast}$	$Na_{fast}$	$Na_{fast}$	$Na_{fast}$
	$K_A$	$K_{slow}$	$K_A$
	$K_{slow}$		
<b>Axon</b>	<b>Axon</b>	<b>Axon</b>	<b>Axon</b>
Leak	Leak	Leak	Leak
$K_{slow}$	$Na_{pp}$	$K_{fast}$	$Na_{pp}$
$K_{fast}$	$K_{fast}$	$Na_{fast}$	$K_{fast}$
$Na_{fast}$	$Na_{fast}$		$Na_{fast}$
	$K_A$		$K_A$

**Figure 2.18** Excitability was fit to empirical data.

**A**, Retraction neurons were modeled with a somatic and axon compartment. The electrical synaptic connection between neurons were primarily between the axon compartments. The conductance of each electrical connection is indicated next to each synapse. The thickness of the lines is proportional to the conductance. **B**, Table of the conductances included in each compartment.

**A. Input resistance****B. Excitability****C1. B4 Excitability****C2. B8 Excitability****Figure 2.19** Fits of input resistance and excitability to empirical data.

**A**, Input resistance of each neuron compared to empirical data (Nargeot et al., 1999, 2009; Sasaki et al., 2013). **B**, Threshold of each neuron compared to empirical data (Nargeot et al., 1999, 2009; Sasaki et al., 2013). **C1**, Excitability of B4 in ganglia (black diamonds) and of B4 model (green line) measured by 5 s intracellular current injections at 2, 4 and 6 nA intensities. **C2**, Excitability of B8 in ganglia (black diamonds) and in B8 model (green line) measured by 5 s intracellular current injections at 1, 2, 3 and 4 nA intensities.



#### 2.3.8.4 Contributions of correlates of OC

To examine the contributions of the correlates of OC, the OC-induced changes observed in B4 excitability, B4-to-B8, and B4-to-B51 synapse were introduced into the model of the feeding CPG. The excitability of B4 was adjusted so that it matched the average pretest activity elicited by a 5 s, 6 nA current injection. Then, the maximum conductance of  $K_{\text{slow}}$  was increased to match the change in the excitability similar to either the yoke or the contingent group (Fig. 2.20A). The maximum conductance of the B4-to-B51 or B4-to-B8 synapse was modified to match the change in IPSP amplitude observed in either the yoke or contingent group (Fig. 2.20B,C). The coupling conductance of the protraction neurons was also increased in all simulations to match the increased coupling observed after OC (Seiling et al., 2009).

With these parameter changes, simulated patterned CPG activity in the yoke and contingent conditions resembled empirical data (Fig. 2.21A, 2.21C). In addition, each of the three parameter changes was simulated separately (e.g. Fig. 2.20B). Patterned activity was elicited by a 2.8 nA current injection into CBI-2 which lasted throughout the simulation. Each condition was simulated in three separate trials, with 600 s simulated each trial. Increasing the amplitude of the B4-to-B8 maximum conductance reduced the number of iBMPs (Fig. 2.21D) presumably by increasing inhibition of B8. Decreasing the excitability of B4 increased the number of iBMPs and the number of B51 plateau potentials (Fig. 2.21B, D) presumably because of the reduced inhibition of B51 and B8. The group where the B4-to-B51 synapse was reduced expressed almost exclusively iBMPs and nearly all these patterns elicited a plateau potential in B51 (Fig. 2.21D). Next, the combined effect of all three contingent

group parameter changes was simulated (Fig. 2.21C), in part to examine whether the increase in the B4-to-B8 IPSP would shunt the effects of the decrease in B4 excitability and in the B4-to-B51 synaptic strength. This group expressed exclusively iBMPs, and all the patterns elicited a plateau potential in B51. These data indicate that the B4-to-B51 inhibitory synapse likely has a greater contribution to the changes in iBMP than changes in B4 excitability. Changes in this synapse sufficed to cause a strong bias towards iBMPs. B4 excitability also strongly biased the CPG towards iBMPs, however this change did not reliably recruit B51. The increase in the B4-to-B8 synapse was not able to dampen the bias towards iBMPs, presumably because of a ceiling effect.

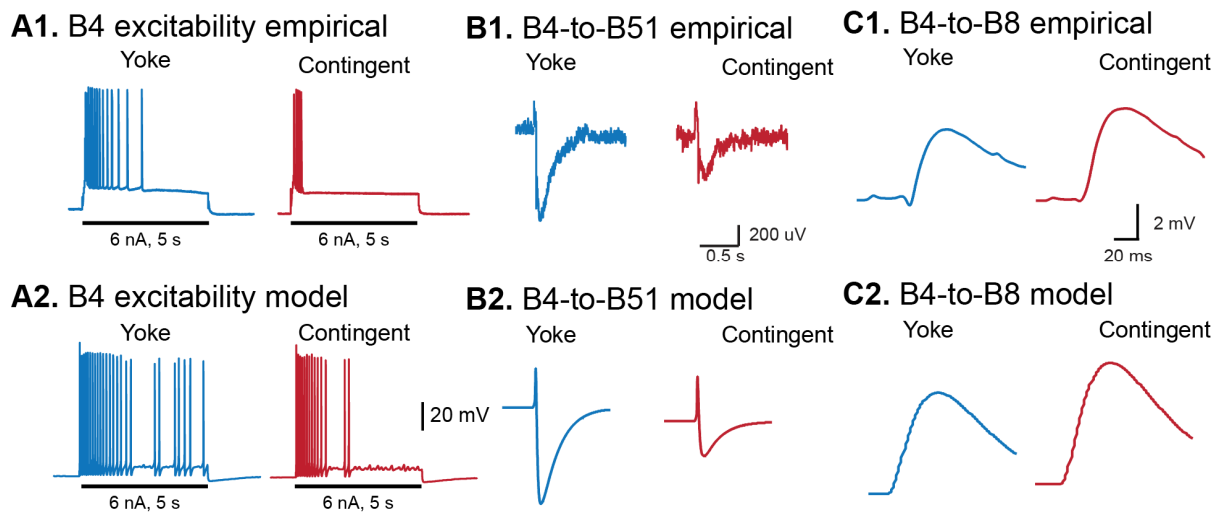
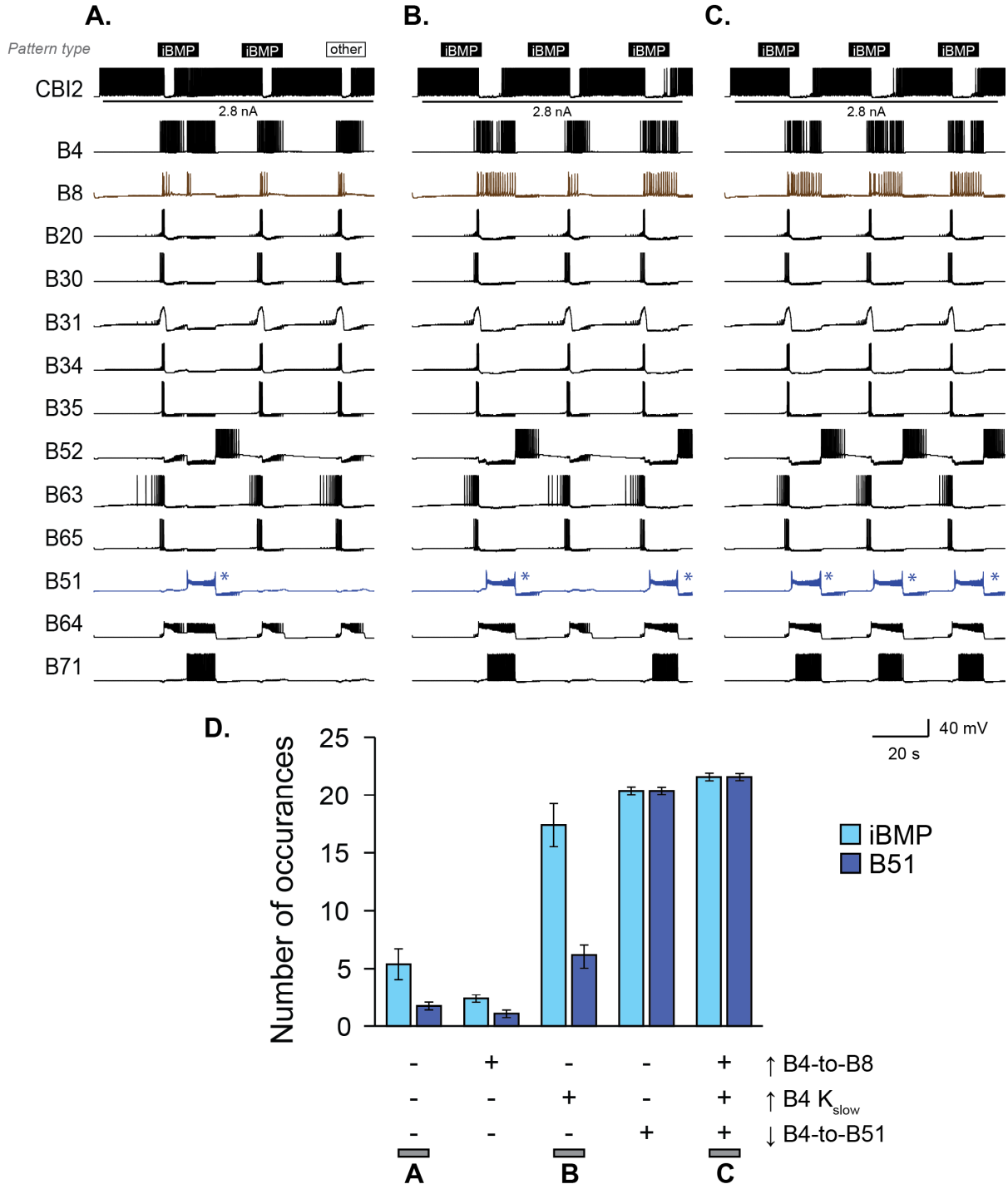


**Figure 2.20** Correlates of OC were introduced into the feeding CPG

**A**, Recordings comparing the excitability of B4 after yoke and contingent training (**A1**) and simulations which were fit to the changes in excitability observed for yoke and contingent groups (**A2**). **B**, Recordings comparing the B4-to-B51 synapse after yoke and contingent training (**B1**) and simulations which were fit to the changes observed in of yoke and contingent groups (**B2**). **C**, Recordings comparing the B4-to-B8 synapse after yoke and contingent training (**C1**) and simulations which were fit to the changes observed in of yoke and contingent groups (**C2**).

**Figure 2.21** Incorporating correlates of OC enhanced number of iBMPs and B51 activity.

Feeding behavior was simulated by activating CBI-2 in the feeding CPG model where the B4-to-B8 maximum conductance, B4 excitability, and the B4-to-B51 maximum conductance were set to their yoke values or modified according to the changes induced by OC. **A**, All three sites were set to their yoke values. The pattern type is indicated at the top of each BMP. Closure motor neuron B8 is colored in brown and B51 colored in blue. **B**, B4 excitability was reduced by increasing  $K_{\text{slow}}$  in this neuron while B4-to-B8 and B4-to-B51 maximum conductances were set to the yoke values. **C**, All three sites were modified according to the changes induced by OC. **D**, Summary data of all the tested variations of the feeding CPG model. \* indicates a B51 plateau potential.



## 2.4 Discussion

This study demonstrates that operant conditioning decreases the intrinsic excitability of B4, decreases the efficacy of the B4-to-B51 inhibitory synaptic connection, tends to increase the B4-to-B8 inhibitory connection, and may increase the B8 sag potential. The results provide several new insights into the mechanisms contributing to operant conditioning. First, these results help explain how multiple sites of plasticity work in concert to reinforce a behavior. Activity in the radula closure motor neuron B8 is a defining feature of iBMPs (see Fig. 1A). B8 is excited by B51 but inhibited by B4 (Fig. 2.1). Part of the increase in B8 activation is due to the conditioning-induced increase in B51 excitability (Nargeot et al., 1999a,b; Lorenzetti et al., 2006, 2008; Mozzachiodi et al., 2008). A simultaneous decrease in excitability of B4 and efficacy of the B4-to-B51 inhibitory synapse would disinhibit B8 and B51. Therefore, the combined effect of modulating each element (B4 and B51) of this “push-pull” circuit would be greater than either effect alone.

Second, this study suggests that similar contingencies between spike activity and DA can lead to different outcomes in neurons within the same circuit. Pairing activity in B51 with DA or En2 increases its excitability (Brembs et al., 2002; Lorenzetti et al., 2008; Nargeot et al., 1999a,b), in contrast, pairing activity in B4 with DA or En2 decreases its excitability (Fig. 2.12 and 2.13). Future experiments will examine whether the differential responses reflect the activation of distinct second-messenger cascades in each cell, or if the same cascade is used, but different membrane channels are targeted.

This study also identified the first two synaptic correlates of operant conditioning in this system, indicating that the memory for operant conditioning is expressed by both changes in synaptic strength and changes in the intrinsic properties of neurons. Indeed, it is becoming increasingly clear that learning and memory involves both types of changes (for review see Mozzachiodi and Byrne, 2010). This study then investigated the relative contributions of the changes in B4 excitability and strength of the B4-to-B51 and the B4-to-B8 synaptic connections. Simulations with the extended CPG model suggest that increasing the B4 excitability alone, and decreasing the B4-to-B51 connection alone, can strongly bias the feeding circuit towards iBMPs. The results from this study set the stage for investigating, within a single circuit, the diversity and relative contributions of synaptic and non-synaptic changes to operant conditioning. Further examination of these issues may provide insights into the design logic of the different sites of plasticity involved in other forms of learning as well.

### **Chapter 3: Unique configurations of compression and truncation of neuronal activity underlie L-DOPA-induced selection of motor patterns in *Aplysia*.**

#### **3.1 Rationale and hypothesis**

Dopamine (DA) is considered to be a ubiquitous modulator of neuronal networks (e.g., Schultz et al., 2013; Wise, 2004). A great deal is known about the cellular and molecular mechanisms of DA modulation (for a review, see Beaulieu and Gainetdinov, 2011), and about DA modulation of the activity of small central pattern generating (CPG) networks such as the 13-neuron lobster pyloric network (Harris-Warrick et al., 1998). However, little is known about DA modulation of individual neuronal activity of larger networks with the ability to select among many complex motor pattern outputs (Frigon, 2012; Schultz et al., 2013; Sharples et al., 2014; Wise, 2004). Investigating such modulation requires monitoring activity in large numbers of individual neurons with high spatiotemporal resolution.

To examine the effects of DA modulation of a relatively complex network, we simultaneously monitored the activity of up to 130 neurons in the feeding circuit of *Aplysia* using voltage-sensitive dye (VSD) imaging combined with extracellular nerve recordings. The combination of VSD and nerve recordings allowed us to record activity in individual neurons, track axonal projections, and monitor fictive motor output. The feeding circuit, which resides primarily in the buccal ganglia, mediates several distinct behaviors, such as biting and swallowing of food and rejection of inedible objects, and generates fictive versions of these behaviors when the ganglia are isolated from the animal (for reviews, see Baxter and Byrne, 2006; Cropper et al.,



2004; Elliot and Susswein, 2002; Nargeot and Simmers, 2012; Wu et al., 1988). Dopaminergic neurons within the buccal ganglia facilitate the genesis of buccal motor patterns (BMPs) and bias the selection towards distinct BMP types (Dacks and Weiss, 2013; Díaz-Ríos and Miller, 2002, 2005, 2006; Due et al., 2004; Jing and Weiss, 2001; Kabotyanski et al., 1998; Nargeot et al., 1999c; Proekt et al., 2004; Rosen et al., 1991; Teyke et al., 1993). Although DA-induced changes of a small number of neurons have been characterized (Kabotyanski et al., 2000), there is no characterization of the circuit-wide changes induced by DA. To study the changes induced by DA in isolated buccal ganglia, we bath applied either low or high concentrations (40 or 250  $\mu$ M) of the DA metabolic precursor L-3,4-dihydroxyphenylalanine (L-DOPA), which enhances the release of endogenous DA with physiologically relevant localization and timing (Abe et al., 2015; Kabotyanski et al., 2000; Pothos et al., 1996). We found that a low concentration of L-DOPA biased motor activity toward intermediate BMPs, whereas a high concentration of L-DOPA biased motor activity towards bite BMPs. We used this concentration-dependent selection of BMPs and VSD imaging to characterize the ways in which different levels of DA modulate neuronal activity to select motor patterns.

## **3.2 Methods**

### **3.2.1 Optical and electrophysiological recording**

*Aplysia californica* (20 – 45 g) were obtained from the University of Miami National Resource for *Aplysia*. Animals were housed in plastic containers inside aerated tanks containing artificial sea water (ASW) (Instant Ocean; Aquarium Systems, Mentor, OH) maintained at 15°C. Animals were fed a ~ 5x3 cm (~ 0.08 g)

piece of seaweed three times per week. Animals were anesthetized by isotonic  $\text{MgCl}_2$  (360 mM) with a volume in milliliters equal to half the animal's body weight in grams. The buccal mass was removed and placed in a Sylgard®-lined dissection chamber containing ASW with a high (3x) concentration of divalent ions (330 mM NaCl, 10 mM KCl, 90 mM  $\text{MgCl}_2(6\text{H}_2\text{O})$ , 20 mM  $\text{MgSO}_4$ , 30 mM  $\text{CaCl}_2(2\text{H}_2\text{O})$ , 10 mM HEPES, pH 7.5). The buccal ganglia were isolated from the buccal mass with nerves intact and pinned down in a Sylgard®-lined imaging chamber with seven custom made suction electrodes fastened radially. The imaging chamber was filled with normal ASW (450 mM NaCl, 10 mM KCl, 30 mM  $\text{MgCl}_2(6\text{H}_2\text{O})$ , 20 mM  $\text{MgSO}_4$ , 10 mM  $\text{CaCl}_2(2\text{H}_2\text{O})$ , 10 mM HEPES, pH 7.5) maintained at room temperature ( $\sim 23^\circ\text{C}$ ) throughout the experiment with no perfusion of the saline to avoid bath agitation. An Olympus® BX50WI upright microscope was equipped with a 20x 0.95 NA XLUMPLFLN water immersion objective (Olympus®). The preparation was stained for 7 min in ASW containing a high concentration of RH-155 (0.25 mg/ml, AnaSpec™), then the bath was exchanged with a lower concentration of RH-155 (0.025 mg/ml) and remained in this solution for the entire experiment (Hill et al., 2012). Preliminary experiments indicated that 0.25 mg/ml RH-155 yielded a greater signal-to-noise ratio compared to 0.1 and 0.05 mg/ml and showed no signs of toxicity. A lamp house was fitted with a 150 W halogen lamp and powered by a Kepco power supply. The light was passed through a 710/40 bandpass filter (BrightLine®) and a 0.8 NA Olympus condenser. The light was then transmitted through the preparation and directed at a 128x128 CMOS camera (NeuroCMOS-DW128, RedShirtImaging™) sampling at 2.5 kHz with a 12 MeV well depth. Motor pattern generation was enhanced by a 15 s phasic stimulus

(0.5 ms, 10 Hz, 100 V) (WPI stimulus isolator 1850A) to buccal nerve 2 immediately prior to recording nerve and VSD signals for 2 min. For pharmacological treatment, each pair of ganglia received a 100  $\mu$ L bolus in close proximity to the ganglia of saline with either ascorbic acid (Veh) alone or L-DOPA (Tocris™) and ascorbic acid, making a final L-DOPA bath concentration of 40  $\mu$ M (Low) or 250  $\mu$ M (High). Treatment was administered 15 min prior to the posttest recording and immediately after bath exchange of the lower concentration of RH-155. The treatment remained in the bath until the end of the experiment. The experiment was designed such that the experimenter was blind to the treatment, practically however this was difficult to achieve because of the dramatic changes in activity induced by L-DOPA.

### 3.2.2 Classification of BMPs

BMPs were monitored by extracellular suction electrode recordings of ipsi- and contralateral buccal nerves 1, 2, and 3 (n1, n2, and n3) and closure activity was monitored by recording either ipsi- or contralateral radula nerve 1 (Rn) (Fig. 3.1A). The start of protraction phase was considered to be the beginning of large-unit activity in n1, and the start of retraction phase was considered to be the end of large-unit activity in n1. The end of retraction phase was considered to be the end of large-unit activity in n2. Similar to previous studies, the *in vitro* preparations expressed four distinct BMP types: rejections, intermediates, bites, and swallows (Baxter and Byrne, 2006; Cropper et al., 2004; Elliot and Susswein, 2002; Kabotyanski et al., 2000; Nargeot and Simmers, 2012; Wu et al., 1988). Consistent with these findings, a histogram of the distribution of BMPs with the overlap of Rn activity with the retraction phase along the x-axis has four reasonably distinguishable peaks (Fig. 3.2.1.1). We

categorized BMPs by setting boundaries at each trough of the histogram. BMPs with less than 10% of closure activity overlap with retraction were classified as retraction, between 10% and 50% overlap were intermediates, between 50% and 90% were bites, and 90% or more overlap were classified as swallows.

### 3.2.3 Analysis of VSD imaging data

Regions of interest (ROI) were drawn manually by a blind observer around each cell with Fiji (Schindelin et al., 2012) using the image frame that had the smallest mean-squared distance from the average of all frames in the recording. VSD signals were acquired by averaging the pixels in the ROI. The ROI was shifted to correct for movements of each cell that occurred during the recording. All MATLAB codes can be found at <https://uni.edu/fakepath> (link to be provided). The raw VSD signals were bandpass filtered in MATLAB (Butterworth,  $F_{pass1} = 15$  Hz,  $F_{stop1} = 0.1$  Hz,  $F_{pass2} = 140$  Hz,  $F_{stop2} = 1$  kHz,  $A_{pass} = 0.1$ ,  $A_{stop1} = 60$ ,  $A_{stop2} = 60$ ).

*VSD spike detection.* Action potentials were detected in the VSD recording data using a variation of the slope threshold method. An action potential was detected if the trace had a downward 4 ms deflection (depolarization) with an amplitude greater than 2.5 times the standard deviation followed 4.8 ms later by an upward deflection (measured from the downward peak) with an amplitude greater than 3.0 times the standard deviation. These time points were chosen because this approximated the shape of a typical action potential in *Aplysia*. A minimum separation between spikes was set to 5.2 ms to prevent counting a single spike more than once. We chose this method of spike detection because it is not computationally intensive and is resistant to changes in baseline.

### 3.2.4 Analysis of extracellular nerve activity

The voltage from the extracellular nerve electrodes was amplified by a differential AC amplifier (A-M Systems 1700) and digitized by the A-D converter of the CMOS camera system. The raw extracellular voltage signals were lowpass filtered in MATLAB (equiripple,  $F_{\text{pass}} = 200$  Hz,  $F_{\text{stop}} = 1$  kHz,  $A_{\text{pass}} = 1$ ,  $A_{\text{stop}} = 60$ , Stopband Shape = flat). The waveforms of action potentials in the nerve had a variety of shapes (Fig. 3.2E1). Therefore, we used a similar spike detection method as for the VSD but with several differences. Nerves had a high baseline activity (e.g., n2 in Fig. 3.1B1), thus the spike detection was ran in multiple iterations to remove spikes in order to gain a more accurate estimation of standard deviation of the noise. The threshold for the initial down-stroke was 3.0 and the upstroke was 3.5 times the standard deviation, which was calculated after the spikes were zeroed out from the previous iteration using a 4 ms prior to 6.8 ms after time window. The width of the spike had to fit one of three empirically determined durations ( $\{1.2/1.2\}$ ,  $\{2.0/2.0\}$ ,  $\{3.2/2.8\}$ ) where the notation is  $\{[\text{duration of downstroke}] / [\text{duration of upstroke}]\}$  in units of ms. In addition, the polarity of the spikes sometimes alternated between preparations, therefore the data was also scanned for the inverse waveform (except the  $\{2.0/2.0\}$  criteria whose inverse was not included because it had a large number of false positives). The spike detection was performed for a total of 5 iterations. The spike times of the final iteration were used for the identification of axonal projections (see below). The multiple criteria were needed to increase the performance of the spike detection algorithm and allow the detection of spikes with different waveforms. The performance of the spike detection of the nerve recordings was confirmed by visual inspection. The parameters

for VSD and nerve spike detection were optimized and fixed before starting the subsequent analyses presented in Figs. 3.3 – 7.

### **3.2.5 Identification of axonal projections from neurons to nerves**

Spike coincidence between each nerve and each neuron was measured by first calculating the probability of an action potential in the nerve given an action potential in the neuron (Fig. 3.2E3) and then subtracting the mean probability of an action potential in the nerve 0 – 50 ms prior to the action potential in the neuron,  $P(\text{nerve} | \text{neuron}) - P(\text{nerve})$ .  $P(\text{nerve} | \text{neuron})$  was calculated by summing the probability of an action potential in the nerve within a window around (2 ms prior to 2 ms after) the highest peak in probability with a positive delay (see peak in Fig. 3.2E3).  $P(\text{nerve})$  estimates the level of activity of the nerve around the same time as the spikes in the neuron. To identify an axonal projection, spike coincidence was required to be at least 0.25.

### **3.2.6 Spike correlation**

Pearson's linear correlation coefficient was calculated for each pair of retraction neurons in each preparation for the entire recording, with a time bin of 0.5 s. The correlation matrix was then clustered using the linkage followed by the cluster and dendrogram functions in MATLAB. The maximum number of clusters was set to 4.

### **3.2.7 Burst analysis**

A burst was considered to be a series of at least three spikes (Cocatre-Zilgien and Delcomyn, 1992) with a maximum inter-spike interval of 400 ms (Chiappalone et al., 2005). To remove neurons with a high baseline firing rate that by chance may meet this threshold, bursting neurons were required to have a substantial difference

in spike frequency within bursts compared to outside of bursts (as indicated by Fisher's Exact Test) (Cocatre-Zilgien and Delcomyn, 1992). Fisher's test was made more conservative by dividing the spike frequency within bursts by four.

Bursting neurons were grouped into those activated primarily during protraction or retraction phase. A cell was considered to be primarily active during either protraction or retraction when at least 75% of its burst activity overlapped with the respective phase. Neurons that shifted phase between recordings were rarely observed. Therefore, the posttest recordings and a 2 min pretest observation period were combined to improve the classification. To confirm the accuracy of our classification, this procedure was applied to 98 published recordings of identified neurons provided in the literature (Bédécarrats et al., 2013; Borovikov et al., 2000; Church and Lloyd, 1994; Jing and Weiss, 2001; Sasaki et al., 2009; Shetreat-Klein and Cropper, 2004; Sieling et al., 2014). The activity of each neuron was obtained by using the snapshot tool in Adobe® Acrobat® X to capture an image of the data and a MATLAB algorithm to convert the pixelated images of the published recordings to spike trains. In 98% of the examples our classification matched what was specified in the literature, indicating that our method agrees with the general consensus.

*Properties of bursts.* Bursts were considered to be associated with a given BMP if for protraction neurons the burst overlapped with the protraction phase. For retraction, Rn, n2, or n3 neurons, the burst was associated with a BMP if the burst overlapped with the retraction phase, because this was the phase in which these neurons were primarily active (see Fig. 3.5). Burst latency was calculated as the delay between start of the first burst of activity in the neuron and the start of the phase

for each BMP. The duration was calculated for each BMP by summing the duration for all bursts in the neuron that overlapped with the phase.

### **3.2.8 Topographical analysis**

Each ganglion was aligned to a universal grid. The orientation of each ganglion was approximated by calculating the mean slope and offset of the ventral neuron cluster and the ganglion as a whole relative to the universal grid. A linear regression was performed on the coordinates of all the pixels of all the neurons having a large area (the largest 50% of neurons in the field of view). These large neurons primarily reside in the ventral neuron cluster, which is composed of large motor neurons that run parallel to the longitudinal axis of the ganglion. The pixels that overlay the entire ganglion were observed to have a light intensity between the 5<sup>th</sup> and 90<sup>th</sup> percentiles of all the pixels within the field of view. Therefore, to improve the estimation of the ganglion orientation, a second linear regression was performed on the pixel coordinates within this range of intensities. The mean slope and offset of these two regression lines relative to the universal grid approximated the orientation of the ganglia. The image was then rotated and shifted in the X-Y direction according to this orientation.

### **3.2.9 Statistical analysis**

All statistics were performed in MATLAB using the statistical toolbox (The Mathworks, Natick, MA, USA). Normality was not assumed for any of the analyses. For the peri-event histograms (Fig. 4) a Kruskal-Wallis test was followed by a multiple comparisons of mean ranks test with Bonferroni correction, which multiplied the p value by the number of time points and the number of treatment groups. For timing



of burst activity analysis (Fig. 3.5), a Kruskal-Wallis test was followed by a pairwise rank sum test with a Bonferroni correction where the  $p$  value was multiplied by the number of neuron subgroups and the number of treatment groups. Heteroscedasticity was not tested prior to the analyses. For all comparisons, a  $p$  value less than 0.05 was considered statistically significant.

### 3.3 Results

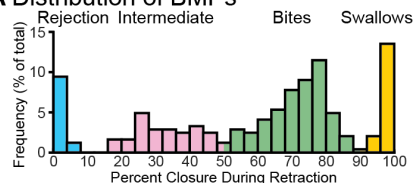
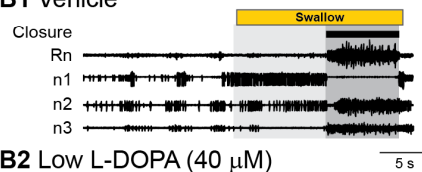
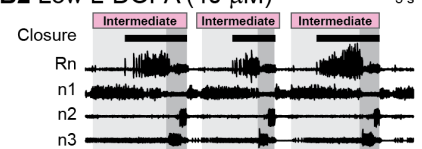
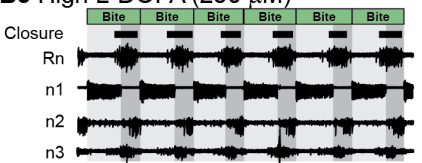
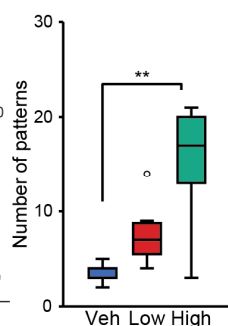
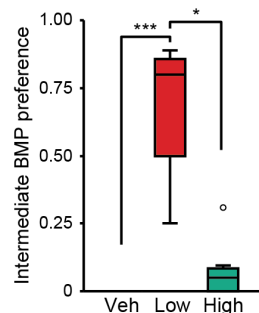
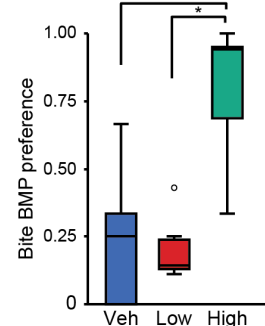
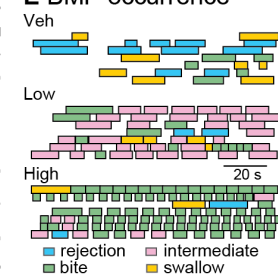
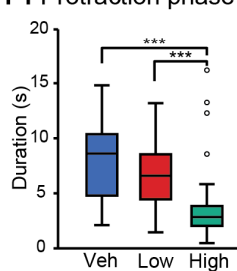
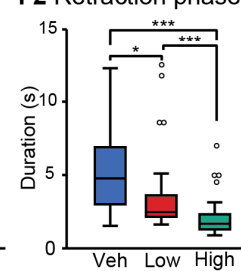
#### 3.3.1 L-DOPA enhances specific fictive behaviors in a concentration dependent manner.

Buccal ganglia were isolated and nerve activity was recorded with suction electrodes to monitor BMPs (see Methods). BMPs consist of two phases. The first phase is protraction, defined here as large unit activity in buccal nerve 1 (n1), and the second phase is retraction, defined here as large unit activity in buccal nerve 2 (n2) and the absence of large unit activity in n1 (see Methods). These phases were previously found to correspond to outward (protraction) and inward (retraction) movement of the radula, a tongue-like structure (Morton and Chiel, 1993a; Neustadter et al., 2002, 2007). Activity of the radula nerve 1 (Rn) mediates closure movement *in vivo*. Greater overlap of Rn activity with retraction corresponds to a larger inward movement of food (Morton and Chiel, 1993a). Therefore, we classified BMPs into four categories based on the overlap of activity in Rn with the retraction phase (Methods and Fig. 3.1A). Two of the BMP categories resembled *in vivo* nerve activity during the ingestion of food (bite and swallow), one category resembled the activity during the rejection of food (rejection), whereas another category resembled nerve activity during

a behavior that resulted in little to no movement of food (intermediate) (Morton and Chiel, 1993a). Each pair of ganglia received treatment of either ascorbic acid (Veh), 40  $\mu$ M (Low) L-DOPA, or 250  $\mu$ M (High) L-DOPA (Fig. 3.1B). Consistent with Kabotyanski et al. (2000), High L-DOPA increased the total number of BMPs (Fig. 3.1B3, 1C) ( $X^2 = 11.513$ ,  $p = 0.003$ ; *post hoc*, Veh vs. High,  $Q = 3.358$ ,  $p = 0.0023$ ; Low vs. High,  $Q = 1.256$ ,  $p = 0.420$ ). Low L-DOPA tended to increase BMPs, but this increase was not significant (Veh vs. Low,  $Q = 2.101$ ,  $p = 0.090$ ). Consistent with Kabotyanski et al. (2000), High L-DOPA increased the preferential expression of bite BMPs (Fig. 3.1B3, 1D2) ( $X^2 = 11.359$ ,  $p = 0.034$ ; *post hoc*, Veh vs. Low,  $Q = 0.086$ ,  $p = 0.996$ ; Veh vs. High,  $Q = 2.875$ ,  $p = 0.011$ ; Low vs. High,  $Q = 2.961$ ,  $p = 0.0086$ ). Low L-DOPA did not increase the preference towards bites but instead increased the preference towards intermediates (Fig. 3.1B2, 1D1) ( $X^2 = 16.145$ ,  $p = 3.1 \times 10^{-4}$ ; *post hoc*, Veh vs. Low,  $Q = 3.947$ ,  $p = 2.3 \times 10^{-4}$ ; Veh vs. High,  $Q = 1.323$ ,  $p = 0.382$ ; Low vs. High,  $Q = 2.624$ ,  $p = 0.024$ ). Veh seemed to express primarily a combination of rejection and swallow BMPs (see Fig. 3.1B1, 1E). These data indicate that L-DOPA increased total BMPs and that different concentrations of L-DOPA can be used to bias selection towards specific BMPs.

### Figure 3.1 Changes in fictive behavior by L-DOPA

Changes in fictive behavior 15 min after treatment with either Vehicle (Veh), 40  $\mu$ M (Low), or 250  $\mu$ M (High) L-DOPA. Each preparation only received a single treatment, which remained in the bath for the duration of the recording. **A**, A histogram of all BMPs recorded in all 21 experiments during the pretreatment observation period and following treatment. Each bin is indicated by a percentage value, calculated by dividing the duration of large unit activity in Rn that occurred during the retraction phase by the total duration of large unit Rn activity during the BMP. This graph indicates that there are four distinct clusters of BMPs that we designate as rejection, intermediate, bites, and swallows. **B**, Nerve recordings for the Vehicle, Low and High treatments showing a 40 s time segment. Protraction phase is marked by light grey and retraction is marked in dark grey. The BMP classification is indicated at the top and closure activity is marked by black boxes. **C**, Summary data for the total number of BMPs. For all box plots, the boundaries of each box are the first and third quartiles ( $Q_1$  and  $Q_3$ ) and the line within the box is the median. The upper and lower extremes are the minimum (or maximum) data value within ( $Q_1$  or  $Q_3$ )  $\pm$  1.5 times the inter-quartile range. Data outside the extremes are marked as open circles. **D1**, Summary data of the preference for intermediate BMPs. A value of one indicates the group exclusively expresses intermediate BMPs. **D2**, Summary data of the preference towards bite BMPs. Sample size for (**C**), (**D1**), and (**D2**) is seven experiments for each group. **E**, The occurrence of BMPs. Each box represents the duration of a single BMP. Each row is an individual experiment. **F1**, Duration of protraction for the different treatment groups. **F2**, Duration of retraction for the different treatment groups. Sample size for the groups in (**F**) is Veh = 24, Low = 54, High = 104 in BMPs. \*  $p < 0.05$ , \*\*  $p < 0.01$ , and \*\*\*  $p < 0.001$ .

**A Distribution of BMPs****B1 Vehicle****B2 Low L-DOPA (40  $\mu$ M)****B3 High L-DOPA (250  $\mu$ M)****C Total BMPs****D1 Intermediates****D2 Bites****E BMP occurrence****F1 Protraction phase****F2 Retraction phase**

To examine whether L-DOPA modified each phase of the BMP, the duration of protraction and retraction was measured for each BMP following treatment. Protraction duration was reduced for High but not Low L-DOPA (Fig. 3.1F1) ( $\chi^2 = 65.499$ ,  $p = 5.9 \times 10^{-15}$ , *Post hoc*, Veh vs. Low,  $Q = 1.034$ ,  $p = 0.555$ , Veh vs. High,  $Q = 6.07$ ,  $p = 4.8 \times 10^{-9}$ , Low vs. High,  $Q = 6.692$ ,  $p = 1.0 \times 10^{-9}$ ). Retraction duration was reduced for Low ( $\chi^2 = 65.232$ ,  $p = 6.9 \times 10^{-15}$ , *Post hoc*, Veh vs. Low,  $Q = 2.635$ ,  $p = 0.023$ )<sup>e</sup> and was reduced to a greater extent by High L-DOPA (Fig. 3.1F2) (Veh vs. High,  $Q = 5.618$ ,  $p = 1.0 \times 10^{-9}$ ; Low vs. High,  $Q = 5.618$ ,  $p = 5.9 \times 10^{-8}$ ). Many neurons in the feeding circuit can be designated as protraction or retraction neurons based on the phase in which they are primarily active. The above results suggest that protraction neurons may be less sensitive to L-DOPA than are retraction neurons. Reduction in retraction neuron activity duration due to Low L-DOPA may bias the network towards intermediate BMPs, whereas combined reductions in protraction and retraction neuron activity duration due to High L-DOPA may bias the network towards bite BMPs. This hypothesis was tested with VSD imaging of neuronal activity.

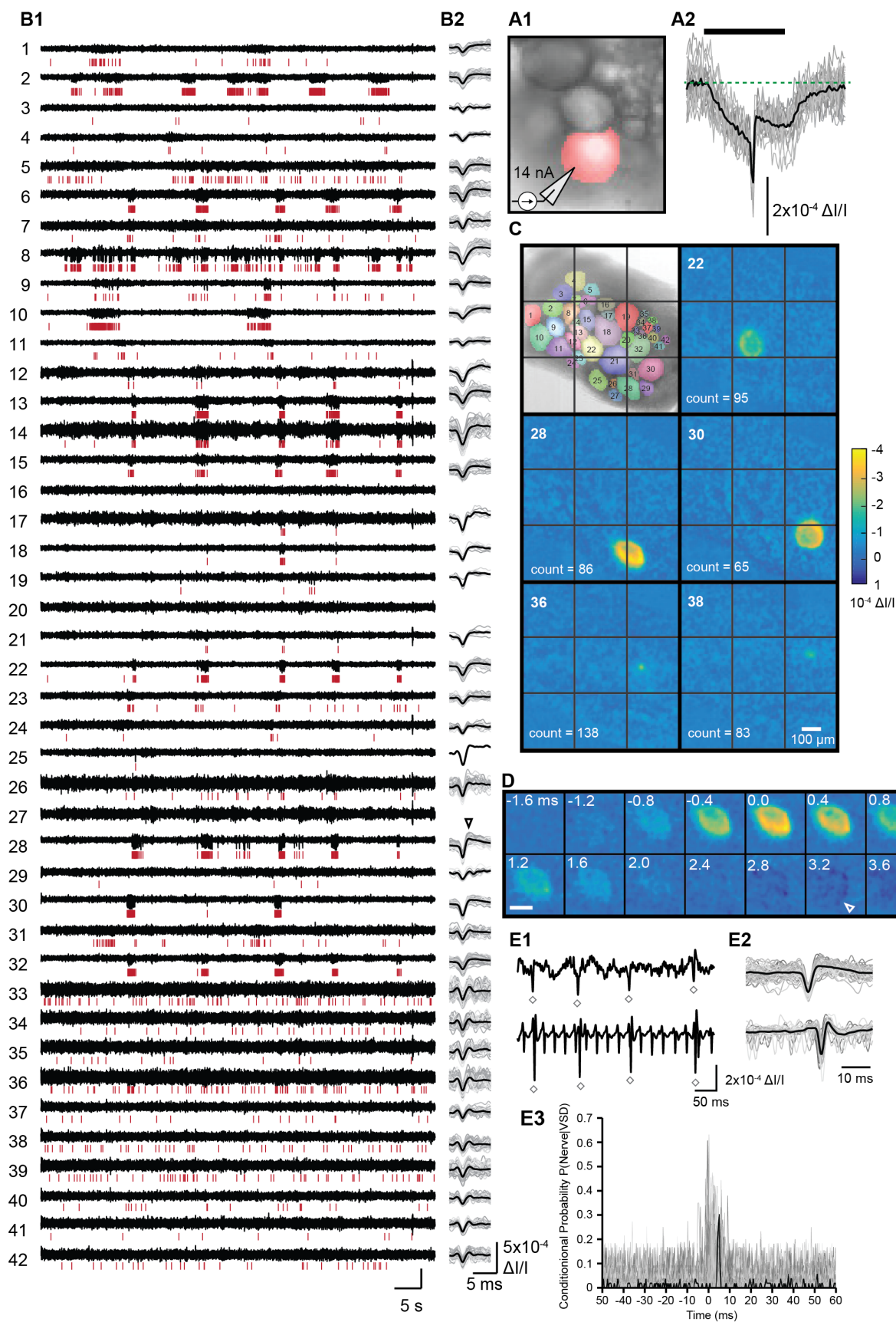
### **3.3.2 VSD imaging captures spike activity in a large number of neurons of the buccal ganglia.**

To gain insight into the ways in which changes in neuronal activity mediate the changes in fictive motor programs induced by L-DOPA, the spiking pattern of neurons in the buccal ganglia was examined using the absorbance voltage-sensitive dye RH-155. This dye has been used in the pedal ganglia of *Aplysia* (Bruno et al., 2015). To confirm its efficacy in the buccal ganglia, changes in light absorbance were recorded in neuron B4 during stimulation of B4 by intracellular depolarizing current pulses (14

nA, 50 ms) (Fig. 3.2A). VSD traces exhibited a prominent downward spike (increase in absorbance) resembling an action potential that was superimposed on a more sustained downward deflection resembling a depolarization induced by the current injection. The action potential was followed by a signal corresponding to the spike afterhyperpolarization.

**Figure 3.2** VSD imaging of neuronal activity in the buccal ganglia.

**A1**, Image of the caudal surface of the ganglion for (**A2**). The pixels that were averaged are highlighted in red. **A2**, VSD responses to 20 intracellular current injections, aligned to the action potential detected in the nerve (n3). Green dotted line marks the baseline prior to current injection. For (**A2**), (**B2**) and (**E2**) individual examples are grey and the average trace is black. Thick black line indicates the current injection. **B1**, VSD (black trace) of 42 neurons recorded simultaneously. Detected spikes are indicated by red vertical lines below each trace. Each trace was generated by averaging the pixels highlighted for each neuron in the top left image of (**C**). **B2**, Temporally aligned action potentials detected in the corresponding trace in (**A1**). Note the prominent AHP in cell 28 (arrowhead). **C**, Image of VSD response during the peak of the waveform of all the detected spikes that occurred in (**B**) for that neuron. The neuron designation is in the top left of each image. Image of the ganglion (caudal surface) with the neuron designations is the top left image. The number of spikes averaged for each neuron is indicated in the bottom left-hand corner. **D**, Individual frames of neuron 28 during and after an action potential. Arrowheads point to the presumed AHP. **E**, Coincidence of spikes between the nerve and neuron indicated the presence of an axonal projection. **E1**, Example recording segment of a neuron whose action potentials detected by VSD (top trace) coincide with a distinct spike in the nerve (bottom trace). **E2**, VSD traces (top) and nerve traces (bottom) of example in (**E1**) aligned by the peak of the VSD signal. Note the nerve spike follows the VSD spike with a constant delay. **E3**, Probability of an action potential in the nerve given a spike in the neuron at time zero. Displayed is every neuron-nerve pair for all experiments in this study. A sharp peak in conditional probability with a time delay of a few ms indicates an axonal projection. Dark line represents the example in (**E1**).





Next, spiking activity was recorded in 20 – 130 neurons simultaneously over a 2 min recording period (Fig. 3.2*B*). Some of this activity occurred in bursts (e.g., cell 28), whereas activity in other neurons was more sparse (e.g., cell 19). We then converted the activity to spike trains using a spike detection algorithm (Methods) and verified that the VSD signals corresponding to the spikes were localized to the neuron of interest (Fig. 3.2*C*). Two frames were averaged during the baseline period just prior to the spike and subtracted from the average of 3 frames at the peak of the spike. This subtracted image was calculated for each detected spike and averaged for all spikes that occurred in that neuron during a 2 min recording period (Fig. 3.2*C*). The averaged subtracted image revealed a VSD signal which closely matched the shape and position of the cell for which the spikes were detected. Importantly, even recordings associated with higher levels of baseline noise (e.g., cell 36) had a signal localized to that particular neuron. Moreover, VSD recordings exhibited signals associated with presumed spike afterhyperpolarizations (AHP) as indicated by an upward deflection after the spike (e.g., arrow in Fig. 3.2*B2*) and decrease in absorbance in the pixels overlaying the neuron (arrows in Fig. 3.2*D*).

Combining VSD with extracellular nerve recordings enables the monitoring of BMPs while also enabling the detection of axonal projections of the recorded neurons. Previous work in the buccal ganglia (Morton et al., 1991) used averaging of extracellular nerve recordings triggered by spikes detected in VSD recordings to detect axonal projections by the emergence of a waveform in the averaged trace. That method requires averaging a large number of action potentials in order to average out randomly occurring large amplitude spikes. Instead, we used spike coincidence to

detect action potentials in the nerve that follow an action potential in the neuron with a relatively constant delay (Fig. 3.2E1-2). To obtain a quantitative method of distinguishing neurons with axonal projections we graphed the probability an action potential occurring in the nerve at different time delays relative to an action potential in the neuron,  $P(\text{nerve} | \text{neuron})$ . We noticed a sharp peak in probability following the action potential in the nerve. This peak was used to estimate the spike coincidence and detect an axonal projection algorithmically (Methods, Fig. 3.2E3).

These data provide evidence that high spatial and temporal resolution imaging can record activity of a large number of neurons simultaneously in the buccal ganglia and can be used to detect axonal projections. We next examined the ways in which L-DOPA reconfigures the activity of neurons mediating the BMPs.

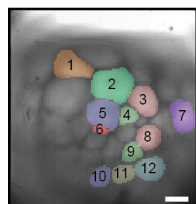
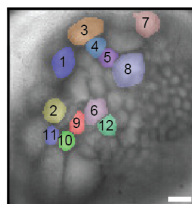
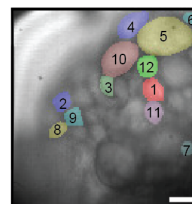
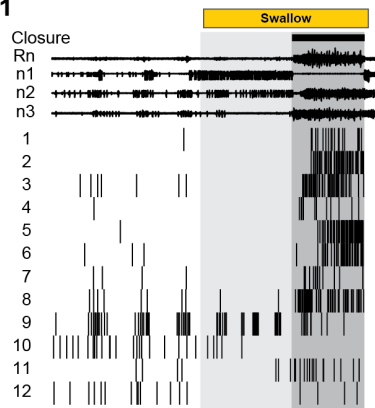
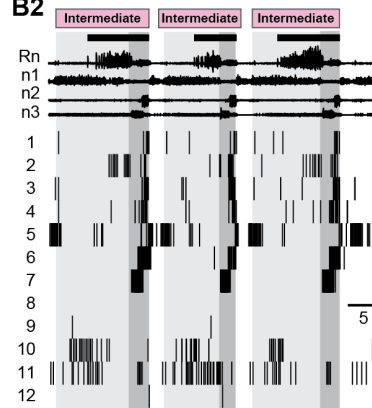
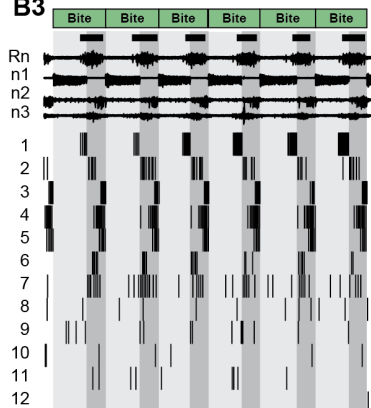
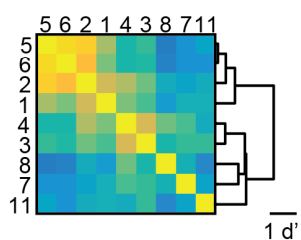
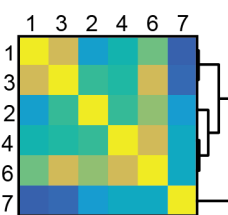
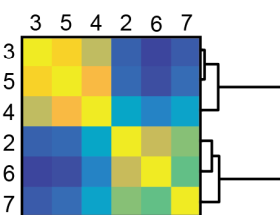
### **3.3.3 L-DOPA modifies neuronal activity without increasing neuronal synchrony.**

As a first step, we examined the extent to which neuronal activity recorded by VSD corresponded to the phases of the BMP. For data analysis we focused only on neurons with bursting activity (for definition, see Methods) and did not include neurons with tonic or sparse activity, because bursting neurons mediate the majority of the features observed during a BMP (Baxter and Byrne, 2006; Cropper et al., 2004; Elliot and Susswein, 2002; Nargeot and Simmers, 2012; Wu et al., 1988). There were  $28.6 \pm 6.0$  (29.6% of total within field of view) neurons per experiment categorized as bursting in Veh,  $25.5 \pm 4.6$  (25.5%) in Low L-DOPA, and  $31.3 \pm 3.2$  (31.3%) in High L-DOPA, with no significant differences among the groups ( $\chi^2 = 1.789$ ,  $p = 0.409$ ). Spike activity was recorded following treatment with either Veh, Low, or High. The

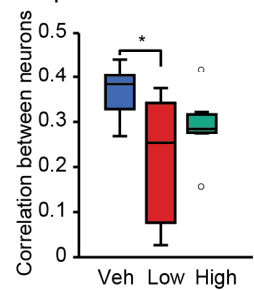
activity of neurons occurred during specific phases of the BMP. For example, in Fig. 3.3*B1* neurons 1 – 8 and 11 seemed to fire primarily during the retraction phase, whereas neuron 1 in Fig. 3.3*B3* was primarily active during the protraction phase. The VSD recordings revealed that the L-DOPA-induced changes in BMPs as monitored via nerve recordings (Fig. 3.1) are due to enhanced rhythmic activity in a large number of neurons in the buccal ganglion. Interestingly, each neuron tended to be recruited at specific times within a particular phase even when the phase was shorter in duration (e.g., in High treated preparations, Fig. 3.3*B3*) suggesting the synchrony of neuronal activity was not increased by L-DOPA.

### Figure 3.3 Changes in fictive behavior and neuronal activity by L-DOPA

Changes in fictive behavior and neuronal activity 15 min after treatment with either Veh, Low or High L-DOPA. A 40 s segment is shown. Recording segment same as for Fig. 1. **A**, Images of the ganglion (caudal surface). Neurons whose activity is shown in (**B**) are highlighted. **B**, (Top) Recordings of Rn and n1-3 nerve activity. (Bottom) Raster of VSD activity recorded simultaneously with nerve activity. Each row is an individual neuron with the location in the image marked in (**A**). Vertical black lines indicate an action potential. Light grey indicates protraction. Dark grey indicates retraction. Closure activity is marked by black boxes. The BMP classification is indicated at the top of the traces. **C**, Correlation matrices for the recordings in (**B**). Numbers correspond to the cell designations in (**A**) and (**B**). Only neurons primarily active during retraction are shown in the correlation matrix. The dendrogram of each matrix is shown on the right. **D**, Mean pairwise correlation between neurons. Sample sizes were seven for each treatment group. Time bin was 0.5 s.

**A1 Veh****A2 Low****A3 High****B1****B2****B3****C1 Veh example****C2 Low example****C3 High example**

Correlation coefficient

**D Mean pairwise correlation**

To analyze neuronal synchrony, the correlation coefficient was examined for each pair of retraction neurons in a given preparation (Fig. 3.3C-D) (for details see Methods). We focused on retraction neurons for the correlation analysis because retraction neurons seemed most reliably activated during BMPs. Pairwise correlation matrices of the examples in Fig. 3.3B revealed high correlation coefficients between several neurons for Veh (e.g., cells  $2 \leftrightarrow 1$ ,  $5 \leftrightarrow 2$ ,  $5 \leftrightarrow 6$ ), Low (e.g., cells  $3 \leftrightarrow 1$ ,  $6 \leftrightarrow 3$ ,  $6 \leftrightarrow 4$ ), and High (e.g., cells  $4 \leftrightarrow 3$ ,  $5 \leftrightarrow 3$ ,  $6 \leftrightarrow 2$ ). If the L-DOPA-induced decrease in retraction phase duration resulted in an increase in synchrony between neurons, the correlation matrix would become more homogenous and the mean pairwise correlation would increase. Cluster analysis of the correlation matrices of Veh, Low, and High identified several groups of neurons. For the preparations of Fig. 3.3C-D, these groups are indicated by the dendrograms to the right of each matrix. In the example for Veh, neurons could be separated into groups {5, 6, and 2}, {4 and 3}, and {8, 7, and 11}, the Low example could be separated into groups {1 and 3}, {2, 4, and 6}, and 7, and the High example could be separated into groups {3, 4, and 5} and {2, 6, and 7}. We next averaged the pairwise correlation coefficient for every pair of retraction neurons for each experiment, and compared the mean correlation coefficient between treatments. Low L-DOPA did not increase but instead decreased the mean pairwise correlation, whereas High L-DOPA led to no significant change ( $X^2 = 6.264$ ,  $p = 0.044$ , *Post hoc*, Veh vs. Low,  $Q = 2.498$ ,  $p = 0.033$ , Veh vs. High,  $Q = 1.378$ ,  $p = 0.352$ , Low vs. High,  $Q = 1.120$ ,  $p = 0.502$ ). These results indicate that L-DOPA did not increase, and indeed Low somewhat decreased (by  $\sim 0.1$ ), the synchrony of neuron activity, suggesting that the unique timing of neuronal activity

remains an important feature even when the durations of the respective phases are substantially shorter. The unique timing of activity of each neuron within a given phase despite reduced phase duration highlights the intricacies of the phasic activity of the neurons within the circuit, warranting a more detailed investigation of L-DOPA-induced changes in the timing of activity of individual neurons during BMPs.

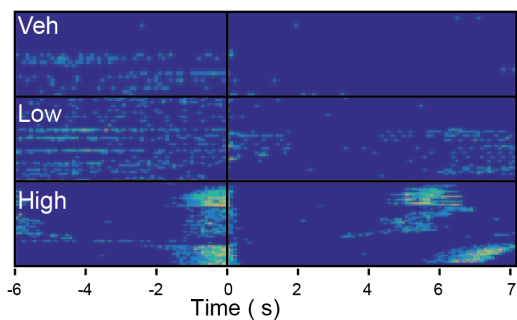
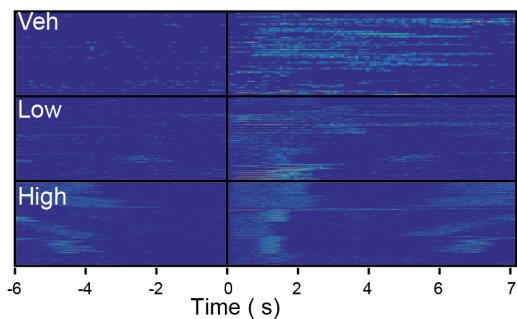
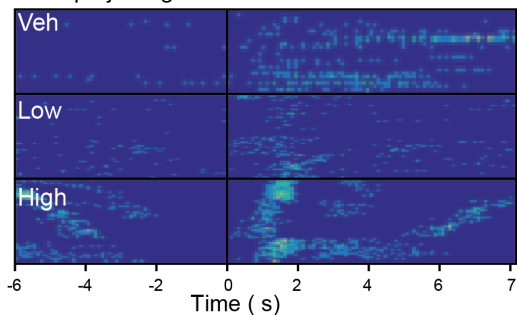
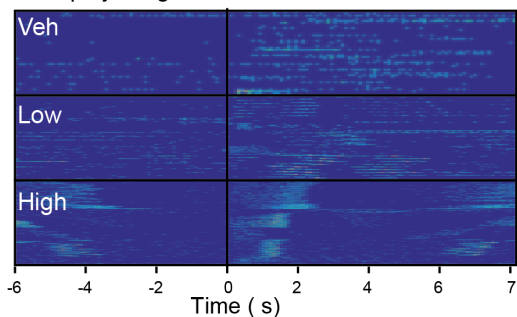
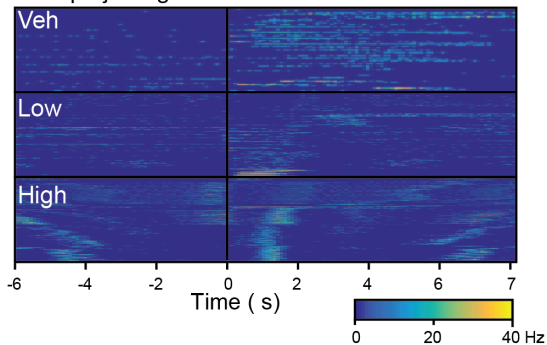
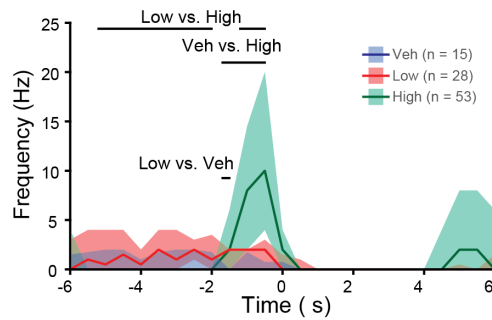
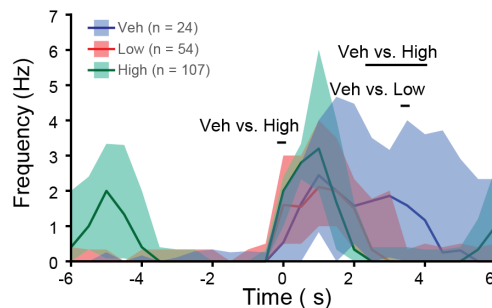
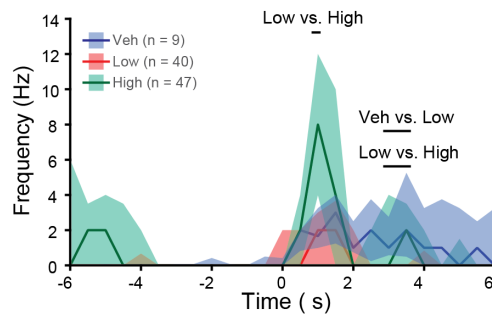
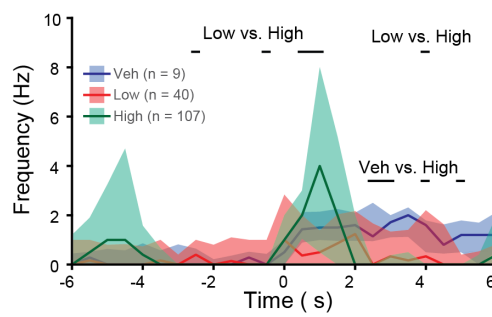
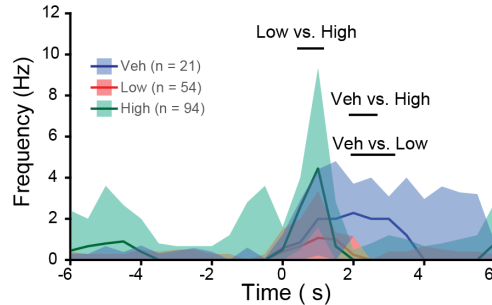
#### **3.3.4 L-DOPA reconfigures activity of specific subgroups of neurons.**

We next examined the ways in which the features of the BMP were associated with changes in the timing of neuronal activity during BMPs. We first separated the neurons according to their preferred phase (protraction or retraction) (see Methods) and then used peri-event histograms aligned to the start of the retraction phase to compare neuronal activity among treatments. A histogram of the average activity of all neurons in each time point was calculated for each BMP in each treatment group. The activity of every bursting neuron in every BMP in each treatment is depicted in Fig. 3.4A and the summary data for all the BMPs in each treatment is depicted in Fig. 3.4B.

**Figure 3.4** The temporal dynamics of specific groups of neurons are modified by L-DOPA.

**A**, The activity of each neuron during each BMP aligned to the start of retraction phase for protraction, retraction, Rn, n2 and n3 projecting neurons following treatment with Veh, Low, or High L-DOPA. Time bin was 0.1 s. **B**, Peri-event histograms for the data in (A). Horizontal bars indicate a significant difference between the specified groups at those time points. Peaks in activity outside  $\pm 4$  s for High are due to activity in adjacent BMPs. The fill represents the interquartile range and the line represents the median level of activity of each time point. Sample size is number of BMPs.



**A1 Protraction****A2 Retraction****A3 Rn projecting****A4 n2 projecting****A5 n3 projecting****B1****B2****B3****B4****B5**

We first examined protraction neurons, which have many important functions such as initiating BMPs and protracting the radula outward to grasp food (Hurwitz et al., 1994, 1996, 1997; Kabotyanski et al., 1998; Susswein and Byrne, 1988; Teyke et al., 1993). Because High L-DOPA yielded the greatest increase in frequency of BMPs, we predicted an increase in activity of protraction neurons in preparations treated with High L-DOPA. The peri-event histogram for protraction neurons (Fig. 3.4B1) indicated a prominent peak of activity prior to the start of the retraction phase, which appeared to have a substantially shorter duration in High L-DOPA (as indicated by a decrease in activity at earlier time points) and a substantially greater level of activity near the end of the protraction phase (Fig. 3.4A1, B1). These data indicated that only High L-DOPA increased the spike frequency and decreased the duration of protraction neuron activity, suggesting that changes in protraction neuron activity may be important for bite, but not intermediate BMPs. These activity changes may help to explain the increase in total patterns in High L-DOPA.

The second group examined was neurons active primarily during retraction. These neurons are important for retracting the radula inward and either releasing or maintaining the grip on food (e.g., Church and Lloyd, 1994; Cropper et al., 2004; Evans and Cropper 1998; Hurwitz and Susswein 1996; Plummer and Kirk, 1990; Sasaki et al., 2013). The peak frequency of retraction neuron activity was not significantly different between the treatments, but the activity was shorter in duration in the Low and High groups as compared to Veh, as indicated by a significant decrease in activity at later time points for Low and High groups compared to Veh (Fig. 3.4A2, B2). The decreased durations for both Low and High L-DOPA suggest

that changes in the activity of retraction neurons may be important for switching to both intermediate and bite BMPs, whereas changes in protraction neurons seemed to be important only for switching to bite BMPs.

We next examined the effects of L-DOPA on neurons that project axons through specific nerves. Neurons projecting through Rn mediate closure of the radula to grip food (Morton and Chiel, 1993b), whereas neurons projecting through n2 and to a lesser extent n3 mediate backward movement of the radula (Church and Lloyd, 1994). Neurons were separated according to whether they projected axons through Rn, n2, or n3, which was determined by the coincidence of spikes in the neuron with spikes in the nerve (see Fig. 3.2E). We only detected a few neurons with an axonal projection through n1 so this group was excluded. Rn, n2, and n3 projecting neurons were active primarily during the retraction phase (Fig. 3.4A3-5, B3-5). The activity of Rn projecting neurons persisted for longer in the Veh group compared to Low L-DOPA, as indicated by less activity in Low at later time points compared to Veh (Fig. 3.4A3, B3). Preparations treated with High L-DOPA had an increase in peak spike frequency compared to Low. These data indicate that Rn neurons in Low L-DOPA had a reduced duration of activity, whereas the High treated group had a boost in frequency and a reduction in duration. n2 projecting neurons had a decrease in duration of activity and increase in spike frequency in High L-DOPA but did not seem to be greatly affected by Low L-DOPA (Fig. 3.4A4, 3.4B4). For n3 projecting neurons, Low L-DOPA reduced the duration of activity without changing the peak frequency (Fig. 3.4A5, B5). However, the peak frequency of n3 neurons was increased in High treated preparations compared to Low. The increase in frequency of n2 and n3

projecting neurons in High L-DOPA may cause downstream activation of the Rn projecting neurons, as well as activating other neurons such as B8 which were outside the focal plane. These effects in concert may drive a switch to predominantly bite BMPs. None of these effects among the treatment groups were associated with any differences in the number of neurons classified as protraction ( $X^2 = 0.998$ ,  $p = 0.607$ ; Veh =  $0.9 \pm 0.3$ ; Low =  $0.9 \pm 0.3$ ; High =  $0.6 \pm 0.2$ ), retraction ( $X^2 = 0.800$ ,  $p = 0.670$ ; Veh =  $4.7 \pm 1.0$ ; Low =  $5.7 \pm 0.6$ ; High =  $5.4 \pm 0.3$ ), Rn projecting ( $X^2 = 0.236$ ,  $p = 0.889$ ; Veh =  $4.6 \pm 2.3$ ; Low =  $4.0 \pm 1.3$ ; High =  $2.6 \pm 0.5$ ), n2 projecting ( $X^2 = 1.051$ ,  $p = 0.591$ ; Veh =  $9.1 \pm 4.7$ ; Low =  $12.6 \pm 4.2$ ; High =  $7.3 \pm 2.0$ ), or n3 projecting ( $X^2 = 1.628$ ,  $p = 0.443$ ; Veh =  $11.9 \pm 4.3$ ; Low =  $17.6 \pm 5.2$ ; High =  $7.4 \pm 2.0$ ).

L-DOPA-induced changes in peri-event histograms indicate that specific features of neuronal activity are modulated in a variety of ways to select for intermediate or bite BMPs. Some of these changes could be mediated by shifting the time at which bursts of activity occur in each neuron, or involve changes in burst duration and spike frequency within bursts. To gain a better understanding of the ways in which L-DOPA modified activity, we next examined the modulation of burst properties in each of these groups of neurons by L-DOPA.

### **3.3.5 L-DOPA uniquely modifies the burst activity of specific subgroups of neurons**

Changes in the timing of burst activity can cause dramatic changes to the characteristics of BMPs (e.g., Jing and Weiss, 2001). The timing of burst activity (latency and duration) and activity within bursts (number of spikes and spike frequency) (Fig. 3.5A) were measured for every bursting neuron in each BMP,

allowing examination of how these features are modified by L-DOPA to switch to intermediate and bite BMPs. For example, a decrease in burst duration and latency combined with an increase in frequency would indicate a compression of spike activity. On the other hand a reduction in duration without any change in frequency or latency would indicate truncation of spike activity. For the neuronal subgroups defined above, the timing of burst activity is shown visually in Fig. 3.5*B* and quantitatively in Fig. 3.5*C*. We delineated the major changes induced by L-DOPA.

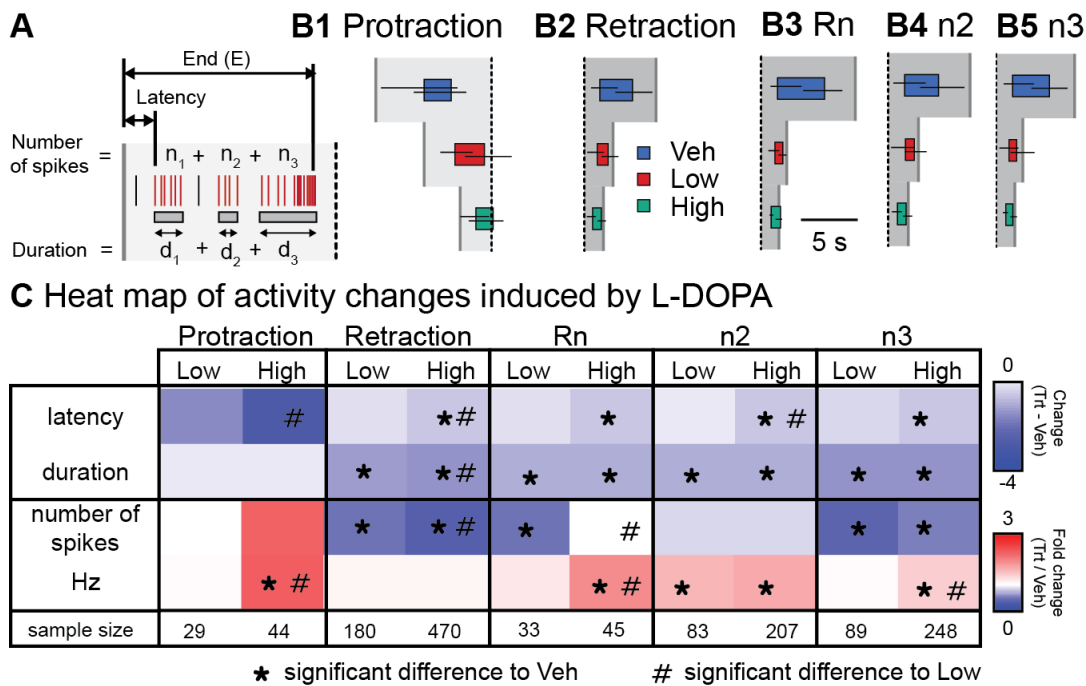


**Figure 3.5** L-DOPA differentially modified the burst properties of neurons.

**A**, A diagram depicting the measurements. The latency is the start of the first burst overlapping with the phase. The duration is the sum of the duration of all bursts for that neuron during the phase. The burst end time is the end of the last burst overlapping with the phase. The number of spikes is the sum of spikes within all the burst overlapping that phase. Frequency is the number of spikes divided by the burst duration. **B**, Graphical representation of the burst timing during a BMP. The colored box represents the median start and end time for bursts in that treatment. The horizontal lines represent the interquartile range for the start and end time of the bursts. The vertical grey lines in B1 indicate the median start of protraction. The vertical grey lines in B2-B5 indicate the median end of retraction. The vertical dotted line indicates the start of retraction. **C**, A matrix of the L-DOPA induced changes in burst times and spiking activity. For display purposes, Veh median start and duration were subtracted from the median start and duration of either Low or High. For spiking activity, the number or frequency of spikes was divided by the median number or frequency of spikes in Veh. \* indicates significance relative to Veh and # indicates significance relative to Low. The sample size is the number of bursts examined.

Protraction neurons were only modified significantly by High L-DOPA. In this treatment group, the burst latency was reduced compared to Low L-DOPA without any change in burst duration for either concentration. In addition, protraction neurons had a significant increase in spike frequency within bursts. These results indicate that the bursts in protraction neurons were shifted to an earlier time in relation to the phase with a concomitant boost in spike activity. For retraction, Rn, and n3 neurons, Low L-DOPA did not change the burst latency or the spike frequency but significantly decreased the burst duration and the number of spikes within bursts, indicating that the spike activity of these neurons was truncated (i.e., blocked at later time points without affecting earlier time points) by Low L-DOPA. For Rn, n2, and n3 neurons, High L-DOPA significantly reduced the burst latency and duration and increased the spike frequency within bursts, suggesting that the spike activity was compressed. For n2 neurons, Low L-DOPA significantly decreased the burst duration and increased the spike frequency without changing the burst latency. It is interesting that despite no apparent change in the activity histogram for n2 neurons in Low L-DOPA (Fig. 3.5*B*, *C*), analysis of individual bursts indicates that changes in n2 were in fact occurring. Retraction neurons treated with High L-DOPA had a decrease in burst latency and duration and in the number of spikes, without a change in spike frequency. These data indicate that Low and High L-DOPA modulate the timing of burst activity for different groups of neurons in different ways. Protraction neurons are most affected by High L-DOPA, whereas retraction, Rn, n2, and n3 projecting neurons are affected by both Low and High L-DOPA, with Low mainly truncating activity and High mainly compressing activity.

### 3.2.6 L-DOPA preferentially activates neurons located in different regions of the ganglia.

Previous studies in *Aplysia* using backfill tracing have found distinct clusters of neurons projecting through individual nerves (Jelescu et al., 2013; Martínez-Rubio et al., 2009; Morton et al., 1991; Scott et al., 1991), however backfill tracing cannot examine the distribution of neurons active at particular time points during a BMP. To examine the spatial organization of neurons using VSD imaging of the feeding circuit we aligned VSD images (see Methods), marked the location of bursting neurons, and pooled the data from all experiments. Analysis of the spatial distribution indicated that protraction, retraction, Rn, n2, and n3 projecting neurons were localized in distinct but overlapping regions of the ganglia (Fig. 3.6). The distribution of Rn, n2, and n3 projecting neurons roughly agrees with previous observations (Jelescu et al., 2013; Morton et al., 1991; Scott et al., 1991). We next compared the spatial distribution of the ensemble of neurons active during BMPs in the pooled data of each treatment group (Fig. 3.7). The locations of neurons were marked if the neuron was active with at least one spike during the 0.5 s time bins. The spatial distribution of active neurons varied greatly between each time bin and for each treatment. Active neurons tended to be clustered in Low L-DOPA (for example Fig. 3.7A3e), whereas in the Veh or High L-DOPA treated groups the neurons were more widely distributed (e.g., Fig. 3.7A4b). The centroid and pairwise distances of the pooled data were used to quantitatively compare the distribution of active neurons among treatment groups. A line that tracked the centroid of all active neurons across experiments was plotted over time (Fig. 3.7B). The centroid of the Veh group tended to be near the center of the ganglia



while the centroids of the Low and High L-DOPA treated groups tended to be localized more to the upper right (ventrolateral) or left (ventromedial), respectively. The path of the centroid of the Low never overlapped with the High and only briefly overlapped with Veh (Fig. 3.7B). This result indicates that neurons active in the different treatment groups tended to be localized in different regions of the ganglia. The width of the spatial distribution was measured by the average pairwise distance between neurons for each time bin. For all treatment groups the average pairwise distance increased shortly after the start of the retraction phase. The average pairwise distance was reduced in the Low treated group as compared to High treated group ( $\chi^2 = 12.192$ ,  $p = 0.0023$ ;  $Q = -3.451$ ,  $p = 0.0016$ )<sup>v</sup> and trended towards a reduction in Low compared to Veh ( $Q = -1.263$ ,  $p = 0.073$ ) indicating that the activated neurons were more tightly clustered in the Low L-DOPA treated group. Taken together, these results indicate that L-DOPA-induced selection of intermediate and bite BMPs recruited groups of neurons that tended to be located in different but overlapping regions of the ganglia.

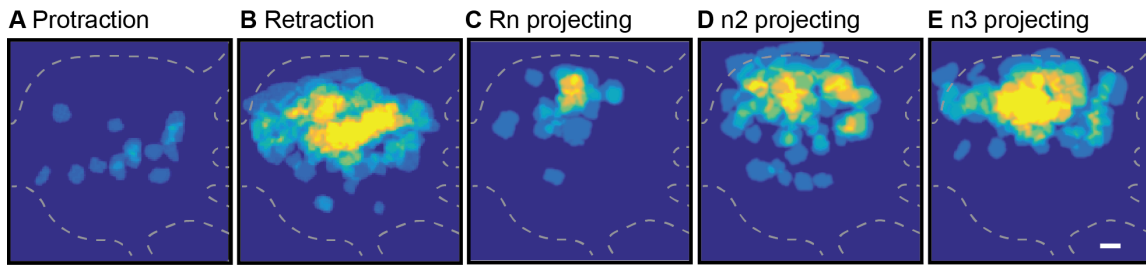


**Figure 3.6** Spatial distribution of protraction, retraction, Rn, n2, and n3 projecting neurons.

**A**, Protraction neurons are clustered near the center. **B**, Retraction neurons are near the upper middle. **C**, Rn projecting neurons are in the center upper region. **D, E**, n2 and n3 neurons are in the top most region of the ganglia. Caudal surface with the buccal commissure on the left. Scale bar is 100  $\mu\text{m}$ .

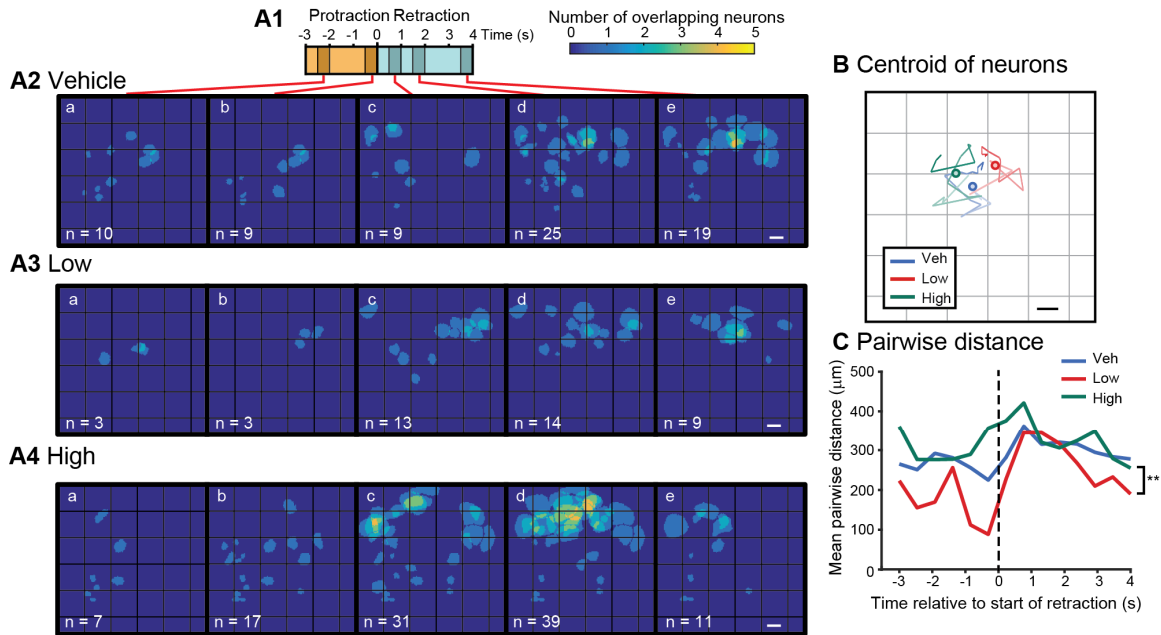


**Figure 3.7** L-DOPA recruits neurons with different spatial distributions.

**A1**, Timeline of a BMP. **A2 – A4**, Images of the locations of all neurons activated at the time bins indicated in (**A1**) from all experiments within a given treatment. The pixels for each overlaying ROI were summed. The number at the bottom left is the number of neurons activated. Caudal surface with the buccal commissure on the left. Scale bar is 100  $\mu\text{m}$ . **B**, The centroid of all neurons as it progresses through each time bin in (**A1**). The path increases in opacity for later time points. The filled circle marks the mean of all the centroids. **C**, Mean pairwise distance between neurons for each time bin. \*\* p < 0.01.

### 3.3 Discussion

Combined VSD and nerve recordings of isolated buccal ganglia revealed that Low L-DOPA biased the feeding network towards intermediate BMPs and High L-DOPA biased the network towards bite BMPs, whereas Veh seemed to express primarily rejections and swallows (Fig. 3.8A). L-DOPA is likely enhancing the release of DA from dopaminergic neurons B65 and B20 (Kabotyanski et al., 1998; Jing and Weiss, 2001). However, increased spontaneous release from dopaminergic afferents is another possibility. Low and High L-DOPA induced a wide variety of effects on neuronal activity (Figs. 3.4 – 5). The differential modulation of neurons suggests that L-DOPA is not acting simply by enhancing or suppressing activity overall, but by specifically modulating neurons in different ways. Currently, it is unclear what molecular mechanisms mediate this differential modulation. In mammals, differential modulation is mediated at least in part by the selective expression of D1-like and D2-like receptors, which have different sensitivities to dopamine (Beaulieu and Gainetdinov, 2011). A D1-like receptor has been characterized in *Aplysia* (Barbas et al., 2006) and some of the components of its downstream signaling cascade have been examined for the identified retraction neuron B51 (Lorenzetti et al., 2008). A genome-wide sequencing has also predicted a D2-like receptor (NCBI: NW\_004797500.1). An intriguing possibility is that neurons express different ratios of D1 and D2-like receptors, similar to the striatum in mammals (Schultz, 2013). Low L-DOPA could predominantly activate high affinity D2 receptors resulting in a switch to intermediate BMPs, while High L-DOPA could predominantly activate low affinity D1 receptors resulting in a switch to bite BMPs.

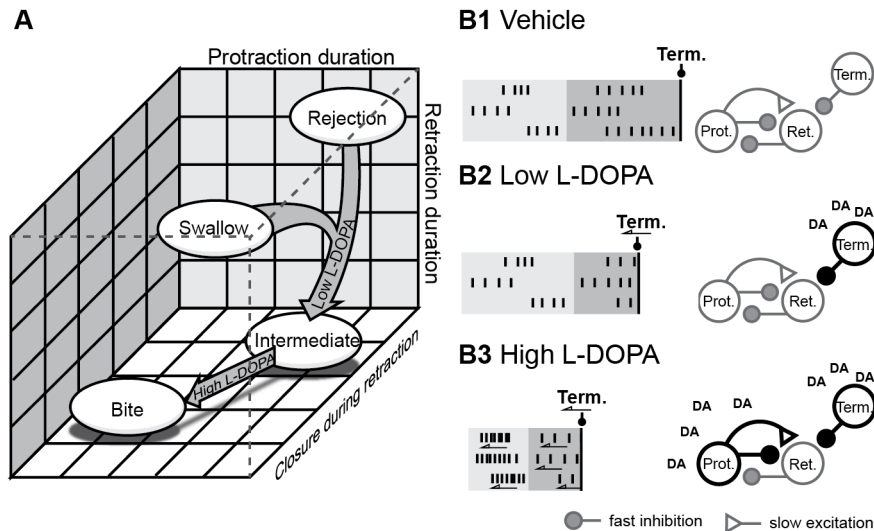


**Figure 4.2.1** Summary of the L-DOPA effects on neuronal activity.

**A**, Low L-DOPA biased the selection of BMPs toward intermediates starting from primarily rejection and to a lesser extent swallows (see Veh in Fig. 1E). High L-DOPA biased the selection of BMPs towards bite BMPs. **B**, Summary of the changes in activity (left) and the proposed mechanism (right). **B1**, Activity in Veh. Vertical lines signify action potentials. Light grey is protraction phase. Dark grey is retraction phase. Black line is the onset of activity of BMP terminating (Term.) neurons. Grey outlines indicate basal conditions while black outlines indicate enhancement. Protraction spike frequency is enhanced. **B2**, Activity in Low L-DOPA. The bursts are truncated because the terminating neurons are being activated sooner (arrow). **B3**, Activity in High L-DOPA. The enhancement of protraction neurons more rapidly activates retraction neurons.

High L-DOPA treatment led to an increase in the number of BMPs (Fig. 3.3) and increase in protraction neuron activity (Fig. 3.4A, 3.5B). This increase could be due to an increase in excitability of protraction neurons. Indeed, increasing the excitability of protraction neurons enhances the frequency of BMPs (Seiling et al., 2014). In addition, DA increases the excitability and spike frequency of a protraction neuron, B67 (Serrano and Miller, 2006). Increased excitability would cause these neurons to be activated more rapidly, decreasing the burst latency (Fig. 3.8B3). The enhanced activation of protraction neurons could, in turn, increase synaptic drive to more rapidly activate retraction, Rn, n2, and n3 neurons, which terminate the protraction phase by feedback inhibition (e.g., Hurwitz and Susswein, 1996). BMPs are terminated by inhibitory neurons (e.g., B52) activated via rebound excitation at the end of the retraction phase (Fig. 3.8B1) (Plummer and Kirk, 1990). DA also increases the rebound excitation and sag potential in neuron B8 (Díaz-Ríos and Miller, 2005; Kabotyanski et al., 1998). One intriguing possibility is that Low and High L-DOPA increase the rebound excitation of BMP-terminating neurons like B52, causing these neurons to activate earlier, in turn terminating the activity of retraction neurons (Fig. 3.8B2-3).

The Rn projecting neuron B8 shifts from being primarily active during protraction in rejection BMPs to being primarily active during retraction in bite and swallow BMPs (Morton and Chiel, 1993b). Unexpectedly, we did not observe a shift in the phase of activity in Rn projecting neurons as we did for the Rn population activity. B8 is typically below the focal plane of our recordings. Thus, an explanation

for this discrepancy is that the Rn projecting neurons we recorded were not likely to be B8 and thus were not likely responsible for large unit activity in Rn.

We also found that neurons with different properties (i.e., preferred phase of activity or axonal projections) are located in distinct but overlapping regions of the ganglia (Fig. 3.7). Neurons with similar properties or functions may be connected with chemical or electrical synapses, which may be facilitated by such topographical organization. For example, the neurons B31 and B32 as well as B4 and B5 are highly coupled to each other and are adjacent to each other (Gardner, 1977; Susswein and Byrne, 1988). In addition, different concentrations of L-DOPA recruited ensembles of neurons with different spatial distributions. These ensembles could be specific to the BMPs (e.g., an intermediate or bite ensemble) or could be specific to the concentrations of L-DOPA. A way of distinguishing between these two possibilities would be to elicit intermediate or bite BMPs using other methods (e.g., neuropeptides or intracellular stimulation of command-like neuron CBI-2 and CBI-11 (Wu et al., 2014)) to examine whether the spatial distribution using other methods is similar to those of Low or High L-DOPA. A finding of similarity would suggest that these ensembles are specific to the BMPs and not the concentrations of L-DOPA.

We observed a general increase in rhythmic motor patterns and alterations to motor patterns depending on the level of L-DOPA and presumably enhancement of DA release by L-DOPA, which is similar to studies in other systems. In leech, DA application elicits rhythmic bursts of motor neurons in a crawl-like pattern (Puhl et al., 2008, 2012), and DA increases the rebound excitation and decreases the AHP to different extents in two crawl-related motor neurons (Crisp et al., 2012). In lamprey,

DA affects swim patterns in a concentration dependent manner, with low concentrations (0.1 – 10  $\mu$ M) increasing swim frequency and higher concentrations decreasing swim behavior. The increase in swim is due to an increase in the excitability (via suppression of AHP) of motor neurons, edge cells, giant interneurons, and dorsal cells, as well as a decrease in inhibition from commissural interneurons (Kemnitz, 1997). DA evokes multirhythmic motor patterns in neonatal mice (Sharples and Whelan, 2017) and increases the excitability of motor neurons and the glutamatergic transmission they receive (Han et al., 2007). In the above studies, a common theme is an enhancement in excitability due to DA-induced reduction in the AHP. Future investigations could examine whether the increases in activity observed in High L-DOPA in *Aplysia* feeding are likewise mediated by a decrease in the AHP or modifications in additional ionic currents. For example, in the lobster pyloric network, bath application of DA produced opposite effects on neurons (e.g., enhancement of the  $I_A$  current in the pyloric dilator neuron, and attenuation of this current in the anterior burster neuron (Harris-Warrick et al., 1998).

In conclusion, the results from this study indicate that different levels of DA enhancement modulate neurons in distinct ways in order to bias the feeding circuit toward specific motor patterns. Additional analysis revealed characteristic alterations in the burst properties and spatial distribution of recruited neurons. Understanding DA modulation of the *Aplysia* feeding central pattern generating network may help to improve understanding of DA modulation of more complex networks in the vertebrate CNS.

## **Chapter 4: Identifying neurons using combined VSD imaging and extracellular nerve recording**

### **4.1 Hypothesis and rationale**

VSD imaging can be used to simultaneously record spike activity in tens to hundreds of neurons, which provides opportunities to understand the dynamics of activity of a large number of neurons. To capitalize on the advantages of this high throughput recording, it is necessary to identify the neurons being recorded to understand the consequences of the observed changes in activity. In mammals, the identification process is aided by the use of genetic techniques to target specific subtypes. Although such genetic resources are currently unavailable for the *Aplysia* nervous system, this model system does have a well characterized neurocircuitry, providing the necessary information to identify neurons. Indeed, the phasic activity of 51 neurons within the feeding circuitry has been characterized, and 47 of these neurons have their morphology and axonal projections delineated. Previous research in the feeding network of *Aplysia* combined extracellular nerve and VSD recordings to characterize neuronal projections of neurons (Morton et al. 1991), but did not attempt to identify the recorded neurons. In this study, VSD and extracellular nerve recordings were combined to identify neurons and ascertain their role in feeding motor patterns.

### **4.2 Results**

#### **4.2.1 Catalogue of feeding CPG neurons**

As a first step to identifying neurons, a catalogue of previously identified neurons was compiled. This catalogue consisted of the phase of activity during a BMP, the axonal projections, and location of the neuron (caudal or rostral). A map of



the location of neurons on each side of the hemiganglia was also created to aid in the identification process (Fig. 5.1).

The phasic activity was categorized as having one of eight possible configurations. Each configuration specified whether the neuron was active in one or more of the phases of the BMP (i.e., protraction, retraction, or post-retraction). For example, one category included neurons which have been observed to be inactive in all three phases. Another category included neurons which could be active only during the retraction phase. For example, B51 can fit in two categories because it can be either inactive in all three phases (e.g., during rBMPs) or be active in only the retraction phase (e.g., during iBMPs) (Evans and Cropper, 1998; Nargeot et al., 1999a,b; Plummer and Kirk, 1990). Some neurons only fit in one category. For example, B64 is always active during a BMP and this activity is always restricted to the retraction phase (Hurwitz and Susswein, 1996). The catalog includes all known activity configurations observed for all identified neurons. A map of the primary activity configuration of each identified neuron is provided in Fig. 5.1A. A superficial analysis of this catalogue revealed that 25 identified neurons can be inactive during a BMP, 26 neurons can be active only during retraction, and 22 neurons can be active only during the protraction phase.

Next the projections were catalogued for the identified neurons. The projections of neurons were derived from neural tracing diagrams or extracellular nerve recordings of previous publications. Neurons which did not have the axonal projections characterized were assumed, for simplicity, to not have any axonal projections through the nerves. In total, there are 14 nerves. 51% of neurons send an

axonal projection through a single ipsilateral nerve while only 17% of neurons send a single projection through a contralateral nerve. 13% of neurons send an axonal projection through a single contralateral and a single ipsilateral nerve. One neuron sends an axonal projection through three ipsilateral and three contralateral nerves. This distribution of projections suggests that information on the projections could aid in the identification of neurons.

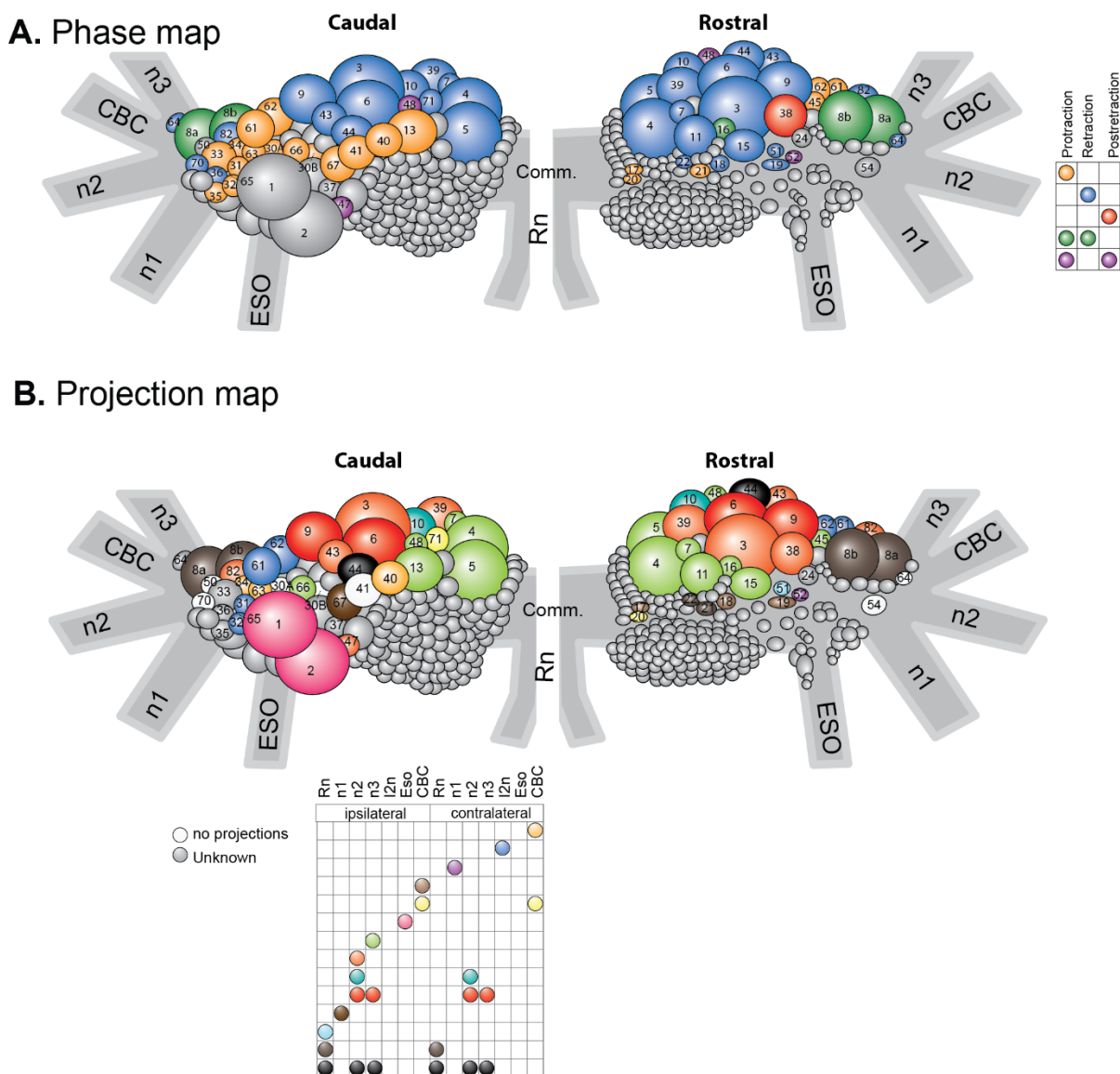


**Figure 4.1** Catalog of all the identified neurons in the buccal ganglia.

**A**, Phase and location of identified neurons in the buccal ganglia. Key: Coloring scheme of the phase map. Each column corresponds to a phase of the pattern. Each row is a group of neurons. Colored circle indicates that this group of neurons is active in this phase. **B**, Projection configuration of all identified neurons in the buccal ganglia. Key: Coloring scheme of the projection map. Columns correspond to specific nerves. Colored circle indicates that this group of neurons has a projection through this nerve.

#### **4.2.2 Neurons could be identified in VSD recordings**

Once the catalogue was compiled, methods were developed to detect axonal projections of neurons in VSD recordings and determine the phasic activity for each recorded neuron. The categorization of phasic activity is discussed in Section 3.2.7 and the identification of axonal projections is discussed in Section 3.2.5. Then, an analysis pipeline was generated to indicate the candidate identified neurons the recorded neuron is likely to be. The final step required human supervision where the identity of the neuron was chosen among the candidates based upon the relative position within the ganglia.

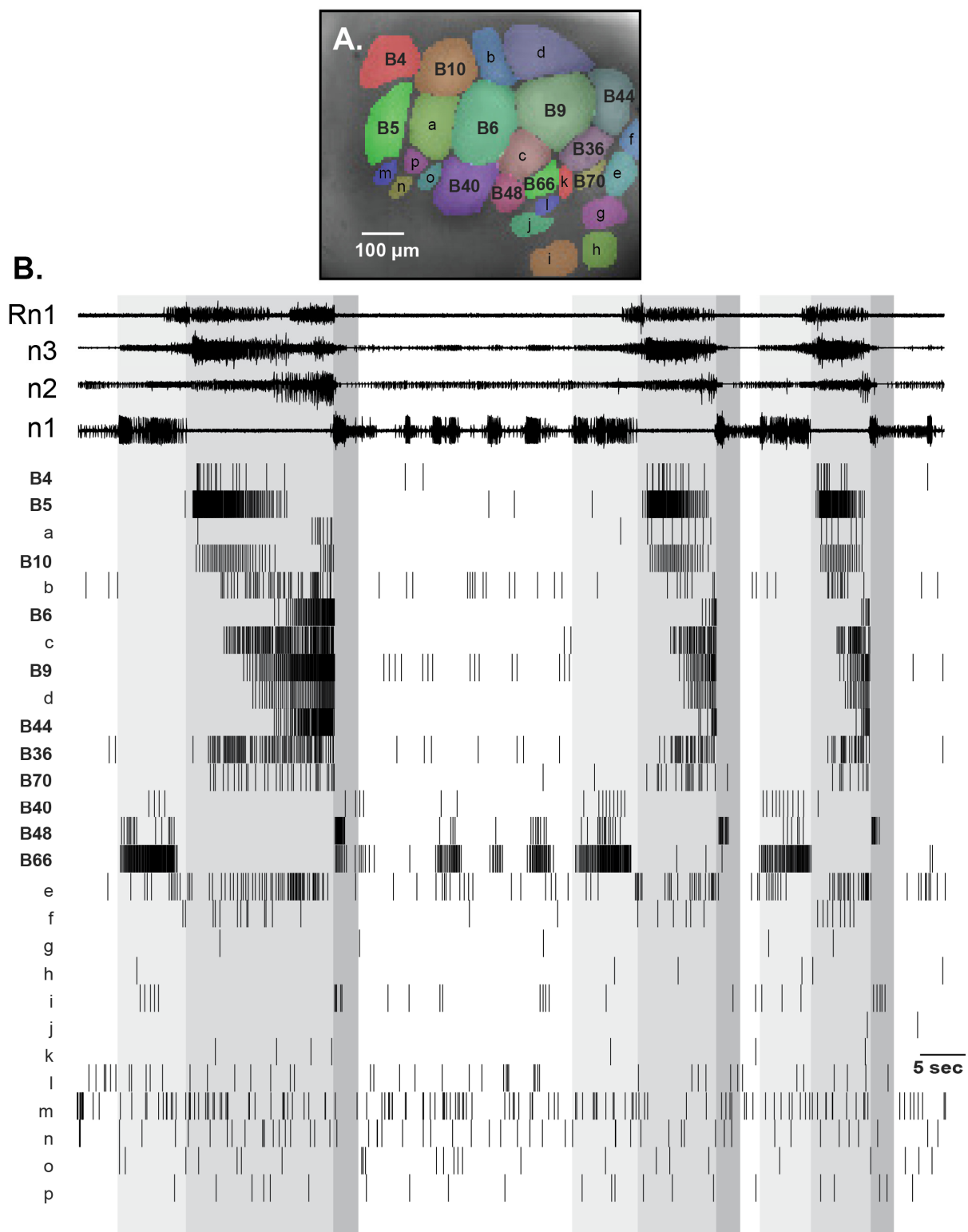
In the first step of the pipeline, the phase of activity was determined. Any neuron whose list of known activity configurations did not include that of the recorded neuron was removed as a potential candidate. For example, if the recorded neuron was designated as only active during retraction, then all except 26 neurons were removed from the list of candidates, because only 26 neurons have a published recording of being active during retraction. Next the axonal projections were determined for the recorded neuron. For example, if an axonal projection was detected in the ipsilateral n2 for this neuron then 18 of the 26 neurons were removed from the list of candidate neurons leaving only 8 neurons. Thus, based on just the phase of activity and the detection of an axonal projection in a single nerve narrowed the possible candidates from 51 neurons to 8 neurons. If an axonal projection was also detected in the contralateral Bn2, then the list of possible candidates is narrowed down to just 4 neurons (B6, B9, B10, B44). Finally, if an axonal projection is detected in Rn then B44 is the only possible candidate because neither B6, B9, nor B10 send

an axonal projection through this nerve. However, if no other axonal projections are detected then spatial information is needed to determine the identity of the neuron. So, if the recorded neuron is on the far upper right of the ganglia, then B10 is the most likely candidate. If, on the other hand, the recorded neuron is on the far lower left of the ganglia, then the neuron is likely to be a new neuron which has yet to be identified. It is currently thought that roughly half of the neurons within the CPG have not been characterized, so the likelihood that the recorded neuron is a new unidentified neuron is approximately 50%. It should be noted that only positive detections of axonal projections were considered informative, the lack of a detection in the recorded neuron was not considered informative and did not exclude candidates because many factors (e.g., recording noise) could cause a bona fide axonal projection to be missed.

This method enabled the identification of 11 neurons in a single recording (Fig. 5.2) indicating that this method is potentially effective in identifying neurons. Some of these identifications are more certain than others. For example, the identification of neurons B4 and B5 is unmistakable, however differentiating B6, B9, and B10 is challenging, thus B6 might be mistaken for B9 or vice versa. Nevertheless, this provides a proof of principle that similar methods can be used to identify neurons in a VSD recording.

**Figure 4.2** Identification of neurons recorded by VSD.

**A**, Image of ganglia showing the pixels that were averaged to obtain the recordings for each neuron. The colors of each neuron in the image are arbitrary. **B**, Example raster plot of a VSD recording (bottom) aligned with nerve recordings (top) during multiple feeding patterns. Each vertical line indicates an action potential detected by VSD. The numbers preceded by a B are neurons that were identified by searching the catalog in Fig. 5.1 for neurons with similar position, phasic activity and the projections as the recorded neuron. Cells that were not identified are arbitrarily labeled with lower case letters. The colors of the spikes correspond to the phase the neuron was active.



### 4.3 Discussion

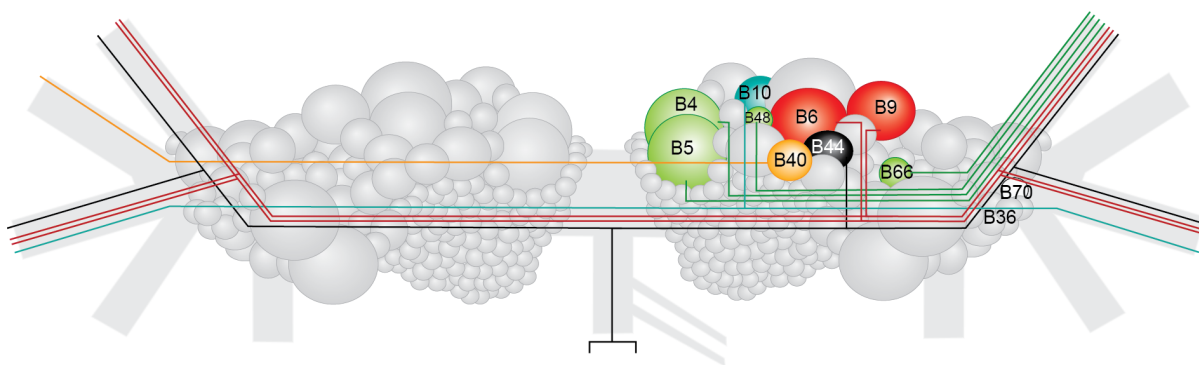
This study has established the groundwork for identifying neurons within the buccal ganglia using combined VSD imaging and extracellular nerve recordings. As a first step, a catalogue of the properties of all the identified neurons was created. This catalogue included the configuration of activity of the identified neurons, the axonal projections and the position of each neuron. This information was then used to identify 11 neurons in a 2 min VSD recording. A map of the identified neurons and their known projections is provided in Fig. 4.3A. Once the neurons are identified, the literature can be searched for synaptic connections that exist between the neurons. For example, as mentioned in the introduction, B4 and its pair B5 send inhibitory connections to nearly every neuron, whereas B36 and B44 connection with other neurons in this recording have yet to be observed. In this manner, the underlying synaptic connections of the recording network can be obtained indirectly through identifying the recorded neurons.

Although this method identified many neurons, a few neuronal features were neglected that may further benefit identification in VSD recordings. One neglected feature is the size and shape of the identified neuron. Occasionally, in this study, the size of the neuron was used by the experimenter to distinguish between neurons but this was not systematically implemented. The size can be a major distinguishing feature. For example, neuron B4 is large but neuron B51 is very small, so these neurons could be distinguished from each other by size alone. In addition, the identification method in this study used a very simple method for characterizing



activity. Activity was encoded in binary form: a neuron was either active during retraction (“1”) or it was inactive during retraction (“0”). Many neurons display different levels of activity during motor patterns. For instance, compare neuron B5 and neuron f in Fig. 4.2. Additionally, many neurons start at different times during retraction (see Fig. 3.3 and Fig. 4.2), therefore future methods should also use the timing of activity to identify neurons. Furthermore, many neurons (e.g., B4, B8, and B51) are active at different levels during different BMP types (e.g., Church and Lloyd, 1994; Evans et al., 1998; Jing and Weiss, 2001; Kabotyanski et al., 1998; Nargeot et al., 1999a,b; Proekt et al., 2007; Sasaki et al., 2009; Teyke et al., 1993). Therefore, comparing the relative levels of activity of each neuron between BMP types could aid in the identification of the recorded neurons. Lastly, this method could be combined with the neurocartography methods pioneered by William Kristan and colleagues (Frady et al., 2016; Kapoor et al., 2015). These methods may be useful in future studies to examine how learning processes like OC modify the activity of identified neurons.

### A. Axonal projections of identified neurons



### B. Network based on previous publications



**Figure 4.3** Neuron identification reveals the functional role of each neuron.

**A**, The projection configuration of each identified neuron. The color scheme legend is on the bottom right. **B**, The synaptic connections of the identified neurons. Information on the connectivity was derived from previous publications.

## **Chapter 5: Discussion and Future Directions**

The studies presented here investigated the modulation of a neuronal circuit by L-DOPA and by a DA-dependent form of learning, OC, using VSD recordings or electrophysiological recordings respectively. In addition, the groundwork was laid for identifying neurons in VSD recordings. The results indicate that OC decreased the excitability of B4 and the B4-to-B51 synaptic connection with a trend towards an enhancement of the B4-to-B8 synaptic connection, and possibly increased the B8 sag potential. The results did not indicate a change in B8 excitability or the B51-to-B8 synaptic connection. A summary of these changes is provided in Fig. 5.1.

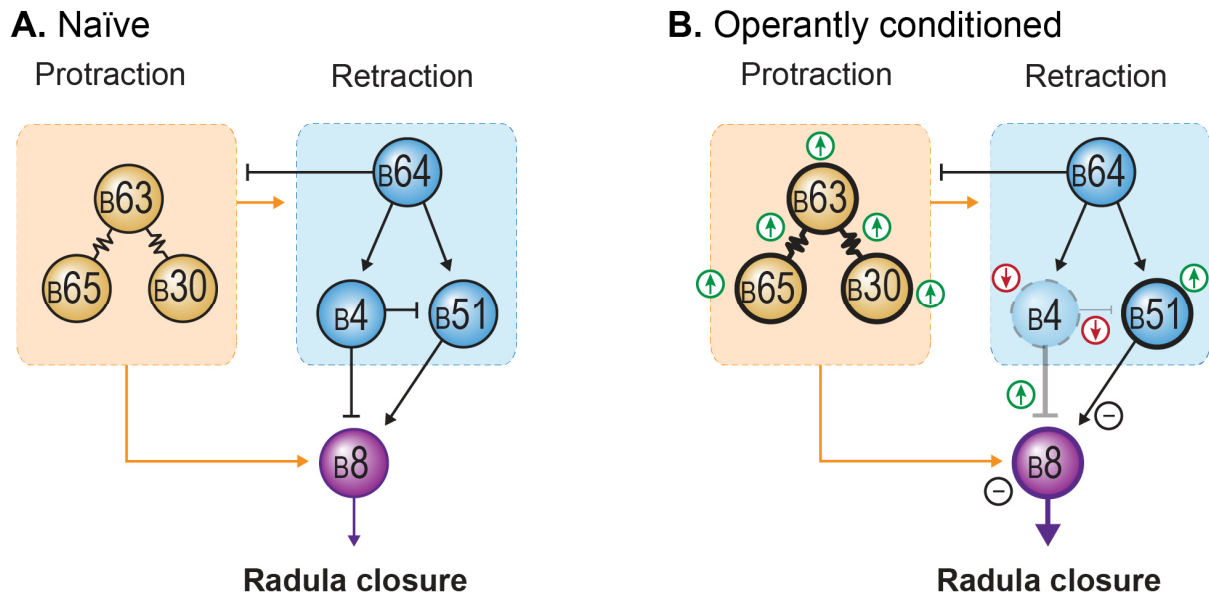


**Figure 5.1** Summary of the OC induced changes in the Feeding CPG

**A**, The naïve circuit. **B**, The OC changes observed in (Nargeot et al., 1999a,b; Seiling et al., 2009) and the results presented in this dissertation. The combined increase in excitability and disinhibition of B51 results in an enhanced B8 activity during retraction. Blue highlights retraction neurons, orange highlights protraction neurons, and purple highlights the B8 closure neuron. Thicker lines indicate enhancement and lighter shaded lines indicate reduction. Enhancement and reduction is also indicated by green upward arrows and red downward arrows, respectively.

The above results indicated that OC reduced the excitability of B4. An unresolved issue is which signaling cascades are responsible for the B4 changes in excitability. In B51,  $\text{Ca}^{2+}$ -dependent PKC and D1 receptor-activated GTPase converge onto adenylyl cyclase leading to an enhancement of cAMP production and the activation of PKA (Lorenzetti et al., 2008). One possibility is that the B51 and B4 excitability changes are mediated by a similar signaling cascades and that the direction of excitability change is determined by downstream processes. Another possibility is that B51 express D1-like receptors that activate stimulatory G-proteins, whereas B4 expresses D2-like receptors that activate inhibitory G-proteins, similar to differential modulation of striatal neurons (Tritsch and Sabatini, 2012). In B4, the activation of D2-like receptors combined with a small increase in  $\text{Ca}^{2+}$  due to electrical activity could lead to the activation of phosphatases such as the  $\text{Ca}^{2+}$ -activated protein phosphatase 2B, or to activation of PKC. Measuring the changes in B4 excitability induced by adenylyl cyclase activators (e.g., forskolin), protein phosphatase inhibitors (e.g., okadaic acid), or PKC inhibitors would help to determine whether these signaling cascades are involved in changes in B4 excitability.

The propensity of a neuron towards increases or decreases in excitability could be determined by interactions between the level of  $\text{Ca}^{2+}$  entry and the proportion of D1 and D2-like receptors. Thus, the timing between neuronal activation ( $\text{Ca}^{2+}$  entry) and DA could be an important factor in determining the direction of the changes in excitability, as suggested by Reynolds and Wickens (2002). The single-cell B4 OC analogue has the ability to test the relationship between the direction of excitability change and the B4 stimulation intensity and duration and the timing of DA. A future

experiment might vary the B4 stimulation intensity and duration, and measure the changes in excitability. A reasonable hypothesis is that low intensities and duration stimulation paired with DA would reduce excitability whereas high intensity and long duration stimulation paired with DA would enhance in excitability. Another experiment could measure the changes in excitability while varying the delay of DA iontophoresis. A reasonable hypothesis is that short delays enhance excitability whereas longer delays reduce excitability. The rationale for these hypotheses is that weaker stimulation might result in lower intracellular  $\text{Ca}^{2+}$  concentrations than strong stimulation, activating distinct signaling cascades. Adding N-, P/Q-, or T- type  $\text{Ca}^{2+}$  channel blockers, or  $\text{Ca}^{2+}$  chelators, would provide insight into the relationship of  $\text{Ca}^{2+}$  and the excitability changes induced by DA.

The molecular mechanisms underlying the changes in the B4-to-B8 and B4-to-B51 synapses is unclear. If B4 does have a higher concentration of D2 receptors, then it is possible that the decrease in the B4-to-B51 synaptic strength may be due to G-protein mediated decreases in ACh release via a reduction in N- and P/Q-type  $\text{Ca}^{2+}$  conductances. Another possibility is a reduction in ACh receptor expression. The increase in B4-to-B8 synaptic connection could be mediated by an increase in the expression or conductance properties of the post synaptic receptors.

It is likely that B4, B30, B51, B63 and B65 are not the only neurons modified by OC. Additional possibilities include two recently identified neurons B70 and B71 (Sasaki et al., 2009, 2013). B70 inhibits B51 and B8 whereas neuron B71 inhibits B4 and excites B8. B70 and B71 are electrically coupled to B51 and B64 (Sasaki et al., 2009, 2013). Because B51 and B71 are the only two retraction neurons known to

excite B8, changes in the excitability of B71 or its synaptic connection could greatly affect B8 activity during retraction. In addition, many protraction neurons (e.g., B20, B30, B34, B40 and B65) have slow excitatory connection to B8. These connections induce PSPs that last for seconds and extend into the retraction phase. Increases in the strength of these slow connections or in the excitability of the presynaptic neuron could also activate B8 to a greater extent during retraction.

The results presented in this dissertation also indicate that VSD imaging can be used to simultaneously record the activity of many neurons in the buccal ganglia. These recordings indicated that a high concentration of L-DOPA increased bite BMPs and that this change correlated with an increase in the level of protraction neuron activity and decrease in the duration of protraction and retraction neuron activity. A logical continuation would be to use VSD imaging to record neuronal activity after OC, to compare the effects of OC on neuronal activity with the changes observed after L-DOPA application. OC increases B51 activity, which prolongs the retraction phase (Nargeot et al., 1999a,b). Therefore, OC is expected to increase the duration of retraction neuron activity rather than decrease it. Through electrical coupling, B51 can also drive activity in retraction neurons. Therefore, an increase in the level of retraction neuron activity is also expected to occur with OC. OC also increases the excitability of protraction neurons B30, B63, and B65, so we would predict that VSD recording of OC would observe an increase the level of protraction neuron activity.

This dissertation also provided the groundwork for identifying buccal ganglia neurons in a VSD recordings. This method was used to identify up to 11 neurons in a single recording. Future methods could incorporate more information about the

dynamics of neuronal activity to facilitate neuron identification. The method could allow for a deeper, more informative, analysis of L-DOPA and OC induced changes. For example, changes in the activity of neurons could be tracked by VSD in multiple preparations. Then, conventional electrophysiological techniques could be used to verify these changes and investigate whether the changes in activity are the result of modification of intrinsic biophysical properties or upstream processes.

The results presented in this dissertation indicate that OC not only increases the excitability but also decreases the excitability and synaptic connections of neurons in the feeding CPG of *Aplysia*. The results also characterized the changes in activity induced by the DA precursor L-DOPA and established a method for identifying neurons in VSD recordings. These results provide a thorough investigation of the modulation of the feeding CPG by DA and DA-dependent forms of learning. The characterization of these changes in a tractable system like *Aplysia* gives insight into other more complex systems which may be modified in similar ways by DA and DA-dependent learning.



## Bibliography

- Abe H, Ino K, Li CZ, Kanno Y, Inoue KY, Suda A, Kunikata R, Matsudaira M, Takahashi Y, Shiku H, Matsue T (2015) Electrochemical imaging of dopamine release from three-dimensional-cultured PC12 cells using large-scale integration-based amperometric sensors. *Anal Chem* 87:6364-6370.
- Abbot A (2010) Levodopa: the story so far. *Nature* 466:S6-7.
- André VM, Cepeda C, Cummings DM, Jocoy EL, Fisher YE, Yang XW, Levine MS (2010) Dopamine modulation of excitatory currents in the striatum is dictated by the expression of D1 or D2 receptors and modified by endocannabinoids. *Eur J Neurosci* 31:14-28.
- Apicella P (2007) Leading tonically active neurons of the striatum from reward detection to context recognition. *Trends Neurosci* 30:299-306.
- Aosaki T, Kiuchi K, Kawaguchi Y (1998) Dopamine D1-like receptor activation excites rat striatal large aspiny neurons *in vitro*. *J Neurosci* 18:5180-5190.
- Bamford NS, Zhang H, Schmitz Y, Wu NP, Cepeda C, Levine MS, Schmauss C, Zakharenko SS, Zablow L, Sulzer D (2004) Heterosynaptic Dopamine Neurotransmission selects sets of corticostriatal terminals. *Neuron* 42:653-663.
- Barbas D, Zappulla JP, Angers S, Bouvier M, Mohamed HA, Byrne JH, Castellucci VF, DesGroseillers L (2006) An *Aplysia* dopamine1-like receptor: molecular and functional characterization. *J Neurochem* 96:414-427.
- Barto AG (1994) Reinforcement learning control. *Curr Biol* 4:888-893.

- Bashford CL (1981) The measurement of membrane potential using optical indicators. *Biosci Rep* 1:183-196.
- Baxter DA, Byrne JH (2006) Feeding behavior of *Aplysia*: a model system for comparing cellular mechanisms of classical and operant conditioning. *Learn Mem* 13:669-680.
- Baxter DA and Byrne JH (2006) Feeding behavior of *Aplysia*: A model system for comparing cellular mechanisms of classical and operant conditioning. *Learn Mem* 13:669-680.
- Beaulieu JM, Gainetdinov RR (2011) The physiology, signaling, and pharmacology of dopamine receptors. *Pharmacol Rev* 63:182-217.
- Bédécarrats A, Cornet C, Simmers J, Nargeot R (2013) Implication of dopaminergic modulation in operant reward learning and the induction of compulsive-like feeding behavior in *Aplysia*. *Learn Mem* 20:318-327.
- Bertoldi M (2014) Mammalian dopa decarboxylase: structure, catalytic activity and inhibition. *Arch Biochem Biophys* 546:1-7.
- Borovikov D, Evans CG, Jing J, Rosen SC, Cropper EC (2000) A proprioceptive role for an exteroceptive mechanoafferent neuron in *Aplysia*. *J Neurosci* 20:1990-2002.
- Bracci E, Centonze D, Bernardi G, Calabresi P (2002) Dopamine excites fast-spiking interneurons in the striatum. *J Neurophysiol* 87:2190-2194.
- Brembs B, Lorenzetti FD, Reyes FD, Baxter DA, Byrne JH (2002) Operant reward learning in *Aplysia*: neuronal correlates and mechanisms. *Science* 296, 1706-1709.

- Brembs B, Baxter DA, Byrne JH (2004) Extending *in vitro* conditioning in *Aplysia* to analyze operant and classical processes in the same preparation. *Learn Mem* 11:412-420.
- Bruno AM, Frost WN, Humphries MD (2015) Modular deconstruction reveals the dynamical physical building blocks of a locomotion motor program. *Neuron* 86: 304-318.
- Byrne JH (1987) Cellular analysis of associative learning. *Physiological Reviews* 67:329-439.
- Calabresi P, Pisani A, Mercuri NB, Bernardi G (1992) Long-term potentiation in striatum is unmasked by removing the voltage dependent magnesium block of NMDA receptor channels. *Eur J Neurosci* 4:929-935.
- Carlsson A (2001) A paradigm shift in brain research. *Science* 294:1021-1024.
- Cataldo E, Byrne JH, Baxter DA (2006) Computational model of a central pattern generator. *Lec Not Comput Sci* 4210: 242-256.
- Centonze D, Bracci E, Pisani A, Gubellini P, Bernardi G, Calabresi P (2002) Activation of dopamine D1-like receptors excites LTS interneurons of the striatum. *Eur J Neurosci* 15:2049-2052.
- Centonze D, Grande C, Usiello A, Gubellini P, Erbs E, Martin AB, Pisani A, Tognazzi N, Bernardi G, Moratalla R, Borrelli E, Calabresi P (2003) Receptor subtypes involved in the presynaptic and postsynaptic actions of dopamine on striatal interneurons. *J Neurosci* 23:6245-6254.

- Chen BT, Bowers MC, Martin M, Hopf FW, Guillory AM, Carelli RM, Chou JK, Bonci A (2008) Cocaine but not natural reward self-administration nor passive cocaine infusion produces persistent LTP in the VTA. *Neuron* 59:288-297.
- Church PJ, Lloyd PE (1991) Expression of diverse neuropeptide cotransmitters by identified motor neurons in *Aplysia*. *J Neurosci* 11:618-625.
- Church PJ, Lloyd PE (1994) Activity of multiple identified motor neurons recorded intracellularly during evoked feeding-like motor programs in *Aplysia*. *J Neurophysiol* 72:1794-1809.
- Chiappalone M, Novellino A, Vajda I, Vato A, Martinoia S, van Pelt J (2005) Burst detection algorithms for the analysis of spatio-temporal patterns in cortical networks of neurons. *Neurocomputing* 65–66:653-662.
- Cocatre-Zilgien JH, Delcomyn F (1992) Identification of bursts in spike trains. *J Neurosci Methods* 41:19–30.
- Cohen LB (2010) Historical overview and general methods of membrane potential imaging. In: *Membrane potential imaging in the nervous system* (Canepari M, Zecevic D, ed), pp 1-11. New York: Springer.
- Costa R, Cohen D, Nicolelis MAL (2004) Differential corticostriatal plasticity during fast and slow motor skill learning in mice. *Curr Biol* 14:1124-1134.
- Cropper EC, Evans CG, Hurwitz I, Jing J, Proekt A, Romero A, Rosen SC (2004) Feeding neural networks in the mollusk *Aplysia*. *Neurosignals* 13:70-86.
- Crisp KM, Gallagher BR, Mesce KA (2012) Mechanism contributing to the dopamine induction of crawl-like bursting in leech motoneurons. *J Exp Biol* 215:3028-3036.

Dacks AM, Siniscalchi MJ, Weiss KR (2012) Removal of default state-associated inhibition during repetition priming improves response articulation. *J Neurosci* 32:17740-17752.

Dacks AM, Weiss KR (2013) Latent modulation: a basis for non-disruptive promotion of two incompatible behaviors by a single network state. *J Neurosci* 33: 3786-3798.

Daubner SC, Le T, Wang S (2011) Tyrosine hydroxylase and regulation of dopamine synthesis. *Arch Biochem Biophys* 508:1-12.

Delgado A, Sierra A, Querejeta E, Valdiosera RF, Aceves J (2000) Inhibitory control of the GABAergic transmission in the rat neostriatum by D2 dopamine receptors. *Neurosci* 95:1043-1048.

Díaz-Ríos M, Oyola E, Miller MW (2002) Colocalization of  $\gamma$ -aminobutyric acid-like immunoreactivity and catecholamines in the feeding network of *Aplysia californica*. *J Comp Neurol* 445:29-46.

Díaz-Ríos M, Miller MW (2005) Rapid dopaminergic signaling by interneurons that contain markers for catecholamines and GABA in the feeding circuitry of *Aplysia*. *J Neurophysiol* 93:2142-2156.

Díaz-Ríos M, Miller MW (2006) Target-specific regulation of synaptic efficacy in the feeding central pattern generator of *Aplysia*: potential substrates of behavioral plasticity? *Biol Bull* 210:215-229.

Due MR, Jing J, Weiss KR (2004) Dopaminergic contributions to modulatory functions of a dual-transmitter interneuron in *Aplysia*. *Neurosci Lett* 358:53-57.

- Elliott CJ and Susswein AJ (2002) Comparative neuroethology of feeding control in mulluscs. *J Exp Biol* 205:877-896.
- Evans CG, Cropper (1998) Proprioceptive input to feeding motor programs in *Aplysia*. *J Neurosci* 18:8016-8031.
- Flores-Hernández J, Cepeda C, Hernández-Echeagaray E, Calvert CR, Jokel ES, Fienberg AA, Greengard P, Levine MS (2002) Dopamine enhancement of NMDA currents in dissociated medium sized neurons: role of D1 receptors and DARPP-32. *J Neurophysiol* 88:3010-3020.
- Frady EP, Kapoor A, Horvitz E, Kristan WB (2016) Scalable semisupervised functional neurocartography reveals canonical neurons in behavioral networks. *Neural Comput* 28:1453-1497.
- Frigon A (2012) Central pattern generators of the mammalian spinal cord. *Neuroscientist* 18:56-69.
- Fromherz P, Müller CO (1993) Voltage-sensitive fluorescence of amphiphilic hemicyanine dyes in neuron membrane. *Biochim Biophys Acta* 1150:111-122.
- Gardner (1971) Bilateral symmetry and interneuronal organization in the buccal ganglia of *Aplysia*. *Science* 173:550-553.
- Gardner and Kandel (1973) Diphasic postsynaptic potential: a chemical synapse capable of mediating conjoint excitation and inhibition. *Science* 176:675-678.
- Gardner D (1977) Interconnections of identified multiaction interneurons in buccal ganglia of *Aplysia*. *J Neurophysiol* 40:349-361.

- Gardner D, Kandel ER (1977) Physiological and kinetic properties of cholinergic receptors activated by multi-action interneurons in buccal ganglia of *Aplysia*. *J Neurophysiol* 40:333-348.
- Gerfen CR, Surmeier JD (2011) Modulation of striatal projection systems by dopamine. *Annu Rev Neurosci* 34:441-466.
- German CL, Baladi MG, McFadden LM, Hanson GR, Flechenstein AE (2015) Regulation of the dopamine and vesicular monoamine transporters: pharmacological targets and implications for disease. *Pharmacol Rev* 67:1005-1024.
- Goetz CG (2011) The history of Parkinson's disease: early clinical descriptions and neurological therapies. *Cold Spring Harb Perspect Med* 1:a008862.
- Grinvald A, Salzberg BM, Lev-Ram V, Hildesheim R (1987) Optical recording of synaptic potentials from processes of single neurons using intracellular potentiometric dyes. *Biophys J* 51:643-651.
- Goldberg JA, Reynolds JNJ (2011) Spontaneous firing and evoked pauses in the tonically active cholinergic interneurons of the striatum. *Neurosci* 198:27-43.
- Guzmán J, Hernández A, Galarraga E, Tapia D, Laville A, Vergara R, Aceves J, Bargas (2003) Dopamine modulation of axon collaterals interconnecting spiny neurons of the rat striatum. *J Neurosci* 23:8931-8940.
- Håkansson K, Galdi S, Hendrick J, Snyder G, Greengard P, Fisone G (2006) Regulation of phosphorylation of the GluR1 AMPA receptor by dopamine D2 receptors. *J Neurochem* 96:482-488.

- Han P, Nakanishi ST, Tran MA, Whelan PJ (2007) Dopaminergic modulation of spinal neuronal excitability. *J Neurosci* 27:13192-13204.
- Harris-Warrick RM, Johnson BR, Peck JH, Kloppenburg P, Ayali A, Sharbinski J (1998) Distributed effects of dopamine modulation in the crustacean pyloric network. *Ann NY Acad Sci* 16:155-167.
- Hernández-López S, Bargas J, Surmeier DJ, Reyes A, Galarraga E (1997) D1 receptor activation enhances evoked discharge in neostriatal medium spiny neurons by modulating an L-type  $\text{Ca}^{2+}$  conductance. *J Neurosci* 17:3334-3342.
- Hernández-López S, Tkatch T, Perez-Garci E, Galarraga E, Bargas J, Hamm H, Surmeier DJ (2000) D2 dopamine receptors in striatal medium spiny neurons reduce L-type  $\text{Ca}^{2+}$  currents and excitability via a novel  $\text{PLC}\beta 1$ - $1\text{P}_3$ -calcineurin-signaling cascade. *J Neurosci* 20:8987-8995.
- Higley MJ, Sabatini BL (2010) Competitive regulation of synaptic  $\text{Ca}^{2+}$  influx by D2 dopamine and A2A adenosine receptors. *Nat Neurosci* 13:958-967.
- Hill ES, Moore-Kochlacs C, Vasireddi SK, Sejnowski TJ, Frost WN (2010) Validation of independent component analysis for rapid spike sorting of optical recording data. *J Neurophysiol* 104:3721-3731.
- Hill ES, Vasireddi SK, Bruno AM, Wang J, Frost WN (2012) Variable neuronal participation in stereotypic motor programs. *PLoS One* 7:e40579.
- Hurwitz I, Goldstein RS, Susswein AJ (1994) Compartmentalization of pattern-initiation and motor functions in the B31 and B32 neurons of the buccal ganglia of *Aplysia californica*. *J Neurophysiol* 71:1514-1527.



- Hurwitz I, Neustadter D, Morton DW, Chiel HJ, Susswein AJ (1996) Activity patterns of the B31/B32 pattern initiators innervating the I2 muscle of the buccal mass during normal feeding movements in *Aplysia californica*. *J Neurophysiol* 75:1309-1326.
- Hurwitz I, Kupfermann I, Susswein AJ (1997) Different roles of neurons B63 and B34 that are active during the protraction phase of buccal motor programs in *Aplysia californica*. *J Neurophysiol* 78:1305-1319.
- Hurwitz I, Susswein AJ (1996) B64, a newly identified central pattern generator element producing a phase switch from protraction to retraction in buccal motor programs of *Aplysia californica*. *J Neurophysiol* 75:1327-1344.
- Jelescu IO, Nargeot R, Bihan DL, Ciobanu L (2013) Highlighting manganese dynamics in the nervous system of *Aplysia californica* using MEMRI at ultra-high field. *Neuroimage* 76:264-271.
- Jing J, Weiss KR (2001) Neural mechanisms of motor program switching in *Aplysia*. *J Neurosci* 21:7349-7362.
- Jocoy EL, André VM, Cummings DM, Rao SP, Wu N, Ramsey AJ, Caron MG, Cepeda C, Levine MS (2011) Dissecting the contribution of individual receptor subunits to the enhancement of N-methyl-D-aspartate currents by dopamine D1 receptor activation in striatum. *Front Syst Neurosci* 5:28.
- Kabotyanski EA, Baxter DA, Byrne JH (1998) Identification and characterization of catecholaminergic neuron B65, which initiates and modifies patterned activity in the buccal ganglia of *Aplysia*. *J Neurophysiol* 79:605-621.

- Kabotyanski EA, Baxter DA, Cushman SJ, Byrne JH (2000) Modulation of fictive feeding by dopamine and serotonin in *Aplysia*. *J Neurophysiol* 83:374-392.
- Kapoor A, Frady EP, Jegelka S, Kristan WB, Horvitz (2015) Inferring and learning from neuronal correspondences. *J of Machine Learn Res.* 1:1-48
- Kandel E (2000) The molecular biology of memory storage: a dialogue between genes and synapses. *Science* 294:1030-1038.
- Kelley AE (2004) Ventral striatal control of appetitive motivation: role in ingestive behavior and reward-related learning. *Neurosci Biobehav Rev* 27:765-776.
- Kemnitz CP (1997) Dopaminergic modulation of spinal neurons and synaptic potentials in the lamprey spinal cord. *J Neurophysiol* 77:289-298.
- Kerr JND, Wickens JR (2001) Dopamine D-1/D-5 receptor activation is required for long-term potentiation in the rat neostriatum *in vitro*. *J Neurophysiol* 85:117-124.
- Kohnomi S, Koshikawa N, Kobayashi M (2012) D2-like dopamine receptors differentially regulate unitary IPSCs depending on presynaptic GABAergic neuron subtypes in rat nucleus accumbens shell. *J Neurophysiol* 107:692-703.
- Koob GF, Volkow ND (2010) Neurocircuitry of addiction. *Neuropsychopharmacology* 35:217-238.
- Leahey TH (2000) A history of psychology: main currents in psychological thought. 5<sup>th</sup> ed. New Jersey: Lehigh Press.

- Lebel D, Grossman Y, Barkai E (2001) Olfactory learning modifies predisposition for long-term potentiation and long-term depression induction in the rat piriform (olfactory) cortex. *Cerebral Cortex* 11:485-489.
- Levitt M, Spector S, Sjoerdsma A, Udenfriend S (1965) Elucidation of the rate-limiting step norepinephrine biosynthesis in the perfused guinea-pig heart. *J Pharmacol Exp Ther* 148:1-8.
- Lorenzetti FD, Baxter DA, Byrne JH (2008) Molecular mechanisms underlying a cellular analog of operant reward learning. *Neuron* 59:815-828.
- London JA, Zečević D, Cohen LB (1987) Simultaneous optical recording of activity from many neurons during feeding in *Navanax*. *J Neurosci* 7:649-661.
- Martínez-Rubio C, Serrano GE, Miller MW (2009) Localization of biogenic amines in the foregut of *Aplysia californica*: catecholaminergic and serotonergic innervation. *J Comp Neurol* 514:329-342.
- Maurice N, Mercer J, Chan CS, Hernández-López S, Held J, Tkatch T, Surmeier DJ (2004) D2 dopamine receptor-mediated modulation of voltage-dependent Na<sup>+</sup> channels reduces autonomous activity in striatal cholinergic interneurons. *J Neurosci* 24:10289-10301.
- Momiyama T, Koga E (2001) Dopamine D2-like receptors selectively block N-type Ca<sup>2+</sup> channels to reduce GABA release onto rat striatal cholinergic interneurons. *J Physiol* 533.2:479-492.
- Morgan PT, Jing J, Vilim FS, Weiss KR (2002) Interneuronal and peptidergic control of motor pattern switching in *Aplysia*. *J Neurophysiol* 87:49-61.

- Morton DW, Chiel HJ, Cohen LB, Wu JY (1991) Optical methods can be utilized to map the location and activity of putative motor neurons and interneurons during rhythmic patterns of activity in the buccal ganglia of *Aplysia*. *Brain Res* 564:45-55.
- Morton DW, Chiel HJ (1993a) *In vivo* buccal nerve activity that distinguishes ingestion from rejection can be used to predict behavioral transitions in *Aplysia*. *J Comp Physiol [A]* 172:17–32.
- Morton DW, Chiel HJ (1993b) The timing of activity in motor neurons that produce radula movements distinguishes ingestion from rejection in *Aplysia*. *J Comp Physiol [A]* 173:519–536.
- Mozzachiodi R, Lorenzetti FD, Baxter DA, Byrne JH (2008) Changes in neuronal excitability serve as a mechanism of long-term memory for operant conditioning. *Nat Neurosci* 11:1146-1148.
- Mozzachiodi R, Byrne JH (2010) More than synaptic plasticity: role of nonsynaptic plasticity in learning and memory. *Trends Neurosci* 33:17-26.
- Nargeot R, Baxter DA, Byrne JH (1997) Contingent-dependent enhancement of rhythmic motor patterns: an *in vitro* analog of operant conditioning. *J Neurosci* 17:8093-8105.
- Nargeot R, Baxter DA, Byrne JH (1999a) *In vitro* analog of operant conditioning in *Aplysia*. I. Contingent reinforcement modifies the functional dynamics of an identified neuron. *J Neurosci* 19:2247-2260.

- Nargeot R, Baxter DA, Byrne JH (1999b) In *vitro* analog of operant conditioning in *Aplysia*. II. Modifications of the functional dynamics of an identified neuron contribute to motor pattern selection. *J Neurosci* 19:2261-2272.
- Nargeot R, Baxter DA, Patterson GW, Byrne JH (1999c) Dopaminergic synapses mediate neuronal changes in an analogue of operant conditioning. *J Neurophysiol* 81:1983-1987.
- Nargeot R, Le Bon-Jego M, Simmers J (2009) Cellular and network mechanisms of operant learning-induced compulsive behavior in *Aplysia*. *Curr Biol* 19:975-984.
- Nargeot R, Petrissans C, Simmers J (2007) Behavioral and *in vitro* correlates of compulsive-like food seeking induced by operant conditioning *Aplysia*. *J Neurosci* 27:8059-8070.
- Nargeot R, Simmers J (2012) Functional organization and adaptability of a decision-making network in *Aplysia*. *Front Neurosci* 6:113. 10.3389/fnins.2012.00113
- Neustadter DM, Drushel RF, Crago PE, Adams BW, Cheil HJ (2002) A kinematic model of swallowing in *Aplysia californica* based on radula/odontophore kinematics and *in vivo* magnetic resonance images. *J Exp Biol* 205:3177-3206.
- Neustadter DM, Herman RL, Drushel RF, Chestek, Cheil HJ (2007) The kinematics of multifunctionality: comparisons of biting and swallowing in *Aplysia californica*. *J Exp Biol* 210:238-260.
- Nirenberg MJ, Chan J, Vaughan RA, Uhl GR, Kuhar Mj, Pickel VM (1997) Immunogold localization of the dopamine transporter: an ultrastructural study of the rat ventral tegmental area. *J Neurosci* 17:4037-4044.

- Nirenberg MJ, Vaughan RA, Uhl GR, Kuhar MJ, Pickel VM (1996) The dopamine transporter is localized to dendritic and axonal plasma membranes of nigrostriatal dopaminergic neurons. *J Neurosci* 16:436-447.
- Niv Y (2009) Reinforcement learning in the brain. *J Math Psychol* 53:139-154.
- Nowak L, Bregestovski P, Ascher P, Herbet A, Prochiantz A (1984) Magnesium gates glutamate-activated channels in mouse central neurones. *Nature* 307:462-465.
- Pacheco-Cano MT, Bargas J, Hernández-López S, Tapia D, Galarraga E (1996) Inhibitory action of dopamine involves subthreshold  $\text{Cs}^+$ -sensitive conductance in neostriatal neurons. *Exp Brain Res* 110:205-211.
- Pisani A, Bonsi P, Centonze D, Calabresi P, Bernardi G (2000) Activation of D2-like dopamine receptors reduces synaptic inputs to striatal cholinergic interneurons. *J Neurosci* 20:RC69.
- Plummer MR, Kirk MD (1990) Premotor neurons B5 1 and B52 in the buccal ganglia of *Aplysia californica*: synaptic connections, effects on ongoing motor rhythms, and peptide modulation. *J Neurophysiol* 63:539-558.
- Pothos E, Desmond M, Sulzer D (1996) L-3,4-dihydroxyphenylalanine increases the quantal size of exocytotic dopamine release *in vitro*. *J Neurochem* 66:629-636.
- Proekt A, Brezina V, Weiss KR (2004) Dynamical basis of intentions and expectations in a simple neuronal network. *Proc Natl Acad Sci U S A*. 101:9447-9452.
- Puhl JG, Mesce KA (2008) Dopamine activates the motor pattern for crawling in the medicinal leech. *J Neurosci* 28:4192-4200.

- Puhl JG, Masino MA, Mesce KA (2012) Necessary, sufficient and permissive: a single locomotor neuron important for intersegmental coordination. *J Neurosci* 32:17646-17657.
- Quinlan EM, Lebel D, Brosh I (2004) A molecular mechanism for stabilization of learning-induced synaptic modifications. *Neuron* 41:185-192.
- Reynolds JNJ, Hyland BI, Wickens JR (2001) A cellular mechanism of reward-related learning. *Nature* 413:67-70.
- Reynold JNJ, Wickens JR (2000) Substantia nigra dopamine regulates synaptic plasticity and membrane potential fluctuations in the rat neostriatum, *in vivo*. *Neuroscience* 99:199-203.
- Reynolds JN, Wickens JR (2002) Dopamine-dependent plasticity of corticostriatal synapses. *Neural Netw* 15:507-521.
- Riolt-Pedotti MS, Friedman, Hess G, Donoghue JP (1998) Strengthening of horizontal cortical connections following skill learning. *Nat Neurosci* 1:230-234.
- Rosen SC, Miller MW, Evans CG, Cropper EC, Kupfermann I (2000) Diverse synaptic connections between peptidergic radula mechanosensory neurons and neurons in the feeding system of *Aplysia*. *J Neurophysiol* 83:1605-1620.
- Rosen SC, Teyke T, Miller MW, Weiss KR, Kupfermann I (1991) Identification and characterization of cerebral-to-buccal interneurons implicated in the control of motor programs associated with feeding in *Aplysia*. *J Neurosci* 11:3630-3655.

- Rosen SC, Weiss KR, Cohen JL, Kupfermann (1982) Interganglionic cerebral-buccal mechanosensors of *Aplysia*: receptive fields and synaptic connections to different classes of neurons involved in feeding behavior. *J Neurophysiol* 48:271-288.
- Ross WN, Salzberg BM, Cohen LB, Davila HV (1974) A large change in dye absorption during the action potential. *Biophys* 14:983-986.
- Ross WN, Salzberg BM, Cohen LB, Grinvald A, Davila HV, Waggoner AS, Wang CH (1977) Changes in absorption, fluorescence, dichroism and birefringence in stained giant axons: optical measurement of membrane potential. *J Membrane Biol* 33:141-183.
- Saar D, Grossman Y, Barkai E (1999) Reduced synaptic facilitation between pyramidal neurons in the piriform cortex after odor learning. *J Neurosci* 19:8616-8622.
- Saar D, Grossman Y, Barkai E (2002) Learning-induced enhancement of postsynaptic potentials in pyramidal neurons. *J Neurophysiol* 87:2358-2363.
- Sasaki K, Brezina V, Weiss KR, Jing J (2009) Distinct inhibitory neurons exert temporally specific control over activity of a motoneuron receiving concurrent excitation and inhibition. *J Neurosci* 29:11732-11744.
- Sasaki K, Cropper EC, Weiss KR, Jing J (2013) Functional differentiation of a population of electrically coupled heterogeneous elements in a microcircuit. *J Neurosci* 33:93-105.
- Schindelin J, Arganda-Carreras I, Frise E et al. (2012) Fiji: an open-source platform for biological-image analysis. *Nat Methods* 9:676-682.



- Schiffmann SN, Lledo PM, Vincent JD (1995) Dopamine D1 receptor modulates the voltage-gated sodium current in rat striatal neurons through a protein kinase A. *J Physiol* 483.1:95-107.
- Schultz W (1986) Responses of midbrain dopamine neurons to behavioral trigger stimuli in monkey. *J Neurophysiol* 56:1439-1461.
- Schultz W (1997) Dopamine neurons and their role in reward mechanisms. *Curr Opin Neurobiol* 7:191-197.
- Schultz W (2013) Updating dopamine reward signals. *Curr Opin Neurobiol* 23:229-238.
- Schultz W (2016) Reward functions of the basal ganglia. *J Neural Transm* 123: 679-693.
- Schultz W, Apicella P, Ljungberg T (1993) Responses of monkey dopamine neurons to reward and conditioned stimuli during successive steps of learning a delayed response task. *J Neurosci* 13:900-913.
- Scott ML, Govind CK, Kirk MD (1991) Neuromuscular organization of the buccal system in *Aplysia californica*. *J Comp Neurol* 312:207-222.
- Serrano GE, Miller MW (2006) Conditional rhythmicity and synchrony in a bilateral pair of bursting motor neurons in *Aplysia*. *J Neurophysiol* 96:2056-2071.
- Sharples AS, Koblinger K, Humphreys JM, Whelan PJ (2014) Dopamine: a parallel pathway for the modulation of spinal locomotor networks. *Front Neural Circuits* 8:55.
- Sharples AS, Whelan PJ (2017) Modulation of rhythmic activity in mammalian spinal networks is dependent on excitability state. *eNeuro* 4: e0368-16.2017 1–18.

- Shepherd JD, Huganir RL (2007) The cell biology of synaptic plasticity: AMPA receptor trafficking. *Annu Rev Cell Dev Biol* 23:613-614.
- Shetreat-Klein AN, Cropper EC (2004) Afferent-induced changes in rhythmic motor programs in the feeding circuitry of *Aplysia*. *J Neurophysiol* 92:2312-2322.
- Sieling F, Bédécarrats A, Simmers J, Prinz Astrid A, Nargeot R (2014) Differential roles of nonsynaptic and synaptic plasticity in operant reward learning-induced compulsive behavior. *Current Biology* 24:941-950.
- Skinner BF (1938) The behavior of organisms: An experimental analysis. New York: Appleton-Century.
- Staddon JER, Cerutti DT (2003) Operant conditioning. *Ann Rev Psychol* 54:115-144.
- Soars-Cunha C, Coimbra B, Sousa N, Rodrigues AJ (2016) Reappraising striatal D1- and D2-neurons in reward and aversion. *Neurosci Biobehav Rev* 68:370-386.
- Snyder GL, Allen PB, Fienberg AA, Valle CG, Huganir RL, Nairn AC, Greengard P (2000) Regulation of phosphorylation of the GluR1 AMPA Receptor in the neostriatum by dopamine and psychostimulants *in vivo*. *J Neurosci* 20:4480-4488.
- Sun XD, Lee EW, Wong EH, Lee KS (2000) ATP-sensitive potassium channels in freshly dissociated rat striatal neurons: activation by metabolic inhibitors and the dopaminergic receptor agonist quipirole. *Eur J Physiol* 440:530-547.
- Sun X, Milovanovic M, Zhao Y, Wolf ME (2008) Acute and chronic dopamine receptor stimulation modulates AMPA receptor trafficking in nucleus accumbens neurons cocultured with prefrontal cortex neurons. *J Neurosci* 28:4216-4230.

- Surmeier DJ, Bargas J, Hemmings HC, Nairn AC, Greengard P (1995) Modulation of calcium currents by a D1 dopaminergic protein kinase/phosphatase cascade in rat neostriatal neurons. *Neuron* 14:385-397.
- Surmeier DJ, Ding J, Day M, Wang Z, Shen W (2007) D1 and D2 dopamine-receptor modulation of striatal glutamatergic signaling in striatal medium spiny neurons. *Trends Neurosci* 30:228:235.
- Susswein AJ, Byrne JH (1988) Identification and characterization of neurons initiating patterned neural activity in the buccal ganglia of *Aplysia*. *J Neurosci* 8:2049-2061.
- Tasaki I, Watanabe A, Sandlin R, Carnay L (1968) Changes in fluorescence, turbidity, and birefringence associated with nerve excitation. *Proc Natl Acad Sci* 61:883-888.
- Taverna S, Canciani B, Pennartz CMA (2005) Dopamine D1-receptors modulate lateral inhibition between principal cells of the nucleus accumbens. *J Neurophysiol* 93:1816-1819.
- Tecuapetla F, Koós T, Tepper JM, Kabbani N, Yeckel MF (2009) Differential dopaminergic modulation of neostriatal synaptic connections of striatopallidal axon collaterals. *J Neurosci* 29:8977-8990.
- Teyke T, Rosen SC, Weiss KR, Kupfermann I (1993) Dopaminergic neuron B20 generates rhythmic neuronal activity in the feeding motor circuitry of *Aplysia*. *Brain Res* 10:226-237.
- Thorndike EL (1911) *Animal Intelligence: Experimental Studies*. New York: Macmillan.
- Tritsch NX, Sabatini BL (2012) Dopaminergic modulation of synaptic transmission in cortex and striatum. *Neuron* 76:33-50.

- Uzakov S, Frey JU, Korz V (2005) Reinforcement of rat hippocampal LTP by holeboard training. *Learn Mem* 12:165-171.
- Waggoner AS, Wang CH, Tolles RL (1977) Mechanism of potential-dependent light absorption changes of lipid bilayer membranes in the presence of cyanine and oxonol dyes. *J Membrane Biol* 33:109-140.
- Wang W, Dever D, Lowe J, Storey GP, Bhansali A, Eck EK, Nitulescu I, Weimer J, Bamford NS (2012) regulation of prefrontal excitatory neurotransmission by dopamine in the nucleus accumbens core. *J Physiol* 590.16:3743-3769.
- Wickens JC, Begg AJ, Arbuthnott GW (1996) Dopamine reverses the depression of rat corticostriatal synapses which normally follows high-frequency stimulation of cortex *in vitro*. *Neuroscience* 70:1-5.
- Wieland S, Du D, Oswald MJ, Parlato R, Köhr G, Kelsch W (2014) Phasic dopaminergic activity exerts fast control of cholinergic interneuron firing via sequential NMDA, D2, and D1 receptor activation. *J Neurosci* 34:11549-11559.
- Wise, R.A. (2004) Dopamine, learning and motivation. *Nat Rev Neurosci* 5:483–494.
- Wu JY, London JA, Zecevic HP, Höpp HP, Cohen LB, Xiao C (1988) Optical monitoring of activity of many neurons in invertebrate ganglia during behaviors. *Experientia* 44:369-376.
- Wu JS, Wang N, Siniscalchi MJ, Perkins MH, Zheng YT, Yu W, Chen SA, Jia RN, Gu JW, Qian YQ, Ye Y, Vilim FS, Cropper EC, Weiss KR, Jing J (2014) Complementary interactions between command-like interneurons that function to activate and specify motor programs. *J Neurosci* 34:6510-6521.

- Xiaochen S, Lin Y (2016) Npas4: linking neuronal activity to memory. *Trends Neurosci* 39:264-275.
- Zhang F, Gradinaru V, Adamantidis AR, Durand R, Airan RD, Lecea LD, Deisseroth K (2010) Optogenetic interrogation of neural circuits: technology for probing mammalian brain structures. *Nat Protoc* 5:439-456.
- Yan Z, Song WJ, Surmeier DJ (1997) D2 dopamine receptors reduce N-type  $\text{Ca}^{2+}$  currents in rat neostriatal cholinergic interneurons through a membrane-delimited, protein-kinase-C-insensitive pathway. *J Neurophysiol* 77:1003-1015.
- Yan Z, Surmeier DJ (1997) D5 dopamine receptor enhance  $\text{Zn}^{2+}$ -sensitive  $\text{GABA}_A$  currents in striatal cholinergic interneurons through a PKA/PP1 cascade. *Neuron* 19:1115-1126.
- Simms BA, Zamponi GW (2014) Neuronal voltage-gated calcium channels: structure, function, and dysfunction. *Neuron* 82:24-45.
- Zečević D, Wu JY, Cohen LB, London JA, Höpp, Falk CX (1989) Hundreds of neurons in the *Aplysia* abdominal ganglion are active during the gill-withdrawal reflex. *J Neurosci.* 9:3681-3689.

**Vita**

Curtis Lynn Neveu was born in Katy, TX on May 13, 1985, the son of Steven Blake Neveu and Daphne Lynn Jech. After graduating from Skiatook High School he received his Bachelors of Science in Biochemistry and Molecular Biology and a Bachelors of Science in Microbiology and Molecular Genetics with a minor in Psychology from Oklahoma State University in 2009. In September of 2009 he entered The University of Texas Graduate School of Biomedical Sciences at Houston.